Role of CHD7 in neural development and maintenance

by

Wanda Sherrie Layman

A dissertation submitted in partial fulfillment
of the requirements for the degree of
Doctor of Philosophy
(Human Genetics)
in The University of Michigan
2011

Doctoral Committee:

Associate Professor Donna M. Martin, Chair
Professor Sally A. Camper
Professor Jeffrey W. Innis
Professor Miriam H. Meisler
Associate Professor Jeffrey R. Martens

Dedication

To my Bear and cub, with your love and support all things are possible…

Acknowledgements

First, I would like to thank Donna Martin for her mentorship and support. I have benefitted greatly from having you as my mentor. I would also like to thank the members of the Martin lab. Liz, you were definitely the best half of the CHD7 dynamic duo. I'm not sure I would have survived the last several years in the lab without you. Jennifer, Mindy, Jillian, and Joe – thank you for all of your help and support.

I also need to thank Jeff Martens and some former members of the Martens lab, Dyke and Paul. When I first started this project, I knew absolutely nothing about olfaction or olfactory tissues. My thesis project was greatly influenced by your help and support.

Many individuals contributed to making this work possible. I am grateful to the members of my thesis committee Sally Camper, Jeff Innis, Miriam Meisler, and Jeff Martens for their support and guidance. I could not have found better scientists and mentors to guide me through this project. Yehoash Raphael and the Raphael lab were also incredibly beneficial to this work. Thanks also to the Program in Biomedical Sciences (PIBS), the Human Genetics department, and the University of Michigan for taking on a graduate student that did not have the best grades, test scores, or experience.

Finally, I would like to thank my family. Brian and Xavier, I don't know how you put up with me all of these years, but I would never have continued on to this point in my life without both of you. Thank you Mom, words cannot express how much I respect

and love you. Dad, I guess that I will finally be Dr. Wanda; I wish you could have lived to see it happen.

Table of Contents

List of Figures

List of Tables

Abstract

Role of CHD7 in neural development and maintenance

by

Wanda Sherrie Layman

Chair: Donna M. Martin

Normal tissue development and maintenance require precise timing and correct localization of gene expression. Several lines of evidence indicate that the chromodomain (CHD) family of proteins are critical regulators of chromatin remodeling and gene expression. In humans, haploinsufficiency for *CHD7* causes CHARGE syndrome, a multiple anomaly condition characterized by ocular coloboma, heart defects, choanal atresia, retarded growth and development, genital hypoplasia and ear abnormalities. Many patients with CHARGE display Kallmann-like features which include olfactory and endocrine dysfunction. Clinical evidence indicates that mutations in *CHD7* lead to pleiotropic developmental defects; however, the mechanisms underlying these defects have not yet been determined.

In order to study the role of CHD7, we generated mice carrying a $Chd7^{Gt}$ allele derived from *Chd7* deficient, gene trapped *lacZ* reporter embryonic stem cells and mice

with a conditional *Chd7* null allele, $Chd7^{flox}$. Homozygous *Chd7* null mice are embryonic lethal by E11. $Chd7^{Gt/+}$ mice exhibit features similar to human CHARGE phenotypes, including postnatal growth delay, vestibular dysfunction, and olfactory defects which include olfactory bulb hypoplasia and severely impaired olfaction. Our data indicate that olfactory dysfunction may primarily result from defects in neural stem cell proliferation and reduced olfactory sensory neurons in the olfactory epithelium. However, defects in neural stem cell proliferation in the subventricular zone of the forebrain may also contribute to olfactory bulb defects which occur in both humans and mice with *Chd7* deficiency. Additionally, decreased cellular proliferation in the E10.5 olfactory placode causes reduced GnRH neurogenesis, and reduced numbers of GnRH neurons in embryonic and adult $Chd7^{Gt/+}$ mice. Expression levels of *GnRH1* and *Otx2* in the hypothalamus and *GnRHR* in the pituitary are significantly reduced in adult $Chd7^{Gt/+}$ mice. Additionally, *Chd7* mutant embryos have CHD7 dosage dependent reductions in expression levels of *Fgfr1*, *Bmp4,* and *Otx2* in the olfactory placode. Together, these data suggest that CHD7 has critical roles in the development and maintenance of GnRH neurons for regulating puberty and reproduction. Overall, our data have shown how defects in neural progenitor proliferation and neurogenesis have contributed to the Kallmann-like features associated with CHD7 deficiency.

Chapter 1

Introduction[1]

Abstract

In humans, heterozygous mutations in the ATP-dependent chromatin remodeling gene *CHD7* cause CHARGE syndrome, a common cause of deaf-blindness, balance disorders, congenital heart malformations, and olfactory dysfunction with an estimated incidence of approximately 1 in 10,000 newborns. The clinical features of CHARGE in humans and mice are highly variable and incompletely penetrant, and most mutations appear to result in haploinsufficiency of functional CHD7 protein. Mice with heterozygous loss of function mutations in *Chd7* are a good model for CHARGE syndrome, and analyses of mouse mutant phenotypes have begun to clarify a role for CHD7 during development and into adulthood. *Chd7* heterozygous mutant mice have postnatal delayed growth, inner ear malformations, anosmia/hyposmia, and craniofacial defects, and *Chd7* homozygous mutants are embryonic lethal. A central question in developmental biology is how chromodomain proteins like CHD7 regulate important developmental processes, and whether they directly activate or repress downstream gene transcription or act more globally to alter chromatin structure and/or function. CHD7 is expressed in a wide variety of tissues during development, suggesting that it has tissue-specific and developmental stage-specific roles. Here we review recent and ongoing analyses of CHD7 function in mouse models and cell based systems. These studies

explore tissue-specific effects of CHD7 deficiency, known CHD7 interacting proteins, and downstream target sites for CHD7 binding. CHD7 is emerging as a critical regulator of important developmental processes in organs affected in human CHARGE syndrome.

Introduction

Regulation of eukaryotic genes is essential for normal tissue and organ development and maintenance. Chromatin structure has a vital role in gene regulation, via its effects on cellular proliferation and maintenance of the differentiated state. A central goal in current developmental biology is to identify molecular pathways that regulate chromatin structure and gene expression, and to understand how this regulation influences organogenesis. In humans, haploinsufficiency for the chromodomain helicase DNA binding gene 7 (*CHD7*) causes CHARGE syndrome, a multiple anomaly condition characterized by ocular coloboma, heart defects, atresia of the choanae, retarded growth and development, genital hypoplasia and ear abnormalities including deafness and vestibular disorders (1). The identification of *CHD7* as the causative gene for CHARGE syndrome has led to several recent advancements in our understanding of this complex disorder. Furthermore, with the establishment of mouse models for CHARGE, it is now possible to begin detailed molecular analyses of how CHD7 functions in specific tissues and cell types both during development and into adulthood. Here we review recent studies which explore the underlying molecular genetic mechanisms by which CHD7 regulates the development and maintenance of various tissues. Researchers are now poised to charge into the future with a well-equipped toolbox for analyzing CHD7 function.

CHD7 mutations cause CHARGE syndrome

In humans, heterozygous *CHD7* mutations cause CHARGE syndrome, a clinically variable, multiple congenital anomaly condition affecting development of the inner ear, central nervous system, olfactory system, eyes, heart, choanae (the region between the oropharynx and nasal passages), genitalia, and craniofacial structures including the hard and soft palates, lip, external ear, and midface (2-6). CHARGE is a common cause of deaf-blindness, balance disorders, olfactory dysfunction, and congenital heart malformations, with an estimated incidence of 1:10,000 in newborns (7-9). The human *CHD7* gene spans 188 kb on chromosome 8q12.1, with a 8994 bp open reading frame and transcription start site in exon 2. Heterozygosity for nonsense, deletion, or missense *CHD7* mutations occurs in 60-80% of patients with CHARGE (2-5, 10, 11). Human *CHD7* mutations are distributed throughout the coding sequence and do not appear to be correlated with specific aspects of the clinical phenotype (2-5, 10, 11). Most human *CHD7* mutations identified thus far are *de novo*; however, evidence for germline mosaicism has been reported in families with multiple affected siblings (3, 12-14).

The clinical features of CHARGE in humans and mice are highly variable and incompletely penetrant. We recently reviewed all reports of *CHD7*-mutation positive CHARGE individuals, and found that the most commonly affected organ in humans with *CHD7* mutations is the ear (2-6, 12-35). Ear defects in CHARGE include temporal bone abnormalities, external ear malformations, and hearing loss (2-6, 12-35). In addition to ear abnormalities, a majority of CHARGE patients are also affected by some combination of the following: ocular coloboma, heart defects, delayed growth and development, and

genital hypoplasia (2-6, 12-35). Although olfactory function is less commonly analyzed in CHARGE patients, a majority of CHARGE patients analyzed have some form of olfactory defect including olfactory bulb hypoplasia and/or aplasia, and impaired olfaction ranging from mild hyposmia to anosmia (16, 24, 26, 28, 36-40). Less commonly reported clinical features associated with CHARGE and *CHD7* mutations include choanal atresia, facial nerve palsy, cleft lip and/or plate, and tracheoesophageal fistula (2-6, 12-35). The variability in CHARGE features suggests that mutations in *CHD7* lead to pleiotropic developmental defects; however, the mechanisms underlying these defects have not yet been determined.

Mouse models of CHARGE and tissue specific defects

Mouse CHD7 protein is comprised of 2985 amino acids, and has a predicted molecular weight of 334 kDa. Both human and mouse *Chd7* genes contain 38 exons, and have similar exon-intron structures. At the protein level, there is 94.7% sequence identity between mouse and human CHD7, which corresponds to 89.7% nucleotide sequence identity. Heterozygous *Chd7* mutant mice were originally identified by ethylnitrosourea (ENU) mutagenesis, with each of nine different lines carrying a single nonsense *Chd7* mutation (41). These nine *Chd7* mutant mouse lines are viable, with phenotypes that include head bobbing, circling behaviors, disrupted lateral semicircular canals, hyperactivity, reduced postnatal growth, variable cleft palate, choanal atresia, cardiac septal defects, hemorrhage, prenatal death, genital abnormalities, keratoconjunctivitis sicca (dry eye), and olfactory defects (41). Our laboratory generated heterozygous loss of function $Chd7^{Gt/+}$ mice using *Chd7* gene trap embryonic stem (ES) cells (42). $Chd7^{Gt/+}$

mice have phenotypic features similar to those generated by ENU mutagenesis (42). *Chd7*$^{Gt/Gt}$ mice are embryonic lethal by E11, and exhibit developmental growth delays such as reduction in size of multiple organs including brain, eyes, ears, and craniofacial structures (42). The intrauterine lethality of homozygous *Chd7*$^{Gt/Gt}$ embryos and the severity of developmental malformations in *Chd7*$^{Gt/+}$ mice indicate a lack of redundancy for prenatal *Chd7* function in the mouse genome, and suggest important roles for CHD7 in organogenesis (42). *Chd7* is expressed in specific tissues during mouse and human embryogenesis including the ear, brain, cranial nerves, olfactory epithelium, olfactory bulb, pituitary, heart, liver, eye, gut, kidney, and craniofacial structures (Figure 1.1) (5, 39, 41, 42). *Chd7* is also expressed in the adult mouse olfactory epithelium, olfactory bulb, and in the rostral migratory stream (39).

Inner ear abnormalities in humans and mice with CHD7 deficiency

The most consistent clinical feature associated with CHARGE syndrome is inner ear defects, including semicircular canal dysplasia that typically affects all three canals, and a Mondini form of cochlear hypoplasia (35, 43-45). In addition, both facial and vestibulocochlear nerve abnormalities are also reported (44, 46). Cochlear implants are a successful treatment for some CHARGE patients, provided there are no underlying nerve abnormalities. CHARGE patients also display vestibular dysfunction, including delayed postural development, abnormal vestibular testing, and balance/motor problems (47, 48). Although absence of the semicircular canals is believed to be a major cause of balance dysfunction, other factors such as ocular malformations, CNS defects, and skeletal abnormalities are also likely contributors.

Heterozygous *Chd7* mice display circling and head-bobbing behaviors consistent with vestibular dysfunction phenotypes (41, 42). Detailed examination of *Chd7* mutant mouse ears indicates a variety of lateral semicircular canal malformations, smaller posterior semicircular canals, and defects in innervation of the posterior crista (Figure 1.2) (42, 49-52). During embryonic development, semicircular canals are formed by sequential outpocketing, fusion of the otic epithelium, and tightly controlled processes to form three canals (53). Semicircular canal dysgenesis can be caused by mutations in a variety of transcription factors and signaling molecules (Table 1). Semicircular canal abnormalities observed in *Chd7* mutant mice are postulated to be the result of smaller posterior and lateral canal outpocketings and delayed fusion of the epithelium (Figure 1.2) (51). Perturbations in signaling cascades both within the inner ear epithelium and surrounding mesenchyme can also result in semicircular canal defects (Table 1.1) (54). In summary, the inner ear phenotypes observed in heterozygous *Chd7* mice are similar to those reported in CHARGE patients and include semicircular canal defects, innervation defects, and vestibular dysfunction. The precise molecular mechanisms of *Chd7* function within the ear are still not understood, but likely involve complex interactions with essential transcription factors expressed during ear development.

Impaired olfaction in humans and mice with CHD7 deficiency

Genital hypoplasia, delayed puberty, and delayed growth are common in CHARGE individuals (16, 24, 26, 28, 40). These features often occur in conjunction with olfactory defects, including hypoplastic olfactory bulbs and reduced olfaction (16, 24, 26, 28, 40). Previous studies of endocrine dysfunction in CHARGE patients reported

growth delays, but only 9% of CHARGE patients had growth hormone deficiency, and growth delay was not associated with thyroid-stimulating hormone or adrenocorticotropic hormone deficiency (40). Analysis of female CHARGE patients over the age of 12 showed lack of spontaneous puberty and no response to stimulation with gonadotropin-releasing hormone (GnRH) (40). A majority of male CHARGE patients had low testosterone levels and cryptorchidism and/or micropenis. In contrast to females, male response to GnRH stimulation was variable and did not always correlate with testosterone levels (40). Endocrine dysfunction in CHARGE individuals is therefore likely to be multifactorial, with variable influence on olfaction, somatic growth, puberty, and fertility.

Mutations in *CHD7* have been reported in individuals with Kallmann syndrome with and without a CHARGE syndrome diagnosis (24, 26). Kallmann syndrome is primarily characterized by idiopathic hypogonadotropic hypogonadism and anosmia (26, 55, 56). Idiopathic hypogonadotropic hypogonadism is characterized by impaired or absent sexual development due to sex steroid hormone deficiency, with low serum levels of the pituitary gonadotropins follicle-stimulating hormone (FSH) and luteinizing hormone (LH) as well as infertility (26, 55, 56). Kallmann-like features in humans are often associated with impairment of embryonic gonadotropin releasing hormone (GnRH) neuronal migration along olfactory neuronal tracts from the olfactory placode to the hypothalamus (26, 55, 56). Kallmann syndrome is genetically heterogeneous, with mutations reported in a variety of genes including *KAL1*, *FGFR1*, *FGF8*, *PROKR2*, *PROK2*, and *CHD7* (26, 55-59). Mouse models exist for several of the genes associated with Kallmann syndrome (hypogonadotropic hypogonadism and reduced olfaction) and are listed in Table 1.2.

Odorant detection is a complex process that requires normal function of several different tissues and organs. Odorants are first detected in the nasal olfactory epithelium by odorants binding to specific odorant receptors located on the surface of olfactory cilia (Figure 1.3). Bound odorants activate olfactory sensory neurons, which are bipolar neurons that project axons to the glomeruli in the olfactory bulb. Olfactory bulb glomeruli contain dendrites of mitral cells and a variety of interneurons and periglomerular cells. Neuronal signals are then relayed to higher brain regions in the central nervous system (CNS).

Since olfactory ability is reliant upon a number of components working in a coordinated fashion, we chose to look at olfactory function in mice utilizing methods that are not influenced by behavioral issues such as circling and hyperactivity. We observed, using electro-olfactogram of the olfactory epithelium, a lack of functional responses in olfactory sensory neurons to a variety of odorants in young (6 week old) adult *Chd7*$^{Gt/+}$ mice (39). Additionally, we found that young adult *Chd7*$^{Gt/+}$ mice have fewer olfactory sensory neurons and olfactory bulb hypoplasia (Figure 1.3) (39). In order to identify the underlying mechanisms by which CHD7 regulates olfactory sensory neurons, we analyzed cell-type specific expression of *Chd7* in the young adult olfactory epithelium (39). CHD7 is present in 97% of proliferating neural stem cells and in Ascl1-positive (Mash1) and NeuroD-positive pro-neuronal cells in the adult mouse olfactory epithelium by immunofluorescence (39). Chemical ablation of the adult mouse olfactory epithelium in *Chd7*$^{Gt/+}$ mice results in reduced regenerative capacity of olfactory sensory neurons, indicating ongoing requirements for CHD7 in adulthood (39). Consequently, we hypothesize that with age or insult, further reductions in olfactory sensory neurons and

olfactory bulb size could occur, but this remains to be formally tested (Figure 1.3). In a concurrent study, *Chd7*$^{Whi/+}$ mice had reduced olfaction (assayed by sniff response to mouse urine compared to water), olfactory bulb hypoplasia, reproductive dysfunction, and decreased fertility compared to wild type mice (60). Taken together, these studies suggest that CHD7 has critical functions in olfactory sensory neuron integrity and odorant detection.

CHD7 and other CHD proteins: classification and characteristics

CHD proteins are a part of the large group of ATP-dependent chromatin remodelers. The mammalian genome encodes approximately 30 such genes that appear to be non-redundant and vital for normal embryonic development (61). Many ATP-dependent chromatin remodeling genes demonstrate haploinsufficiency, indicating that their products may be involved in rate-limiting steps during development (61). CHD7 is one of nine ATP-dependent chromatin remodeling CHD enzymes that are characterized by the presence of two chromodomains, centrally located helicase domains, and less well defined carboxy terminal domains (Figure 1.4) (61-63). CHD proteins use ATP hydrolysis to regulate access to DNA by altering nucleosomes (61-63). The nine CHD proteins are broadly classified into three subfamilies based upon their amino acid sequence and functional protein domains (61-63). CHD7 is a member of the class III chromodomain proteins together with CHD5, CHD6, CHD8, and CHD9 (61-63). CHD7 contains a SANT (SWI3, ADA2, N-COR, and TFIIB) domain, which is conserved among many regulators of transcription and chromatin structure, and is believed to function as a histone tail binding module (64). CHD7, CHD8, and CHD9 contain two BRK domains,

the function of which appears to be specific to higher eukaryotes since it is not present in yeast chromatin remodeling factors (63). CHD7 and the other eight CHD proteins are an interesting class of novel ATP-dependent chromatin remodelers with unique protein motifs that are incompletely characterized. To date, CHD7 is the only member of this class of proteins for which mutations have been associated with a well described human syndrome.

CHD7 binding sites and interacting proteins

Recent studies have begun to clarify a role for CHD7 in regulating gene expression during tissue development and maintenance. In a study using chromatin immunoprecipitation followed by microarray based sequence analysis (ChIP-chip), CHD7 has been shown to bind in a cell type specific manner to methylated histone H3 lysine 4 in enhancer regions of numerous genes in human colorectal carcinoma cells, human neuroblastoma cells, and mouse embryonic stem cells before and after differentiation, indicating that CHD7 may have temporal and tissue-specific functions (65). CHD7 has also been implicated to regulate multipotent neural crest-like cells by binding to PBAF components including BRG1, BAF170, BAF155, BAF57, PB1, ARID2, and BRD7 (66). In mesenchymal stem cells, CHD7 regulates cell fate specification during osteoblast and adipocyte differentiation (67). CHD7 forms a complex with NLK, SETDB1, and PPAR-γ, and binds to methylated lysine 4 and lysine 9 residues on histone H3 at PPAR-γ target promoters, which suppresses ligand-induced transactivation of PPAR-γ target genes (67). Additionally, the *CHD7 Drosophila* orthologue, *Kismet*, is involved in transcriptional elongation by RNA polymerase II

through recruitment of ASH1 and TRX and may help maintain stem cell pluripotency by regulating methylation of histone H3 lysine 27 (68). Together, these data indicate multiple roles for CHD7 in regulating transcription, potentially affecting tissue and developmental stage-specific processes (Figure 1.5).

Summary and future studies

In summary, CHARGE syndrome is a monogenic disease which exhibits highly variable expressivity. Organs affected in CHARGE during development include neural tube, neural crest, and placodal derivatives. Certain tissues such as the inner ear and olfactory system appear to be highly sensitive to *CHD7* dosage, whereas other organs such as the heart, kidney, and skeletal systems are more variably affected. *CHD7* haploinsufficiency occurs in 60-80% of CHARGE patients and mutations in *CHD7* are distributed throughout the coding sequence. Further studies are necessary to determine whether the remaining 20-40% of CHARGE patients have mutations in *CHD7* regulatory elements or in other genes. It is also possible that unidentified environmental factors contribute to the phenotype. Heterozygous *Chd7* mutant mice and *in vitro* ES cell analyses have begun to clarify a role for CHD7 in the development and maintenance of a variety of tissues (39, 41, 42, 60, 65-68). These studies suggest that CHD7 has roles in stem cell maintenance and cell fate specification (39, 65-68). *In vitro* analyses have implicated that CHD7 is a member of the PBAF complex in neural crest-like cells (66) and that CHD7 forms a complex with NLK, SETDB1, and PPAR-γ (67). These studies open the door for further *in vivo* assays which should identify important downstream effectors of CHD7. Taken together, these observations suggest that CHD7 is likely to

participate in combinatorial protein complexes which bind DNA in enhancer regions and regulate gene transcription in a temporal and tissue-specific manner.

To date, much has been learned about CHARGE syndrome, but several important questions remain unanswered. Is there a core set of CHD7 binding partners that regulate CHD7 function, and if so are they tissue and age-specific? What are the upstream regulators of *CHD7*? Finally, can we use information about CHD7 function in cells to help design therapies for patients diagnosed with CHARGE syndrome?

Chapter 1 Notes

[1]A revised version of Chapter 1 was published as Layman WS, Hurd EA, Martin DM. (2010). Chromodomain Proteins in Development: Lessons from CHARGE Syndrome. *Clinical Genetics*: Jul;78(1):11-20.

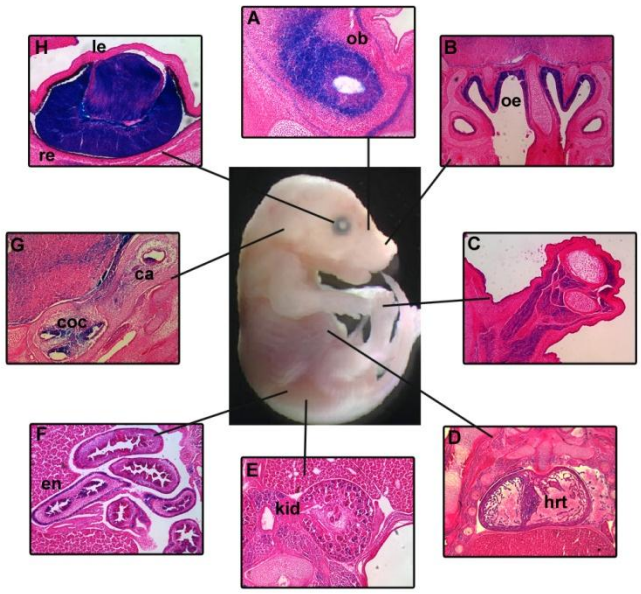

Figure 1.1 *Chd7* is expressed in CHARGE related tissues during development. Frozen sections from E14.5 $Chd7^{Gt/+}$ embryos demonstrate β-galactosidase (X-gal staining) in CHARGE-related organs including (A) olfactory bulbs (ob), (B) olfactory epithelium (oe), (C) limb, (D) heart (hrt), (E) kidney (kd), (F) enteric neurons of the gut (en), (G) crista (ca) and cochlea (coc) of the inner ear and (H) lens (le) and retina (re) of the eye. All sections are in the coronal orientation.

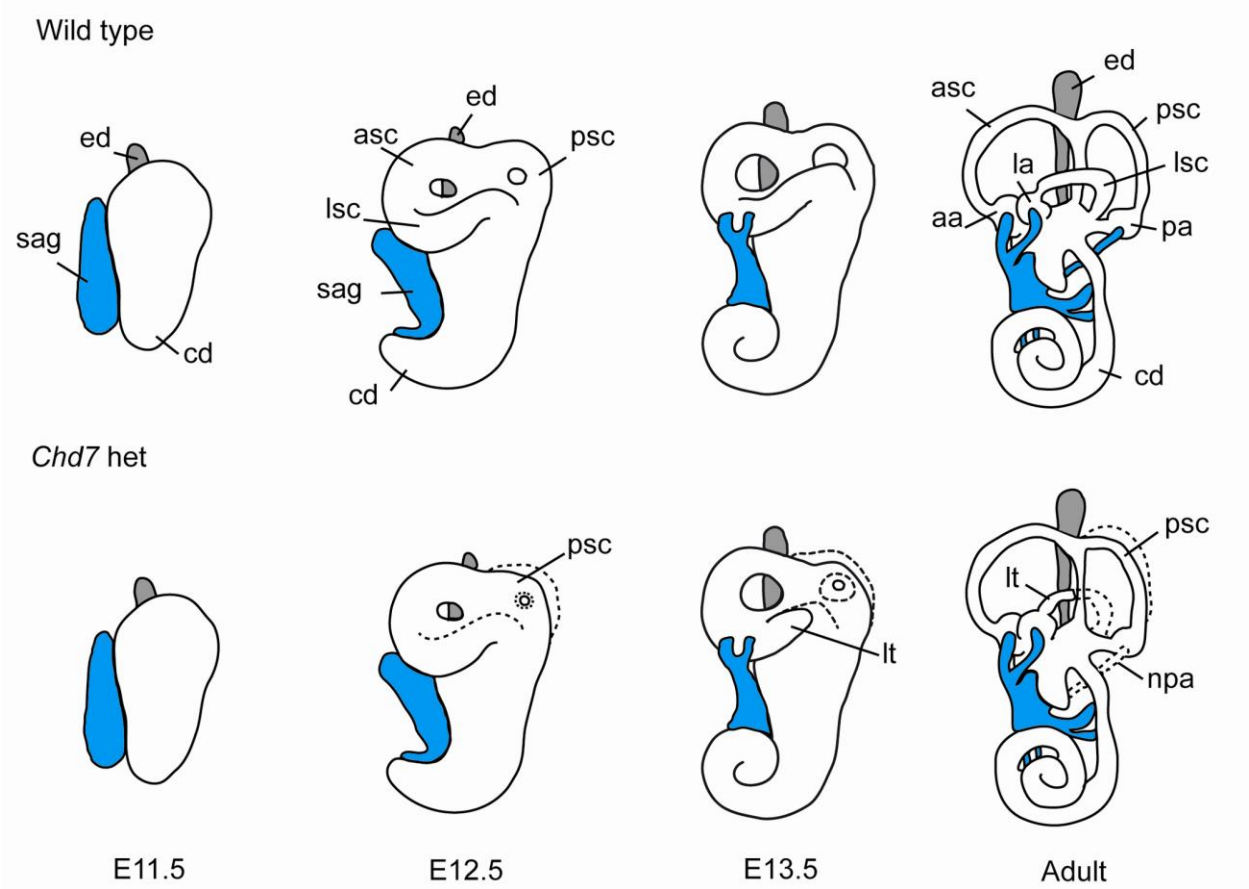

Figure 1.2 Model of inner ear development in wild type and Chd7 heterozygous mutant mice. The E11.5 otocyst extends dorsally to form the endolymphatic duct (ed, grey) and ventrally to form the cochlea (coc), and neuroblasts delaminate from the ventral epithelium to occupy the statoacoustic ganglion (sag, shown in blue). By E12.5, the epithelium of the canal pouches fuses to form the anterior (asc), posterior (psc) and lateral (lsc) semicircular canals. Between E13.5 and adulthood, the vestibular apparatus continues to mature, the cochlea completes its coiling, and the sensory epithelium becomes completely innervated. In *Chd7* heterozygous mutant ears the lateral and posterior semicircular canals are truncated (lt), small, or misshapen. In addition, the nerve to the posterior ampulla (npa) is disrupted. Normal developmental structures are shown by a dashed line in *Chd7* heterozygous mutants.

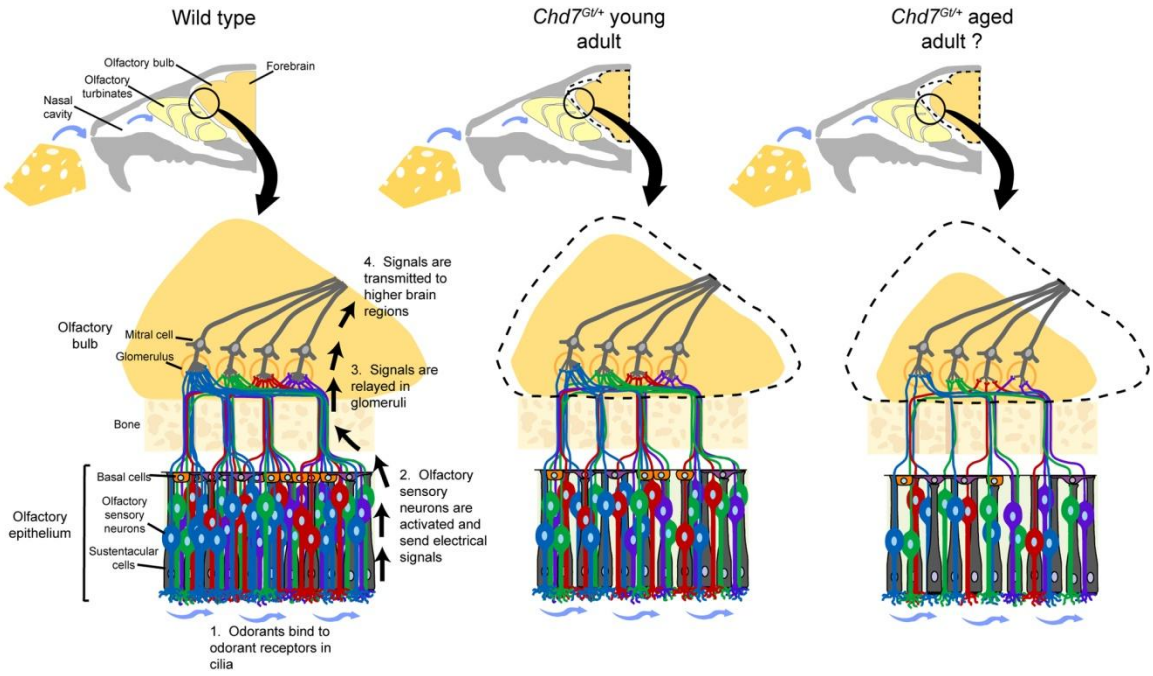

Figure 1.3 Model of olfactory function in wild type and Chd7$^{Gt/+}$ mice. Following inhalation, odorants are detected in the olfactory epithelium by binding to specific odorant receptors located on the surface of olfactory cilia. Bound odorants activate olfactory sensory neurons, which are bipolar neurons that project axons to the glomeruli in the olfactory bulb. Each olfactory sensory neuron (ex. blue, red, green, and purple) contains one type of odorant receptor in the cilia and each neuron with that type of odorant receptor projects an axon to the same glomerulus in the olfactory bulb. Electrical signals sent by olfactory sensory neurons are detected by mitral cell dendrites in the glomeruli. These signals are then sent to higher brain regions in the central nervous system. Wild type mouse olfactory epithelium contains densely packed olfactory sensory neurons which project to the olfactory bulb. However, *Chd7*$^{Gt/+}$ young adult mice have 30% fewer olfactory sensory neurons and olfactory bulb hypoplasia. We hypothesize that aged *Chd7*$^{Gt/+}$ mice have a greater reduction in both olfactory sensory neurons and size of the olfactory bulb.

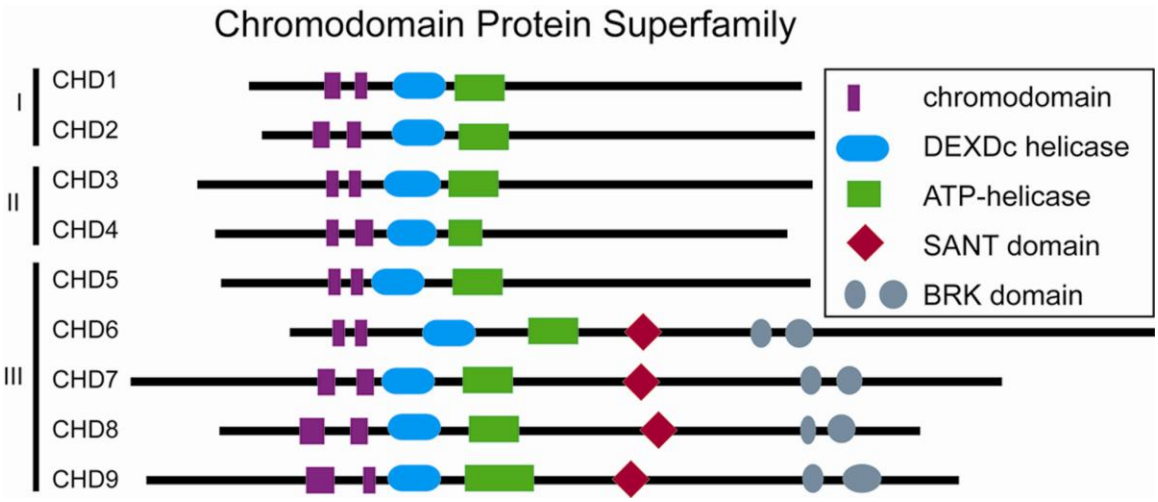

Figure 1.4 The chromodomain family of proteins contains 9 members that are subdivided into 3 classes on the basis of shared protein motifs. CHD7 is a member of the third class together with CHD5, CHD6, CHD8, and CHD9.

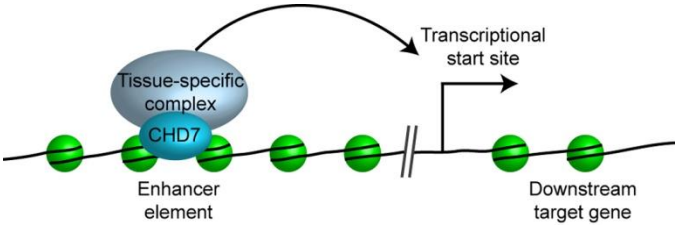

Figure 1.5 Model for CHD7 transcriptional regulation. CHD7 binds to enhancer regions of target genes together with a tissue-specific complex of proteins. The CHD7 tissue-specific complex either activates or represses downstream target gene expression in a developmental stage specific manner.

Gene	Type of protein	Mouse inner ear defects	Human inner ear defects	References
Brn4 (Pou3f4)	Pou-domain transcription factor	ASC abnormalities	X-linked hereditary deafness type 3: Dysplasia of cochlea and semicircular canals and deafness	(69, 70)
Chd7	Chromodomain helicase DNA binding protein	LSC, PSC and associated crista abnormalities	CHARGE Syndrome: Outer and inner ear abnormalities including semicircular canal defects and deafness	(41, 42, 49)
Eya1	Transcription factor	ASC, PSC, LSC and associated crista absent	Branchio-oto-renal syndrome: Outer, Middle and Inner ear abnormalities and deafness	(71, 72)
Fgf3	Fibroblast growth factor	ASC, PSC and LSC abnormalities	Syndromic deafness: Inner ear agenesis and deafness	(73-75)
Fgf10	Fibroblast growth factor	ASC, PSC, LSC and associated crista abnormalities	LADD syndrome: Outer ear abnormalities, Inner ear abnormalities and deafness	(76, 77)
Jag1	Notch receptor ligand	ASC, PSC and LSC abnormalities	Alagille syndrome: Posterior semicircular canal defects	(51, 78)
Six1	Transcription factor	ASC, PSC and LSC absent	Branchio-oto-renal syndrome: Outer, Middle and Inner ear abnormalities and deafness	(79-81)

Table 1.1 Mouse models of human semicircular canal dysgenesis. Abbreviations: ASC, anterior/superior semicircular canal; LSC, lateral semicircular canal; PSC, posterior semicircular canal.

Gene	Type of Protein	Reference(s)
Chd7	Chromodomain helicase DNA binding protein	(39, 60)
Fgf8	Fibroblast growth factor	(57, 82, 83)
Fgfr1	Fibroblast growth factor receptor	(57)
Prok2 (*Pk2*)	Prokineticin	(84, 85)
Prokr2 (*Pkr2*)	Prokineticin receptor	(86)

Table 1.2 Mouse models of human Kallmann syndrome (idiopathic hypogonadotropic hypogonadism and olfactory dysfunction)

References

1 Hall, B.D. (1979) Choanal atresia and associated multiple anomalies. *J Pediatr*, **95**, 395-398.

2 Aramaki, M., Udaka, T., Kosaki, R., Makita, Y., Okamoto, N., Yoshihashi, H., Oki, H., Nanao, K., Moriyama, N., Oku, S. *et al.* (2006) Phenotypic spectrum of CHARGE syndrome with CHD7 mutations. *J Pediatr*, **148**, 410-414.

3 Jongmans, M.C., Admiraal, R.J., van der Donk, K.P., Vissers, L.E., Baas, A.F., Kapusta, L., van Hagen, J.M., Donnai, D., de Ravel, T.J., Veltman, J.A. *et al.* (2006) CHARGE syndrome: the phenotypic spectrum of mutations in the CHD7 gene. *J Med Genet*, **43**, 306-314.

4 Lalani, S.R., Safiullah, A.M., Fernbach, S.D., Harutyunyan, K.G., Thaller, C., Peterson, L.E., McPherson, J.D., Gibbs, R.A., White, L.D., Hefner, M. *et al.* (2006) Spectrum of CHD7 Mutations in 110 Individuals with CHARGE Syndrome and Genotype-Phenotype Correlation. *Am J Hum Genet*, **78**, 303-314.

5 Sanlaville, D., Etchevers, H.C., Gonzales, M., Martinovic, J., Clement-Ziza, M., Delezoide, A.L., Aubry, M.C., Pelet, A., Chemouny, S., Cruaud, C. *et al.* (2006) Phenotypic spectrum of CHARGE syndrome in fetuses with CHD7 truncating mutations correlates with expression during human development. *J Med Genet*, **43**, 211-217.

6 Vissers, L.E., van Ravenswaaij, C.M., Admiraal, R., Hurst, J.A., de Vries, B.B., Janssen, I.M., van der Vliet, W.A., Huys, E.H., de Jong, P.J., Hamel, B.C. *et al.* (2004) Mutations in a new member of the chromodomain gene family cause CHARGE syndrome. *Nat Genet*, **36**, 955-957.

7 Harris, J., Robert, E. and Kallen, B. (1997) Epidemiology of choanal atresia with special reference to the CHARGE association. *Pediatrics*, **99**, 363-367.

8 Issekutz, K.A., Graham, J.M., Jr., Prasad, C., Smith, I.M. and Blake, K.D. (2005) An epidemiological analysis of CHARGE syndrome: preliminary results from a Canadian study. *Am J Med Genet A*, **133**, 309-317.

9 Kallen, K., Robert, E., Mastroiacovo, P., Castilla, E.E. and Kallen, B. (1999) CHARGE Association in newborns: a registry-based study. *Teratology*, **60**, 334-343.

10 Sanlaville, D. and Verloes, A. (2007) CHARGE syndrome: an update. *Eur J Hum Genet*, **15**, 389-399.

11 Vuorela, P., Ala-Mello, S., Saloranta, C., Penttinen, M., Poyhonen, M., Huoponen, K., Borozdin, W., Bausch, B., Botzenhart, E.M., Wilhelm, C. *et al.* (2007) Molecular analysis of the CHD7 gene in CHARGE syndrome: identification of 22 novel mutations and evidence for a low contribution of large CHD7 deletions. *Genet Med*, **9**, 690-694.

12 Delahaye, A., Sznajer, Y., Lyonnet, S., Elmaleh-Berges, M., Delpierre, I., Audollent, S., Wiener-Vacher, S., Mansbach, A.L., Amiel, J., Baumann, C. *et al.* (2007)

Familial CHARGE syndrome because of CHD7 mutation: clinical intra- and interfamilial variability. *Clin Genet*, **72**, 112-121.

13 Jongmans, M.C., Hoefsloot, L.H., van der Donk, K.P., Admiraal, R.J., Magee, A., van de Laar, I., Hendriks, Y., Verheij, J.B., Walpole, I., Brunner, H.G. *et al.* (2008) Familial CHARGE syndrome and the CHD7 gene: a recurrent missense mutation, intrafamilial recurrence and variability. *Am J Med Genet A*, **146**, 43-50.

14 Pauli, S., Pieper, L., Haberle, J., Grzmil, P., Burfeind, P., Steckel, M., Lenz, U. and Michelmann, H.W. (2009) Proven germline mosaicism in a father of two children with CHARGE syndrome. *Clin Genet*, **75**, 473-479.

15 Alazami, A.M., Alzahrani, F. and Alkuraya, F.S. (2008) Expanding the "E" in CHARGE. *Am J Med Genet A*, **146A**, 1890-1892.

16 Asakura, Y., Toyota, Y., Muroya, K., Kurosawa, K., Fujita, K., Aida, N., Kawame, H., Kosaki, K. and Adachi, M. (2008) Endocrine and radiological studies in patients with molecularly confirmed CHARGE syndrome. *J Clin Endocrinol Metab*, **93**, 920-924.

17 Bergman, J.E., de Wijs, I., Jongmans, M.C., Admiraal, R.J., Hoefsloot, L.H. and van Ravenswaaij-Arts, C.M. (2008) Exon copy number alterations of the CHD7 gene are not a major cause of CHARGE and CHARGE-like syndrome. *Eur J Med Genet*, **51**, 417-425.

18 Chopra, C., Baretto, R., Duddridge, M. and Browning, M.J. (2009) T-cell immunodeficiency in CHARGE syndrome. *Acta Paediatr*, **98**, 408-410.

19 Felix, T.M., Hanshaw, B.C., Mueller, R., Bitoun, P. and Murray, J.C. (2006) CHD7 gene and non-syndromic cleft lip and palate. *Am J Med Genet A*, **140**, 2110-2114.

20 Fujita, K., Aida, N., Asakura, Y., Kurosawa, K., Niwa, T., Muroya, K., Adachi, M., Nishimura, G. and Inoue, T. (2009) Abnormal basiocciput development in CHARGE syndrome. *AJNR Am J Neuroradiol*, **30**, 629-634.

21 Gennery, A.R., Slatter, M.A., Rice, J., Hoefsloot, L.H., Barge, D., McLean-Tooke, A., Montgomery, T., Goodship, J.A., Burt, A.D., Flood, T.J. *et al.* (2008) Mutations in CHD7 in patients with CHARGE syndrome cause T-B + natural killer cell + severe combined immune deficiency and may cause Omenn-like syndrome. *Clin Exp Immunol*, **153**, 75-80.

22 Hoover-Fong, J., Savage, W.J., Lisi, E., Winkelstein, J., Thomas, G.H., Hoefsloot, L.H. and Loeb, D.M. (2009) Congenital T cell deficiency in a patient with CHARGE syndrome. *J Pediatr*, **154**, 140-142.

23 Johnson, D., Morrison, N., Grant, L., Turner, T., Fantes, J., Connor, J.M. and Murday, V. (2006) Confirmation of CHD7 as a cause of CHARGE association identified by mapping a balanced chromosome translocation in affected monozygotic twins. *J Med Genet*, **43**, 280-284.

24 Jongmans, M.C., van Ravenswaaij-Arts, C.M., Pitteloud, N., Ogata, T., Sato, N., Claahsen-van der Grinten, H.L., van der Donk, K., Seminara, S., Bergman, J.E., Brunner, H.G. *et al.* (2009) CHD7 mutations in patients initially diagnosed with Kallmann syndrome--the clinical overlap with CHARGE syndrome. *Clin Genet*, **75**, 65-71.

25 Jyonouchi, S., McDonald-McGinn, D.M., Bale, S., Zackai, E.H. and Sullivan, K.E. (2009) CHARGE (coloboma, heart defect, atresia choanae, retarded growth and development, genital hypoplasia, ear anomalies/deafness) syndrome and chromosome 22q11.2 deletion syndrome: a comparison of immunologic and nonimmunologic phenotypic features. *Pediatrics*, **123**, e871-877.

26 Kim, H.G., Kurth, I., Lan, F., Meliciani, I., Wenzel, W., Eom, S.H., Kang, G.B., Rosenberger, G., Tekin, M., Ozata, M. *et al.* (2008) Mutations in CHD7, encoding a chromatin-remodeling protein, cause idiopathic hypogonadotropic hypogonadism and Kallmann syndrome. *Am J Hum Genet*, **83**, 511-519.

27 Lee, Y.W., Kim, S.C., Shin, Y.L., Kim, J.W., Hong, H.S., Lee, Y.K. and Ki, C.S. (2009) Clinical and genetic analysis of the CHD7 gene in Korean patients with CHARGE syndrome. *Clin Genet*, **75**, 290-293.

28 Ogata, T., Fujiwara, I., Ogawa, E., Sato, N., Udaka, T. and Kosaki, K. (2006) Kallmann syndrome phenotype in a female patient with CHARGE syndrome and CHD7 mutation. *Endocr J*, **53**, 741-743.

29 Sanka, M., Tangsinmankong, N., Loscalzo, M., Sleasman, J.W. and Dorsey, M.J. (2007) Complete DiGeorge syndrome associated with CHD7 mutation. *J Allergy Clin Immunol*, **120**, 952-954.

30 Udaka, T., Okamoto, N., Aramaki, M., Torii, C., Kosaki, R., Hosokai, N., Hayakawa, T., Takahata, N., Takahashi, T. and Kosaki, K. (2007) An Alu retrotransposition-mediated deletion of CHD7 in a patient with CHARGE syndrome. *Am J Med Genet A*, **143**, 721-726.

31 Van de Laar, I., Dooijes, D., Hoefsloot, L., Simon, M., Hoogeboom, J. and Devriendt, K. (2007) Limb anomalies in patients with CHARGE syndrome: an expansion of the phenotype. *Am J Med Genet A*, **143A**, 2712-2715.

32 Wincent, J., Holmberg, E., Stromland, K., Soller, M., Mirzaei, L., Djureinovic, T., Robinson, K., Anderlid, B. and Schoumans, J. (2008) CHD7 mutation spectrum in 28 Swedish patients diagnosed with CHARGE syndrome. *Clin Genet*, **74**, 31-38.

33 Wright, E.M., O'Connor, R. and Kerr, B.A. (2009) Radial aplasia in CHARGE syndrome: a new association. *Eur J Med Genet*, **52**, 239-241.

34 Writzl, K., Cale, C.M., Pierce, C.M., Wilson, L.C. and Hennekam, R.C. (2007) Immunological abnormalities in CHARGE syndrome. *Eur J Med Genet*, **50**, 338-345.

35 Zentner, G.E., Layman, W.S., Martin, D.M. and Scacheri, P.C. (2010) Molecular and phenotypic aspects of CHD7 mutation in CHARGE syndrome. *Am J Med Genet A*, **152A**, 674-686.

36 Azoulay, R., Fallet-Bianco, C., Garel, C., Grabar, S., Kalifa, G. and Adamsbaum, C. (2006) MRI of the olfactory bulbs and sulci in human fetuses. *Pediatr Radiol*, **36**, 97-107.

37 Blustajn, J., Kirsch, C.F., Panigrahy, A. and Netchine, I. (2008) Olfactory anomalies in CHARGE syndrome: imaging findings of a potential major diagnostic criterion. *AJNR Am J Neuroradiol*, **29**, 1266-1269.

38 Chalouhi, C., Faulcon, P., Le Bihan, C., Hertz-Pannier, L., Bonfils, P. and Abadie, V. (2005) Olfactory evaluation in children: application to the CHARGE syndrome. *Pediatrics*, **116**, e81-88.

39 Layman, W.S., McEwen, D.P., Beyer, L.A., Lalani, S.R., Fernbach, S.D., Oh, E., Swaroop, A., Hegg, C.C., Raphael, Y., Martens, J.R. *et al.* (2009) Defects in neural stem cell proliferation and olfaction in Chd7 deficient mice indicate a mechanism for hyposmia in human CHARGE syndrome. *Hum Mol Genet*, **18**, 1909-1923.

40 Pinto, G., Abadie, V., Mesnage, R., Blustajn, J., Cabrol, S., Amiel, J., Hertz-Pannier, L., Bertrand, A.M., Lyonnet, S., Rappaport, R. *et al.* (2005) CHARGE syndrome includes hypogonadotropic hypogonadism and abnormal olfactory bulb development. *J Clin Endocrinol Metab*, **90**, 5621-5626.

41 Bosman, E.A., Penn, A.C., Ambrose, J.C., Kettleborough, R., Stemple, D.L. and Steel, K.P. (2005) Multiple mutations in mouse Chd7 provide models for CHARGE syndrome. *Hum Mol Genet*, **14**, 3463-3476.

42 Hurd, E.A., Capers, P.L., Blauwkamp, M.N., Adams, M.E., Raphael, Y., Poucher, H.K. and Martin, D.M. (2007) Loss of Chd7 function in gene-trapped reporter mice is embryonic lethal and associated with severe defects in multiple developing tissues. *Mamm Genome*, **18**, 94-104.

43 Glueckert, R., Rask-Andersen, H., Sergi, C., Schmutzhard, J., Mueller, B., Beckmann, F., Rittinger, O., Hoefsloot, L.H., Schrott-Fischer, A. and Janecke, A.R. (2010) Histology and synchrotron radiation-based microtomography of the inner ear in a molecularly confirmed case of CHARGE syndrome. *Am J Med Genet A*, **152A**, 665-673.

44 Morimoto, A.K., Wiggins, R.H., 3rd, Hudgins, P.A., Hedlund, G.L., Hamilton, B., Mukherji, S.K., Telian, S.A. and Harnsberger, H.R. (2006) Absent semicircular canals in CHARGE syndrome: radiologic spectrum of findings. *AJNR Am J Neuroradiol*, **27**, 1663-1671.

45 Satar, B., Mukherji, S.K. and Telian, S.A. (2003) Congenital aplasia of the semicircular canals. *Otol Neurotol*, **24**, 437-446.

46 Arndt, S., Laszig, R., Beck, R., Schild, C., Maier, W., Birkenhager, R., Kroeger, S., Wesarg, T. and Aschendorff, A. (2010) Spectrum of hearing disorders and their management in children with CHARGE syndrome. *Otol Neurotol*, **31**, 67-73.

47 Abadie, V., Wiener-Vacher, S., Morisseau-Durand, M.P., Poree, C., Amiel, J., Amanou, L., Peigne, C., Lyonnet, S. and Manac'h, Y. (2000) Vestibular anomalies in

CHARGE syndrome: investigations on and consequences for postural development. *Eur J Pediatr*, **159**, 569-574.

48 Wiener-Vacher, S.R., Amanou, L., Denise, P., Narcy, P. and Manach, Y. (1999) Vestibular function in children with the CHARGE association. *Arch Otolaryngol Head Neck Surg*, **125**, 342-347.

49 Adams, M.E., Hurd, E.A., Beyer, L.A., Swiderski, D.L., Raphael, Y. and Martin, D.M. (2007) Defects in vestibular sensory epithelia and innervation in mice with loss of Chd7 function: Implications for human CHARGE syndrome. *J Comp Neurol*, **504**, 519-532.

50 Hawker, K., Fuchs, H., Angelis, M.H. and Steel, K.P. (2005) Two new mouse mutants with vestibular defects that map to the highly mutable locus on chromosome 4. *Int J Audiol*, **44**, 171-177.

51 Kiernan, A.E., Erven, A., Voegeling, S., Peters, J., Nolan, P., Hunter, J., Bacon, Y., Steel, K.P., Brown, S.D. and Guenet, J.L. (2002) ENU mutagenesis reveals a highly mutable locus on mouse Chromosome 4 that affects ear morphogenesis. *Mamm Genome*, **13**, 142-148.

52 Pau, H., Hawker, K., Fuchs, H., De Angelis, M.H. and Steel, K.P. (2004) Characterization of a new mouse mutant, flouncer, with a balance defect and inner ear malformation. *Otol Neurotol*, **25**, 707-713.

53 Martin, P. and Swanson, G.J. (1993) Descriptive and experimental analysis of the epithelial remodellings that control semicircular canal formation in the developing mouse inner ear. *Dev Biol*, **159**, 549-558.

54 Salminen, M., Meyer, B.I., Bober, E. and Gruss, P. (2000) Netrin 1 is required for semicircular canal formation in the mouse inner ear. *Development*, **127**, 13-22.

55 Bhagavath, B., Podolsky, R.H., Ozata, M., Bolu, E., Bick, D.P., Kulharya, A., Sherins, R.J. and Layman, L.C. (2006) Clinical and molecular characterization of a large sample of patients with hypogonadotropic hypogonadism. *Fertil Steril*, **85**, 706-713.

56 Kim, H.G., Bhagavath, B. and Layman, L.C. (2008) Clinical manifestations of impaired GnRH neuron development and function. *Neurosignals*, **16**, 165-182.

57 Chung, W.C., Moyle, S.S. and Tsai, P.S. (2008) Fibroblast growth factor 8 signaling through fibroblast growth factor receptor 1 is required for the emergence of gonadotropin-releasing hormone neurons. *Endocrinology*, **149**, 4997-5003.

58 Falardeau, J., Chung, W.C., Beenken, A., Raivio, T., Plummer, L., Sidis, Y., Jacobson-Dickman, E.E., Eliseenkova, A.V., Ma, J., Dwyer, A. *et al.* (2008) Decreased FGF8 signaling causes deficiency of gonadotropin-releasing hormone in humans and mice. *J Clin Invest*, **118**, 2822-2831.

59 Hardelin, J.P. and Dode, C. (2008) The complex genetics of Kallmann syndrome: KAL1, FGFR1, FGF8, PROKR2, PROK2, et al. *Sex Dev*, **2**, 181-193.

60 Bergman, J.E., Bosman, E.A., van Ravenswaaij-Arts, C.M. and Steel, K.P. (2009) Study of smell and reproductive organs in a mouse model for CHARGE syndrome. *Eur J Hum Genet*.

61 Ho, L. and Crabtree, G.R. (2010) Chromatin remodelling during development. *Nature*, **463**, 474-484.

62 Hall, J.A. and Georgel, P.T. (2007) CHD proteins: a diverse family with strong ties. *Biochem Cell Biol*, **85**, 463-476.

63 Marfella, C.G. and Imbalzano, A.N. (2007) The Chd family of chromatin remodelers. *Mutat Res*, **618**, 30-40.

64 Boyer, L.A., Latek, R.R. and Peterson, C.L. (2004) The SANT domain: a unique histone-tail-binding module? *Nat Rev Mol Cell Biol*, **5**, 158-163.

65 Schnetz, M.P., Bartels, C.F., Shastri, K., Balasubramanian, D., Zentner, G.E., Balaji, R., Zhang, X., Song, L., Wang, Z., Laframboise, T. *et al.* (2009) Genomic distribution of CHD7 on chromatin tracks H3K4 methylation patterns. *Genome Res*.

66 Bajpai, R., Chen, D.A., Rada-Iglesias, A., Zhang, J., Xiong, Y., Helms, J., Chang, C.P., Zhao, Y., Swigut, T. and Wysocka, J. (2010) CHD7 cooperates with PBAF to control multipotent neural crest formation. *Nature*, **463**, 958-962.

67 Takada, I., Mihara, M., Suzawa, M., Ohtake, F., Kobayashi, S., Igarashi, M., Youn, M.Y., Takeyama, K., Nakamura, T., Mezaki, Y. *et al.* (2007) A histone lysine

methyltransferase activated by non-canonical Wnt signalling suppresses PPAR-gamma transactivation. *Nat Cell Biol*, **9**, 1273-1285.

68 Srinivasan, S., Dorighi, K.M. and Tamkun, J.W. (2008) Drosophila Kismet regulates histone H3 lysine 27 methylation and early elongation by RNA polymerase II. *PLoS Genet*, **4**, e1000217.

69 Phippard, D., Lu, L., Lee, D., Saunders, J.C. and Crenshaw, E.B., 3rd (1999) Targeted mutagenesis of the POU-domain gene Brn4/Pou3f4 causes developmental defects in the inner ear. *J Neurosci*, **19**, 5980-5989.

70 Vore, A.P., Chang, E.H., Hoppe, J.E., Butler, M.G., Forrester, S., Schneider, M.C., Smith, L.L., Burke, D.W., Campbell, C.A. and Smith, R.J. (2005) Deletion of and novel missense mutation in POU3F4 in 2 families segregating X-linked nonsyndromic deafness. *Arch Otolaryngol Head Neck Surg*, **131**, 1057-1063.

71 Abdelhak, S., Kalatzis, V., Heilig, R., Compain, S., Samson, D., Vincent, C., Weil, D., Cruaud, C., Sahly, I., Leibovici, M. *et al.* (1997) A human homologue of the Drosophila eyes absent gene underlies branchio-oto-renal (BOR) syndrome and identifies a novel gene family. *Nat Genet*, **15**, 157-164.

72 Xu, P.X., Adams, J., Peters, H., Brown, M.C., Heaney, S. and Maas, R. (1999) Eya1-deficient mice lack ears and kidneys and show abnormal apoptosis of organ primordia. *Nat Genet*, **23**, 113-117.

73 Hatch, E.P., Noyes, C.A., Wang, X., Wright, T.J. and Mansour, S.L. (2007) Fgf3 is required for dorsal patterning and morphogenesis of the inner ear epithelium. *Development*, **134**, 3615-3625.

74 Mansour, S.L. (1994) Targeted disruption of int-2 (fgf-3) causes developmental defects in the tail and inner ear. *Mol Reprod Dev*, **39**, 62-67; discussion 67-68.

75 Tekin, M., Hismi, B.O., Fitoz, S., Ozdag, H., Cengiz, F.B., Sirmaci, A., Aslan, I., Inceoglu, B., Yuksel-Konuk, E.B., Yilmaz, S.T. *et al.* (2007) Homozygous mutations in fibroblast growth factor 3 are associated with a new form of syndromic deafness characterized by inner ear agenesis, microtia, and microdontia. *Am J Hum Genet*, **80**, 338-344.

76 Milunsky, J.M., Zhao, G., Maher, T.A., Colby, R. and Everman, D.B. (2006) LADD syndrome is caused by FGF10 mutations. *Clin Genet*, **69**, 349-354.

77 Pauley, S., Wright, T.J., Pirvola, U., Ornitz, D., Beisel, K. and Fritzsch, B. (2003) Expression and function of FGF10 in mammalian inner ear development. *Dev Dyn*, **227**, 203-215.

78 Koch, B., Goold, A., Egelhoff, J. and Benton, C. (2006) Partial absence of the posterior semicircular canal in Alagille syndrome: CT findings. *Pediatr Radiol*, **36**, 977-979.

79 Laclef, C., Souil, E., Demignon, J. and Maire, P. (2003) Thymus, kidney and craniofacial abnormalities in Six 1 deficient mice. *Mech Dev*, **120**, 669-679.

80 Ruf, R.G., Xu, P.X., Silvius, D., Otto, E.A., Beekmann, F., Muerb, U.T., Kumar, S., Neuhaus, T.J., Kemper, M.J., Raymond, R.M., Jr. *et al.* (2004) SIX1 mutations cause branchio-oto-renal syndrome by disruption of EYA1-SIX1-DNA complexes. *Proc Natl Acad Sci U S A*, **101**, 8090-8095.

81 Zheng, W., Huang, L., Wei, Z.B., Silvius, D., Tang, B. and Xu, P.X. (2003) The role of Six1 in mammalian auditory system development. *Development*, **130**, 3989-4000.

82 Kawauchi, S., Shou, J., Santos, R., Hebert, J.M., McConnell, S.K., Mason, I. and Calof, A.L. (2005) Fgf8 expression defines a morphogenetic center required for olfactory neurogenesis and nasal cavity development in the mouse. *Development*, **132**, 5211-5223.

83 Meyers, E.N., Lewandoski, M. and Martin, G.R. (1998) An Fgf8 mutant allelic series generated by Cre- and Flp-mediated recombination. *Nat Genet*, **18**, 136-141.

84 Ng, K.L., Li, J.D., Cheng, M.Y., Leslie, F.M., Lee, A.G. and Zhou, Q.Y. (2005) Dependence of olfactory bulb neurogenesis on prokineticin 2 signaling. *Science*, **308**, 1923-1927.

85 Zhang, C., Ng, K.L., Li, J.D., He, F., Anderson, D.J., Sun, Y.E. and Zhou, Q.Y. (2007) Prokineticin 2 is a target gene of proneural basic helix-loop-helix factors for olfactory bulb neurogenesis. *J Biol Chem*, **282**, 6917-6921.

86 Matsumoto, S., Yamazaki, C., Masumoto, K.H., Nagano, M., Naito, M., Soga, T., Hiyama, H., Matsumoto, M., Takasaki, J., Kamohara, M. *et al.* (2006) Abnormal

development of the olfactory bulb and reproductive system in mice lacking prokineticin receptor PKR2. *Proc Natl Acad Sci U S A*, **103**, 4140-4145.

Chapter 2

Defects in neural stem cell proliferation and olfaction in *Chd7* deficient mice indicate a mechanism for hyposmia in human CHARGE syndrome[1]

Abstract

Mutations in *CHD7,* a chromodomain gene, are present in a majority of individuals with CHARGE syndrome, a multiple anomaly disorder characterized by ocular coloboma, heart defects, atresia of the choanae, retarded growth and development, genital hypoplasia, and ear anomalies. The clinical features of CHARGE syndrome are highly variable and incompletely penetrant. Olfactory dysfunction is a common feature in CHARGE syndrome and has been potentially linked to primary olfactory bulb defects, but no data confirming this mechanistic link have been reported. Based on these observations, we hypothesized that loss of *Chd7* disrupts mammalian olfactory tissue development and function. We found severe defects in olfaction in individuals with *CHD7* mutations and CHARGE, and loss of odor evoked electro-olfactogram responses in *Chd7* deficient mice, suggesting reduced olfaction is due to a dysfunctional olfactory epithelium. *Chd7* expression was high in basal olfactory epithelial neural stem cells and down-regulated in mature olfactory sensory neurons. We observed smaller olfactory bulbs reduced olfactory sensory neurons, and disorganized epithelial ultrastructure in

Chd7 mutant mice, despite apparently normal functional cilia and sustentacular cells. Significant reductions in proliferation of neural stem cells and regeneration of olfactory sensory neurons in the mature *Chd7*$^{Gt/+}$ olfactory epithelium indicate critical roles for *Chd7* in regulating neurogenesis. These studies provide evidence that mammalian olfactory dysfunction due to *Chd7* haploinsufficiency is linked to primary defects in olfactory neural stem cell proliferation, and may influence olfactory bulb development.

Introduction

CHD7 haploinsufficiency in humans causes CHARGE syndrome, a clinically variable, multiple anomaly condition with an estimated incidence of 1:8500-1:12,000 (1-3). CHARGE is characterized by ocular coloboma, heart defects, atresia of the choanae, retarded growth and development, genital hypoplasia, and ear abnormalities including deafness and vestibular disorders (4). CHARGE individuals also have variably penetrant craniofacial abnormalities, hypogonadotropic hypogonadism, and olfactory dysfunction (4-11). Heterozygosity for nonsense, deletion, or missense *CHD7* mutations is estimated to occur in 60-80% of patients with CHARGE syndrome; these mutations are distributed throughout the coding sequence and do not appear to be correlated with specific aspects of the clinical phenotype (5-11). Most human *CHD7* mutations identified thus far are *de novo*; however, evidence for germline mosaicism has been suggested for families with multiple affected siblings (6, 12-14). Magnetic resonance imaging shows olfactory bulb defects ranging from hypoplasia to complete absence in all CHARGE individuals tested, and olfactory dysfunction in a majority of patients (15-20).

Chd7 is widely expressed during murine and human embryonic development, and in many neural tissues including forebrain, midbrain, hindbrain, optic nerve, retina, trigeminal ganglion, facial ganglion, glossopharyngeal ganglion, dorsal root ganglion, and enteric neurons (8, 21, 22). *Chd7* is also expressed in developing human and mouse olfactory bulb and olfactory epithelium (8, 21, 22), suggesting a role for CHD7 in olfaction. The olfactory system provides a unique model in which to analyze the role of CHD7 in neuronal development, due to the rapid turnover of the olfactory epithelium with continuous neurogenesis of olfactory sensory neurons during development and into adulthood. A better understanding of the mechanisms underlying olfaction and neuronal regeneration in adult tissues could give insights into therapies directed toward neural regeneration, and elucidate the role of CHD7 in olfactory development and maintenance.

CHD7 is one of nine members of a family of chromatin remodeling proteins that are characterized by the presence of two chromodomains, a centrally located helicase domain, and less well defined carboxyl terminal domains (23, 24). These nine CHD proteins are subdivided into three classes based upon their amino acid sequence and functional protein domains (25-29). CHD proteins use ATP hydrolysis to regulate access to DNA by altering nucleosome structure (25-29). There is also evidence that CHD7 may regulate transcription elongation. The *CHD7 Drosophila* orthologue *Kismet* down regulates transcriptional elongation by RNA polymerase II through recruitment of ASH1 and TRX and may be involved in maintenance of stem cell pluripotency by regulating methylation of histone H3 lysine 27 (30). CHD7 is also implicated in cell fate specification of mesenchymal stem cells (31). During osteoblast and adipocyte differentiation, CHD7 forms a complex with NLK, SETDB1, and PPAR-γ, then binds to

methylated lysine 4 and lysine 9 residues on histone H3 at PPAR-γ target promoters and suppresses ligand-induced transactivation of PPAR-γ target genes which leads to a change in cell fate (31). Together, these data suggest that CHD7 regulates gene transcription with effects on stem cell differentiation.

Here, we show that CHARGE individuals with mutations in *CHD7* have variably impaired olfaction, and *Chd7* deficient mice also have severely impaired olfaction with hypoplastic olfactory bulbs. We found high *Chd7* expression in adult mouse olfactory epithelial stem cells including proliferating basal cells and pro-neuronal basal cells, but no detectable *Chd7* expression in the adult olfactory bulb. *Chd7* deficient mice have a significant decrease in olfactory neural stem cell proliferation, leading to a reduction in olfactory sensory neurons. These data help to clarify the structural impact of *Chd7* deficiency on olfactory neuronal production and regeneration, and implicate a role for CHD7 in neural stem cell differentiation.

Results

Olfaction is reduced in human CHARGE patients and in mice with *Chd7* deficiency

Olfactory defects and olfactory bulb hypoplasia have previously been reported in CHARGE individuals (15-20, 32). However, there is minimal information about olfactory status in individuals with CHARGE phenotypes and documented *CHD7* mutations. We analyzed eight individuals with CHARGE (and confirmed mutations in *CHD7)* (7) for defects in olfaction, using The Brief Smell Identification Test (B-SIT) (Table 2.1). B-SIT is a self-administered, scratch and sniff test booklet that measures whether an individual can accurately identify 12 different odorants. It is important to

note that random guessing would result in a score of 3. We found that 6 of 8 individuals with CHARGE aged 10 years or older had B-SIT scores of 8 or lower, whereas a score of 9-12 is considered to reflect normal olfactory function. The 8 scores from individuals with CHARGE ranged from 0 to 11, and included misidentification of all odorants represented in the test. Interestingly, individuals 6, 7, and 8 all did well on the B-SIT test, with scores of 8 or higher. These individuals all have mutations in exon 33 (individuals 6 and 7 have missense mutations, whereas individual 8 has a nonsense truncating mutation). Exon 33 is a 3' exon that does not encode any of the well characterized protein domains in CHD7 (chromodomain, helicase, SNF2, BRK, or SANT). Further analyses are needed to determine whether olfactory ability correlates with specific *CHD7* genotypes, and whether certain CHD7 protein domains are more important than others for olfactory function.

Based on the high prevalence of olfactory defects in individuals with CHARGE, we hypothesized that similar defects might be present in *Chd7* deficient mice. To test this hypothesis, we used $Chd7^{Gt/+}$ mice which are heterozygous for a gene trapped *lacZ* allele (22). Homozygous $Chd7^{Gt/Gt}$ mice are embryonic lethal after E10.5, presumably from cardiac or other internal organ defects (21, 22). To test for olfactory function in $Chd7^{Gt/+}$ mice, we analyzed six-week old wild type (N = 8) and $Chd7^{Gt/+}$ (N = 7) sex-matched littermate mice by electro-olfactogram (Figure 2.1). Mice were tested with amyl acetate at four different concentrations (Figure 2.1A), as well as five additional odorants (octanal, haptaldehyde, hexanal, eugenol, carvone) at 10^{-3}M (Figure 2.1B). $Chd7^{Gt/+}$ mice had little to no response to any odorant at the concentrations tested by electro-olfactogram (Figure 2.1). These data provide definitive evidence that $Chd7^{Gt/+}$ mice have

severely impaired olfactory function compared to wild type littermates, for all odorants tested and they demonstrate for the first time that this impairment occurs at the level of the olfactory epithelium.

Chd7 is expressed in developing and mature olfactory epithelium

Chd7 mRNA is expressed in developing mouse olfactory tissues (21, 22). To localize CHD7 protein in the olfactory system, we used two independent approaches. We used $Chd7^{Gt/+}$ mice that express β-galactosidase from the *Chd7* locus (22), and compared β-galactosidase expression with immunofluorescence for CHD7 using anti-CHD7 antibody (Figure 2.2). We detected high β-galactosidase activity (Figure 2.2A, B) and anti-CHD7 immunofluorescence (Figure 2.2C-F) in the developing olfactory epithelium and olfactory bulb. There was a slight reduction in anti-CHD7 immunofluorescence in the olfactory epithelium of $Chd7^{Gt/+}$ embryos compared to wild type littermates (Figure 2.2C, D), consistent with *Chd7* haploinsufficiency at the $Chd7^{Gt}$ allele.

To test whether *Chd7* expression continues into adulthood in mouse olfactory tissues, we performed antibody staining with anti-CHD7 on the 6 week-old adult mouse olfactory epithelium and olfactory bulb. We found that *Chd7* is expressed in the mature olfactory epithelium (Figure 2.2G-L) and is significantly down-regulated in the adult olfactory bulb (data not shown). We observed some regional differences in the distribution of CHD7-positive cells in both the wild type and $Chd7^{Gt/+}$ olfactory epithelium (Figure 2.2G, H). In wild type mice, a majority of the olfactory epithelium contained CHD7-positive cells in the basal portion of the epithelium with a small proportion of CHD7-positive cells residing in the apical portion. $Chd7^{Gt/+}$ mice appeared

to have fewer CHD7-positive cells in the olfactory epithelium, most of which resided in the basal portion of the epithelium (Figure 2.2G, H). Olfactory epithelial crypts (recessed regions) in both wild type and *Chd7*$^{Gt/+}$ mice had CHD7-positive cell nuclei occupying the basal, medial, and apical portions of the epithelium (Figure 2.2K, L). These data indicate that *Chd7* expression is regionally distributed throughout the adult olfactory epithelium of both wild type and *Chd7*$^{Gt/+}$ mice.

Chd7 is expressed in olfactory neural stem cells

The olfactory epithelium contains a variety of well defined, functionally, and structurally distinct cell types (33). In order to identify CHD7-positive cell types within the adult olfactory epithelium, we used immunofluorescence with anti-CHD7 and cell type specific antibodies. Olfactory marker protein (OMP) labels mature olfactory sensory neurons in the postnatal olfactory epithelium (33, 34). We found that most CHD7-positive cells in the olfactory epithelium were OMP-negative in both wild type and *Chd7*$^{Gt/+}$ mice (Figure 2.3A, B). However, the distribution and intensity of OMP immunofluorescence in *Chd7*$^{Gt/+}$ olfactory epithelium was altered compared to wild type littermates (Figure 2.3B). There was 16% less anti-OMP immunofluorescence of mature olfactory sensory neurons measured by ImageJ software in the *Chd7*$^{Gt/+}$ olfactory epithelium, and this OMP label appeared disorganized compared to wild type (Figure 2.3B). These data are consistent with an abnormality in olfactory sensory neurons in *Chd7*$^{Gt/+}$ mice.

Since a majority of CHD7-positive cells are located in the basal portion of the epithelium (Figure 2.2I, J), it was important to distinguish which population of basal cells

was CHD7-positive. To characterize the CHD7-positive basal cells in the mature olfactory epithelium, we used antibodies against Mash-1 and NeuroD, markers of early (Mash1) and late (NeuroD) pro-neuronal basal stem cells. Mash1 is a basic helix-loop-helix (bHLH) transcription factor thought to be a pro-neuronal determination gene that initiates neuronal differentiation (33). NeuroD is a bHLH transcription factor whose expression is thought to drive cell cycle exit and determination of neuronal cell fate (33). We detected co-localization of CHD7 with Mash1 (Figure 2.3C, D) and NeuroD (Figure 2.3E, F) in basal cells of wild type and *Chd7*$^{Gt/+}$ olfactory epithelium. These observations provide evidence that *Chd7* is expressed in pro-neuronal basal cells of the adult olfactory epithelium, in both wild type and *Chd7*$^{Gt/+}$ mice.

Sustentacular cells and microvillar cells are the two known cell types located in the apical portion of the olfactory epithelium. Sustentacular cells comprise the majority of apical cells and are thought to represent a glial-like population of cells. To test whether CHD7-positive cells in the apical portion of the epithelium represented sustentacular cells, we used an antibody against receptor expression-enhancing protein 6 (Reep6) (35). We found colocalization between CHD7 and REEP6 in both wild type and *Chd7*$^{Gt/+}$ olfactory epithelium (Figure 2.3G, H). We also found colocalization of CHD7 and Sus1, another marker of sustentacular cells (Figure 2.3I, J). In addition, anti-Sus1 appeared to label a subset of microvillar cells, based upon cellular morphology. CHD7 colocalized with Sus1 in some of these microvillar appearing cells (arrow, Figure 2.3I). These data indicate that *Chd7* is expressed in sustentacular cells and perhaps also in some microvillar cells of the olfactory epithelium.

Olfactory bulb neuronal defects in *Chd7*$^{Gt/+}$ mice

Clinical data in humans with CHARGE have suggested a high prevalence of olfactory bulb defects, ranging from complete absence of the bulbs to mild hypoplasia or asymmetry (15-20). We found statistically significant differences in brain, telencephalon, and olfactory bulb length between adult wild type and *Chd7*$^{Gt/+}$ mutant mice (Figure 2.4A, B, I, J). There were no differences in olfactory bulb width (Figure 2.4A, B, I, J) or morphology, based on H&E staining of wild type and *Chd7*$^{Gt/+}$ mutant mice (Figure 2.4C, D, I). Olfactory bulb hypoplasia in *Chd7*$^{Gt/+}$ mice is consistent with olfactory bulb defects found in CHARGE individuals. However, *Chd7*$^{Gt/+}$ mice may also have a subtle abnormality in olfactory bulb neuronal architecture or function. To test this, we used anti-OMP which marks olfactory sensory neuron projections in the olfactory bulb glomeruli. We found intact OMP-positive glomeruli in both wild type and *Chd7*$^{Gt/+}$ olfactory bulb (Figure 2.4E, F), arguing against a major defect in olfactory sensory neuronal architecture. To further analyze olfactory sensory neuron activity, we labeled dopaminergic interneurons which surround the glomeruli with anti-tyrosine hydroxylase. Tyrosine hydroxylase is expressed in these interneurons in response to signal transduction from the olfactory sensory neurons (36). We found a significant reduction in tyrosine hydroxylase label around the glomeruli in the *Chd7*$^{Gt/+}$ olfactory bulb (Figure 2.4G, H). These data demonstrate that while *Chd7*$^{Gt/+}$ olfactory sensory neurons appear to project normally to the olfactory bulb, olfactory bulb interneuron activity is reduced.

Analysis of cell type specific functions in *Chd7*$^{Gt/+}$ olfactory epithelium

The absence of response to odorants by electro-olfactogram in *Chd7*$^{Gt/+}$ mice demonstrates an inability of the *Chd7*$^{Gt/+}$ epithelium to generate or conduct an electrical current after exposure to chemical stimuli. In order to test the function of olfactory sensory neurons, we used calcium imaging in olfactory epithelium slices to analyze whether individual olfactory sensory neurons elicit a signal in response to odorants (37). We found that *Chd7*$^{Gt/+}$ pups had functional OSN responses to odorants similar to wild type littermates (Figure 2.5A-F). These data show that early postnatal olfactory sensory neurons are intact in *Chd7*$^{Gt/+}$ mice, and exclude developmental delay as a cause of mature olfactory epithelium dysfunction.

Because sustentacular cells are essential for normal olfactory function (33), we tested whether olfactory dysfunction in *Chd7*$^{Gt/+}$ mice was due to defects in sustentacular cells. To test this, we measured sustentacular cell function by examining glutathione-S transferase (GST) activity (Figure 2.5G). GST expression is restricted to sustentacular cells and Bowman's glands (and not olfactory sensory neurons) in the olfactory epithelium (38, 39), and is necessary for sustentacular cells to properly detoxify the olfactory environment which is under constant environmental stress (33). We found normal GST activity in *Chd7*$^{Gt/+}$ mice compared to wild type littermates (Figure 2.5G). Together, these data suggest a mechanism of reduced olfaction in *Chd7*$^{Gt/+}$ mice that is independent of GST activity in sustentacular cells, and suggest that olfactory dysfunction is not simply due to an unhealthy olfactory epithelium.

Analysis of other mouse mutants with reduced olfaction has indicated that all of the necessary components for odorant detection need to be properly localized in the cilia

(40) and that proper cilia structure and function are essential for normal odorant detection (41, 42). To test whether cilia structure and function are altered in *Chd7*$^{Gt/+}$ mice, we measured ciliary adenylyl cyclase activity and analyzed cilia by immunofluorescence with antibodies against cilia components. Adenylyl cyclase activity in the cilia is essential for canonical G-protein coupled receptor signaling in most olfactory sensory neurons (43). We detected normal basal and forskolin-stimulated adenylyl cyclase activity in adult *Chd7*$^{Gt/+}$ mice (Figure 2.5H).

Interestingly, immunofluorescence label for cilia markers in *Chd7*$^{Gt/+}$ mice was consistently patchy between mice and between sections within a given mouse, with some regions appearing to have normal antibody label and other regions showing decreased label, consistent with regional differences in cilia distribution (Figure 2.6A, B). We also found intact but variable immunofluorescence for several cilia components in *Chd7*$^{Gt/+}$ mice, including acetylated α-tubulin (Figure 2.6A-D), $G_{\gamma}13$ (Figure 2.6E, F), adenylyl cyclase III (Figure 2.6G, H), CNGA2, and γ-tubulin (data not shown). These data indicate that abnormalities in cilia components are not a likely contributor to reduced olfactory function in *Chd7*$^{Gt/+}$ mice, but that regional decreases in the amount of cilia present may potentially contribute to olfactory dysfunction.

Olfactory sensory neurons are reduced and disorganized in *Chd7*$^{Gt/+}$ mice

The cytoarchitecture of the postnatal olfactory epithelium is highly organized, and each cell type can be distinguished by its gene expression profile, apical-basal location, and morphology. We examined the ultrastructure of the olfactory epithelium in wild type and *Chd7*$^{Gt/+}$ mice using scanning electron microscopy (SEM). By SEM, we observed

wild type OSN cell bodies organized in parallel stacked columns within the epithelium (Figuer 2.7A). In contrast, *Chd7*$^{Gt/+}$ OSN cell bodies appeared to have lost this highly ordered arrangement (Figure 2.7B). We also observed patchy cilia distribution on the apical surface of the *Chd7*$^{Gt/+}$ epithelium consistent with the immunofluorescence for cilia components (Figure 2.7C, D). These data indicate that olfactory sensory neurons in *Chd7*$^{Gt/+}$ olfactory epithelium are disorganized but retain some dendritic projections to the apical surface.

We closely examined olfactory epithelial cell types by transmission electron microscopy (TEM). We found that wild type and *Chd7*$^{Gt/+}$ olfactory sensory neurons appear to extend dendrites which end in a dendritic knob on the apical surface of the epithelium and project cilia along the nasal mucosa (Figure 2.7E, F). We then directly quantified the numbers of various cell types in the olfactory epithelium by light microscopic analysis of tissues that had been processed for TEM (Figure 2.7G-I). Cell types were classified based upon their location in the epithelium and their morphology. The number of cells of each type was compared to the average known percentages of each cell type of the adult olfactory epithelium: apical cells 15%, olfactory sensory neurons 75-80%, and basal (globose and horizontal) cells 10% (33). The apical-most and basal-most populations of cell nuclei could not be differentiated into further subclasses. The remaining cell bodies located in the medial portion of the epithelium were counted as olfactory sensory neurons (Figure 2.7G, H). We detected a significant reduction (30%) in the number of olfactory sensory neurons in *Chd7*$^{Gt/+}$ mice (Fig. 7H, I), consistent with our previous observation of decreased OMP staining (Fig. 3A, B). There was also a small (10%) yet significant reduction in the number of basal cells in *Chd7*$^{Gt/+}$ mice

(Figure 2.7H, I). We found no statistically significant difference in the number of apical cells in *Chd7*$^{Gt/+}$ mice compared to wild type (Figure 2.7H, I). The smaller reduction in basal cells compared to the larger reduction observed in olfactory sensory neurons is likely due to the olfactory epithelium having two populations of basal cells: horizontal basal cells (HBCs) and globose basal cells (GBCs). Since HBCs are typically quiescent (33), their cell numbers may not be as influenced by reduced *Chd7* dosage as GBCs. Reduced GBCs with no change in HBCs could also skew the data toward the small difference in total basal cell number. These data indicate that the appearance of disorganized olfactory sensory neurons in *Chd7*$^{Gt/+}$ mice could be related to an overall reduction in the number of olfactory sensory neurons and GBCs.

Neural stem cell proliferation in the olfactory epithelium requires CHD7

Basal cells are the stem cell progenitors in the postnatal olfactory epithelium, and GBCs are known to be a highly dynamic pro-neuronal basal cell population (33, 44-48). Since Mash1/NeuroD labeling showed that *Chd7* is expressed in pro-neuronal basal cells, we tested whether *Chd7*$^{Gt/+}$ olfactory epithelia have defects in cellular proliferation. For these studies, we used a BrdU incorporation assay to identify S-phase cells in the wild type and *Chd7*$^{Gt/+}$ olfactory epithelium. Colocalization between anti-BrdU and anti-CHD7 immunofluorescence allowed us to visualize and quantify CHD7-positive and BrdU-positive proliferating basal cells (Figure 2.8A-D). We found that *Chd7* is expressed in 98% of BrdU-positive proliferating basal cells in both wild type and *Chd7*$^{Gt/+}$ mice (Figure 2.8A-D). *Chd7* expression was high in crypt regions, which also appeared to be sites of high cellular proliferation in the olfactory epithelium (Figure

2.8A, B). Previous reports indicate that there are regions of the olfactory epithelium where proliferation is more active (49). These crypt regions appear to have high levels of CHD7-positive proliferating basal cells. Quantification of CHD7-positive and BrdU-positive cells revealed a 50% reduction in proliferating basal cells in the olfactory epithelium in adult *Chd7*$^{Gt/+}$ mice compared to wild type littermates (Figure 2.8E). There was also a 50% reduction in the number of CHD7-positive cells in the apical region of the epithelium (Fig. 8E). Together, these data indicate a requirement for CHD7 in proliferating cells in the basal olfactory epithelium. Reduced numbers of proliferating GBCs could translate into fewer apical CHD7-positive cells and lead to fewer mature olfactory sensory neurons, as predicted by the reduced intensity of olfactory epithelium OMP staining (Figure 2.3A, B).

Neuronal regeneration is altered in *Chd7*$^{Gt/+}$ mice

Neuronal regeneration throughout adulthood is an essential characteristic for continued function of the olfactory epithelium, since the olfactory epithelium is continuously exposed to environmental stresses and must recover to maintain its primary function of odorant detection. To determine whether defects in *Chd7*$^{Gt/+}$ olfaction were associated with abnormalities in neuronal regeneration, we chemically ablated the olfactory epithelium and assayed neuronal regeneration in wild type and *Chd7*$^{Gt/+}$ mice. Six-week old wild type (N = 9) and *Chd7*$^{Gt/+}$ (N = 8) sex-matched littermates were given a 25 μl intranasal infusion of 1% Triton-X 100 in saline. Two weeks post-ablation, one wild type mouse was sacrificed to determine efficiency of the ablation technique. The olfactory epithelium was completely ablated at two weeks post-ablation, with no

observable OMP or Reep6 staining. Four weeks post-ablation, wild type (N = 4) and *Chd7*$^{Gt/+}$ (N = 4) mice were sacrificed and analyzed for neuronal regeneration by immunofluorescence using anti-OMP (Figure 2.9A, B). Wild type and *Chd7*$^{Gt/+}$ mice both had some degree of OMP staining and neuronal regeneration. However, *Chd7*$^{Gt/+}$ mice had reduced OMP-positive cells which also appeared to be disorganized compared to wild type littermates. At eight weeks post-ablation, wild type (N = 4) mice had almost complete recovery of olfactory sensory neurons in the olfactory epithelium at eight weeks post-ablation (Figure 2.9C, E), whereas *Chd7*$^{Gt/+}$ (N = 4) mice had regional differences in neuronal regeneration with some regions of the epithelium appearing normal while others exhibited little to no neuronal regeneration (Figure2. 9D, F). These data indicate that adult *Chd7*$^{Gt/+}$ mice have delayed or impaired ability to regenerate the olfactory epithelium compared to wild type mice. Delays or reductions in the ongoing formation of new olfactory sensory neurons under normal conditions could also contribute to the olfactory defects observed in *Chd7*$^{Gt/+}$ mice.

Discussion

Here we have shown that both humans and mice with *CHD7* deficiency have impaired olfaction. We observed *Chd7* expression during development in restricted cell types of the olfactory epithelium and olfactory bulb, and *Chd7* expression in the adult mouse olfactory epithelium in proliferating basal cells and in pro-neuronal basal cells. We also found that *Chd7* deficient mice have a significant reduction in basal cell proliferation, which translates into a reduction in both basal cells and olfactory sensory neurons. Figure 2.10 depicts a diagram of the olfactory epithelium in both wild type and

Chd7 mutant mice. The reduction in olfactory sensory neurons caused by *Chd7* deficiency leads to regional variability in cilia density and disorganization of the *Chd7* mutant olfactory epithelium, which may influence tight junctions required for signal transduction. Additionally, *Chd7* deficient mice have a reduced capacity for regeneration of olfactory sensory neurons following chemical ablation of the olfactory epithelium. These data together suggest a critical role for *CHD7* in olfactory tissues not only during development but also into adulthood.

Our data provide the first evidence that CHD7 functions in cellular proliferation and neuronal differentiation in the olfactory epithelium. The mechanism by which CHD7 regulates cell cycle progression and stem cell differentiation is not yet understood. DNA chromatin structure has a vital role in gene regulation, cellular proliferation and maintenance of the differentiated state. However, little is known about the cell and tissue specific functions of chromodomain proteins. Protein-protein interactions involving cell cycle progression and gene expression have been reported for some CHD family members (50-56). Proteins such as histone deacetylases and nuclear receptor corepressor 1 are involved in protein interactions with CHD proteins (50-56) and are also known to be critical for neuronal differentiation (57, 58). In a recent study using ChIP-chip analysis, CHD7 was shown to bind to methylated histone H3 K4 enhancer regions of numerous genes in the mammalian genome (59). These data suggest a role for CHD7 in regulating transcription, potentially affecting multiple developmental processes during cell fate specification.

CHD7 and other chromodomain proteins are also thought to regulate access to chromatin by binding and unwinding it (25-29). CHD7 could work in conjunction with

other transcription factors involved in cell cycle progression and neuronal differentiation. Otx2, a paired-like homeodomain transcription factor, is critical for normal cellular proliferation and neuronal differentiation (60). *Otx2* mutant mice lack the pro-neuronal transcription factor *Mash1* (60). Mash1 induces the expression of later bHLH transcription factors like *Ngn1* and *NeuroD*, driving cell cycle exit and neuronal differentiation (33). We found that CHD7 colocalizes with BrdU-positive proliferating cells and with Mash1 and NeuroD in basal cells. Since Otx2 is involved in cellular proliferation and induces the expression of Mash1 and NeuroD, CHD7 may be necessary for access to Otx2 target genes in the olfactory epithelium. Our data indicate that *Chd7* deficiency may impact the expression and/or function of transcription factors dependent upon CHD7 for access to target genes through chromatin modifications.

Neural progenitor cells in the adult olfactory epithelium possess an extensive capacity for ongoing cellular proliferation and differentiation. These neural progenitors must be tightly regulated developmentally, temporally, and spatially to maintain the integrity of the epithelium over time. *Chd7* is expressed in both the embryonic and adult olfactory epithelium, and targets of CHD7 are likely to include factors involved in regulation of neurogenesis, neuronal regeneration and cell cycle progression. CHD7 could be involved in expression of morphogens such as the bone morphogenetic proteins (BMPs) or fibroblast growth factors (FGFs). Previous studies have shown that BMP4 has dosage dependent opposing effects on neurogenesis in the olfactory epithelium (61, 62). BMP2, BMP4, and BMP7 at high concentrations have anti-neurogenic effects on progenitors (61, 62). However, low concentrations of BMP4 increase neurogenesis in the olfactory epithelium while BMP2 and BMP7 retain their anti-neurogenic effects at low

concentrations (61, 62). Although low concentrations of BMP4 increase neurogenesis in the olfactory epithelium, BMP4 does not cause an increase in cellular proliferation (61), in contrast to the decreased cellular proliferation we observed with *Chd7* deficiency. FGF2 induces neurogenesis and increases cellular proliferation of progenitors in the olfactory epithelium (61). Together these data suggest that BMP and FGF signaling may be sensitive to changes in *CHD7* dosage in the olfactory epithelium.

Interestingly, *Chd7* deficiency does not appear to affect the structure, function, or localization of olfactory cilia components. However, we observed regional cilia reductions in $Chd7^{Gt/+}$ mice that could contribute to defects in odorant detection. These data indicate that unlike other mouse models with defects in olfaction, olfactory dysfunction in $Chd7^{Gt/+}$ mice is not caused by defects in cilia structure, function (41, 42), or protein transport (40). Instead, reduced numbers of olfactory sensory neurons and cilia could contribute to impaired olfaction in mature $Chd7^{Gt/+}$ mice, perhaps through altered electrical signal transmission. The apparently normal calcium responses in neurons of the neonatal *Chd7* mutant mouse olfactory epithelium suggest that the developing mutant epithelium is relatively normal. Therefore, later defects in EOG, olfactory bulb tyrosine hydroxylase label, reduced olfactory bulb size, and reduced olfactory performance in CHARGE patients could be a result of ongoing abnormalities in neural stem cell proliferation and reduced/disorganized olfactory sensory neurons. Future studies of developing *Chd7* mutant olfactory tissues and olfactory behaviors in *Chd7* mutant mice should help clarify these pleiotropic effects.

Olfactory dysfunction in CHARGE has typically been associated with defects in the olfactory bulb which ranged from hypoplasia to complete absence of one or both

lobes of the olfactory bulb (15-20). *Chd7* mutant mice have olfactory bulb hypoplasia, consistent with the observed human phenotype. However, the olfactory bulb defects observed in CHARGE individuals often consist of more severe hypoplasia or complete absence of one or both olfactory bulb lobes. Since we detected olfactory hypoplasia in young adult mice (6 weeks) it is also possible that the olfactory bulb hypoplasia could become progressively more severe as the animals age. Defects in the olfactory epithelium have not previously been analyzed in humans or mice with *CHD7* mutations (15-20). We found that $Chd7^{Gt/+}$ mice have severely impaired olfaction by electro-olfactogram, which measures odorant detection directly from the surface of the epithelium independent of the olfactory bulb. Our data indicate that olfactory dysfunction in CHARGE individuals may be attributed to primary defects in the olfactory epithelium, and raises the possibility that reduced sensory input from olfactory sensory neurons could contribute to later and more severe olfactory bulb defects.

Prior studies of olfaction in CHARGE have also been limited because the mutation status of the individuals was not reported (15-18, 20) in all but one study of a female with CHARGE and Kallmann (19), and in a recent report of three individuals ascertained on the basis of a Kallmann syndrome phenotype (63). The eight patients in our study have *CHD7* mutations that span the gene, and one functional domain (SNF domain) of the CHD7 protein (Table 1). Ours is the first report of measured reduction in olfaction in CHARGE patients with known *CHD7* mutations. We chose the B-SIT to analyze olfactory dysfunction in CHARGE individuals because it is a rapid test that is readily available and inexpensive, especially compared to physiological measures of olfactory function in humans (64). The B-SIT is easy to perform, even for children.

However, the B-SIT is not reliable for distinguishing degrees of hyposmia and anosmia (64). Also, our results could be potentially influenced by cognitive impairment, as is true for the University of Pennsylvania Smell Identification Test (UPSIT), from which the B-SIT is based. Our B-SIT data were obtained from individuals who took the test at home, which could also have influenced test results. Despite these limitations, the B-SIT showed reduced olfaction in a majority of *CHD7* mutation-positive CHARGE individuals. A better understanding of the mechanisms involved in the pathogenesis of CHARGE will help facilitate both diagnosis and therapies for CHARGE syndrome. Our data suggest that the B-SIT could be used in a clinical setting as an additional diagnostic tool for evaluating children and adults with suspected CHARGE phenotypes.

We have identified a novel role for CHD7 in neural stem cells of the olfactory epithelium, which could provide insight into a similar role for *Chd7* in regulating cell cycle and cell fate specification in other sensory and non-sensory tissues. Our data also demonstrate a novel mechanism for olfactory dysfunction in mammals caused by reduced olfactory sensory neurons. How does a reduction in olfactory sensory neurons lead to impaired olfaction? We hypothesize that fewer olfactory sensory neurons are insufficient to generate an electrical potential, leading to reduced neuronal electrical transmission to the olfactory bulb. Reduced tyrosine hydroxylase in the $Chd7^{Gt/+}$ olfactory bulb is consistent with this notion. A reduction in olfactory sensory neurons in $Chd7^{Gt/+}$ mice may also alter the integrity of the olfactory epithelium such that critical cell-cell contacts are disrupted, impairing the ability of the olfactory sensory neurons to process and maintain electrical signals. It will be important to identify whether there are critical genes dysregulated by loss of *Chd7* function. We expect some genes regulated by CHD7

to influence proliferation, while others may control aspects of cellular differentiation. Generation and characterization of conditional *Chd7* null mutants could also enable further analysis of the roles of CHD7 during olfactory development. Since *Chd7* null mice are embryonic lethal by E11 (21, 22), tissue specific and inducible knockouts would enable research on homozygous phenotypes that are currently not amenable for study in heterozygous mouse models. Our work also opens new questions for future research on the function of CHD7 in stem cells in the olfactory system and elsewhere.

Materials & Methods

Human olfactory testing

We used the B-SIT (Brief Smell Identification Test™, Sensonics, Inc., Haddon Heights, NJ) as a measure of olfactory function in individuals with CHARGE syndrome. The B-SIT is a 12 item, self-administered test booklet which contains odorants embedded on scent strips that are released by scratching with a pencil (40, 64-67). Answers are given as multiple choices among four alternative responses. Individuals with CHARGE who were 10 years or older, and their parents or unaffected siblings, were recruited for participation by mail inquiries, and then subsequently sent test booklets for scoring. Individuals were provided with detailed instructions for completing the test. All aspects of the study were approved by the IRB medicine review committees of The University of Michigan and Baylor College of Medicine.

Mice

Chd7$^{Gt/+}$ mice were generated by backcrossing with 129S1/Sv1mJ (Jackson Laboratory) mice to generation N5-N7 and genotyped using methods as previously described (22). We found no detectable CHD7 immunofluorescence in *Chd7*$^{Gt/Gt}$ E10.5 embryos using a polyclonal anti-CHD7 antibody, confirming that *Chd7*^{Gt} is a null allele (unpublished observations). All procedures were approved by the University Committee on Use and Care for Animals at The University of Michigan and Michigan State University.

Immunofluorescence and immunohistochemistry

Six week-old *Chd7*$^{+/+}$ and *Chd7*$^{Gt/+}$ sex-matched littermate mice were anaesthetized with 250 mg/kg body weight tribromoethanol and perfusion fixed with 4% paraformaldehyde. Mice were then decapitated and heads placed in 4% paraformaldehyde overnight at 4°C. Heads were incubated in RDO Rapid Decalcifier (Apex Engineering, Aurora, IL) for 4-6 hours followed by 30% sucrose protection overnight at 4°C. Tissue was flash frozen in O.C.T. embedding medium (Tissue Tek, Torrance, CA) for sectioning. Following cryosectioning, 14 μm sections were processed for hematoxylin/eosin staining or immunofluorescence with antibodies against adenylyl cyclase III (1:500; Santa Cruz, Santa Cruz, CA), CNGA2 (1:200; Alomone Labs, Jerusalem, Israel), acetylated α-tubulin (1:1000; Sigma, St. Louis, MO), $G_{\gamma}13$ (1:200; gift of Robert Margolskee, Mt. Sinai School of Medicine, New York, NY), γ-tubulin (1:500; Sigma), OMP (1:200; Wako Chemicals USA, Inc, Richmond, VA), CHD7 (1:1000; Abcam, Cambridge, MA), β-galactosidase (1:1000; gift of Thomas Glaser), BrdU (1:100;

Immunologicals Direct, Raleigh, NC), NeuroD (1:1000; gift of Jacques Drouin), Mash1 (1:150; Abcam, Cambridge, MA), Tyrosine hydroxylase (1:150; Pel-Freez, Rogers, AR), Sus1 (1:20; gift of Frank Margolis) or Reep6 (1:500). Rabbit antisera against mouse REEP6 peptides (1-16; MDGLRQRFERFLEQKN and 188-201; STSEPPAALELDPK) were generated by Zymed Laboratories Inc. (South San Francisco, CA). Specificity to REEP6 was confirmed in cell-based transfection assays. Secondary antibodies used at 1:200 were conjugated with Alexa 488, Alexa 555, or biotin with streptavidin-HRP (Vector Laboratories) and diaminobenzidine (DAB) with urea/peroxide tablets (Sigma) or biotinylated secondary antibodies conjugated with streptavidin-Alexa488 or streptavidin-Alexa555 Molecular Probes, Eugene, OR and Invitrogen, Carlsbad, CA). NIH ImageJ software (Bethesda, MD) was used to analyze fluorescence intensity over at least 30 images. Fluorescence intensity was measured in restricted areas of the epithelium encompassing the olfactory sensory neurons but excluding cilia label, and background was subtracted to obtain the final measurements. Images were captured on a confocal microscope (Olympus IX-81 inverted scope) using the Olympus FluoView 500 software and processed in Photoshop CS2 version 9.0.

β-Galactosidase assay

Timed pregnancies were established between *Chd7*$^{Gt/+}$ and wild type mice, with the morning of plug identification designated E0.5. Embryos were collected at E12.5 after cervical dislocation and hysterectomy. Embryos were briefly washed in PBS and amniotic sacs were collected for DNA isolation and PCR genotyping. Embryos were processed for X-gal staining as previously described (68). X-gal stained sections were

post-fixed in 4% paraformaldehyde and counterstained in eosin. Sections were visualized with a Leica DMRA microscope and digital images processed with Adobe Photoshop CS2 V9.0 software.

Proliferation assays

Mice were injected intraperitoneally with 0.1 g/g body weight 5-bromo-2-deoxyuridine (BrdU) 30 minutes prior to sacrifice. Tissues were then processed for anti-BrdU and anti-CHD7 immunofluorescence as above. Secondary antibodies were conjugated with Alexa 488, Alexa 555, or biotin, as above. For quantitation of S-phase cells, confocal images from three regions of the olfactory epithelium were analyzed in eight different mice ($N = 4$ wild type, $N = 4$ *Chd7*$^{Gt/+}$ sex-matched littermates). From each tissue section, 4-6 images were analyzed using Olympus FluoView 500 software for number of CHD7-positive, BrdU-positive, and CHD7/BrdU-positive cells, and the data tested for significance by t-test using two-tailed unequal variance.

Scanning and transmission electron microscopy

Six week- old *Chd7*$^{+/+}$ and *Chd7*$^{Gt/+}$ sex-matched littermate mice were anaesthetized with 250 mg/kg body weight tribromoethanol and perfusion fixed with 2% glutaraldehyde. Mice were decapitated, the head bisected along the midline and further dissected to expose the olfactory epithelium. The olfactory epithelium was dissected from the head and fixed in 2% glutaraldehyde overnight. The tissue was then prepared for scanning electron microscopy (SEM) using the OTOTO fixation method (69). Scanning electron microscopy was performed at the University of Michigan Microscope

and Image Analysis Laboratory using the AMRAY 1910 Field Emission Scanning Electron Microscope.

For transmission electron microscopy (TEM), perfusion fixed and dissected olfactory tissues were processed for TEM as previously described (70-72). Transmission electron microscopy was done at the University of Michigan Microscope and Imaging Analysis Laboratory using the Philips CM-100 transmission electron microscope. For quantifying numbers of cells in the olfactory epithelium, tissues processed for TEM were sectioned (1 μm). Olfactory tissue sections from each pair of littermate mice (N = 3 wild type, N = 3 *Chd7*$^{Gt/+}$ sex-matched littermates) were collected randomly from three different regions of the epithelium. Within each section, cells in 10 images were counted, taking into consideration their location in the epithelium and their cellular morphology. Sections were visualized with a Leica DMRA microscope and digital images processed with Adobe Photoshop CS2 V9.0 software. Cell numbers were analyzed for significance by t-test using two-tailed unequal variance.

Electro-olfactograms

Six week- old *Chd7*$^{+/+}$ and *Chd7*$^{Gt/+}$ sex-matched littermate mice were sacrificed by CO_2 inhalation then decapitated, the head bisected along the midline, and tissues dissected to expose the turbinates of the olfactory epithelium. Electrodes ranging from 4-8 MΩ in resistance filled with Ringers containing 0.1% agarose were placed on either turbinates II or IIb for recording. Vapor-phase odor stimuli were generated from 10mL of solution in a sealed 50mL bottle. The odorants were delivered as a 20mL pulse injected into a continuous stream of humidified air flowing over the tissue sample. The

data were then analyzed with Clampfit (Molecular Devices Corp., Sunnyvale, CA) and peak heights determined from pre-pulse baseline. Data were normalized to a pulse of pure amyl acetate given later in the same trace. *Chd7* mutant data were normalized to the average response of the *Chd7* wild type mouse for a specific dose of the odorant. For each mouse tested (N = 8 wild type, N = 7 $Chd7^{Gt/+}$ sex-matched littermates), four different concentrations of amyl acetate were delivered as well as five additional odorants (octanal, heptaldehyde, hexanal, eugenol, and carvone) each tested at a concentration of 10^{-3} M of the respective odorant.

Adenylyl cyclase/cAMP accumulation assay

Six week-old $Chd7^{+/+}$ and $Chd7^{Gt/+}$ sex-matched littermate mice were sacrificed by CO_2 inhalation then decapitated. Cilia membranes were isolated essentially as described previously (73). Briefly, olfactory epithelia from either wild type or $Chd7^{Gt/+}$ mice were dissected into small pieces. Cilia were removed from the epithelium by agitation in Ringers solution supplemented with 10 mM $CaCl_2$ and Complete Protease Inhibitor tablets (Roche, Indianapolis, IN). Tissue was rocked for 15 min at 4 °C followed by centrifugation at 7700 x g for 5 min. The supernatant was collected in a separate tube and the agitation/centrifugation steps were repeated two more times. The pooled supernatants were centrifuged for 30 min at 27,000 x g to pellet the ciliary membranes. The supernatants were discarded and the pellet was resuspended in GTPγS buffer (100 mM NaCl, 5 mM $MgCl_2$, 20 mM Tris-Cl, 0.8 mM EDTA, pH7.4) supplemented with Complete Protease Inhibitors.

To start the adenylyl cyclase assay, 15-20 μg of the isolated cilia prep was added to the assay mix containing 1x GTPγS buffer, 1x ATP regenerating mix, 10 μM GTP, and 1 mM IBMX in the presence or absence of 10 μM forskolin. After 10 min at 37 °C, the reaction was stopped by replacing the medium with ice-cold 3% perchloric acid. After at least 30 min at 4 °C, 0.4 ml was removed from each sample, neutralized with 0.08 ml of 2.5 M $KHCO_3$, vortexed, and centrifuged at 15,000 x *g* for 1 min. A 20 μl aliquot was taken from the supernatant of each sample, and accumulated cAMP was quantified using a [^{3}H]cAMP assay kit according to manufacturer's instructions (GE Healthcare, Chalfont St. Giles, Buckinghamshire, UK). The total pmol cAMP produced per mg protein was calculated for each condition. All data are presented as a percent of basal, unstimulated cyclase activity for the wild type mouse. Statistical significance was determined using one-way ANOVA analysis with GraphPad Prism 5 software.

Calcium imaging

Slices were essentially prepared as previously described (37). Neonatal mice (postnatal day 1-2) were killed by decapitation and the lower jaw was removed. Tissue was mounted onto a vibratome-cutting block, supported by carrots, and 400μm thick slices were cut. Ice-cold slices were transferred to oxygenated Ringer solution until ready to load with dye. Ringer solution contained 140 mM NaCl, 5 mM KCl, 1 mM $MgCl_2$, 2 mM $CaCl_2$, 10 mM HEPES, 10 mM glucose, and 0.5 mM probenicid (to prevent dye loss). To identify the presence of the *lacZ* gene in the heterozygous mice, one slice from each mouse was incubated in fluorescein digalactoside (Invitrogen, Carlsbad, CA) according to manufacturers instruction to test for β-galactosidase activity. Genotyping

was confirmed by PCR analysis of genomic DNA isolated from the mouse tail snips. Prior to calcium imaging, all slices were loaded with 18 μM fluo-4 AM (Invitrogen) for 60-90 min at 25°C.

Fluo-4 loaded olfactory epithelial slices in a laminar flow chamber (Warner Instruments, Hamden, CT) were measured for odorant-evoked calcium using laser scanning confocal imaging as described previously (37). Ringer solution was continuously perfused over the slice at a flow rate of 1.5–2.0 ml/min throughout the length of the experiment. Images were taken at least 100 μm below the top of the slice to avoid damaged neurons. An odorant mixture consisting of 200 μM each of amyl acetate, carvone, eugenol, cineole, octanal, heptanal, and hexanal was made fresh in Ringer solution was applied using bath exchange and a 200-μl-volume loop injector. Images were acquired on an Olympus FluoView 1000 confocal laser scanning system and data analysis was performed using Olympus software and NIH ImageJ. Images were acquired approximately every 1 second for 2-3 minutes. For all traces, odorant was added after 15 s of recording to allow for baseline stabilization, and all data were normalized to the average of the first 15 s of recording during which odorant was absent.

Glutathione S-Transferase assay

Six week-old *Chd7*$^{+/+}$ and *Chd7*$^{Gt/+}$ sex-matched littermate mice were sacrificed by CO_2 inhalation then decapitated. Heads were bisected along the midline to expose the olfactory epithelium. The olfactory epithelium was dissected from the head and processed for glutathione S-transferase enzymatic activity using the Glutathione S-Transferase Assay Kit as per manufacturer's instructions (Sigma).

Olfactory epithelium chemical ablation studies

Six week-old *Chd7*$^{+/+}$ and *Chd7*$^{Gt/+}$ sex-matched littermate mice were anesthetized with 100 mg/kg ketamine/10mg/kg xylazine intraperitoneal injection and given a single intranasal irrigation with 20µl of 1% TritonX-100 in 0.15M NaCl, based on methods previously described (36). Mice were sacrificed at 2, 4, and 8 weeks post-ablation and processed for immunofluorescence using anti-CHD7, anti-OMP, and anti-BrdU as described above.

Acknowledgments

The authors thank all of the families that participated in our olfactory testing and John Belmont for helpful discussions and assistance with patient recruitment. We also thank Jacques Drouin at the Institut de Recherches Cliniques de Montréal for the use of the NeuroD antibody, Thomas Glaser at the University of Michigan for providing the β-galactosidase antibody, and Frank Margolis at the University of Maryland for the SUS-1 antibody. We are grateful to Karen Steel, Anne Hansen, Miriam Meisler, Jeff Innis, and Sally Camper for insightful discussions.

Chapter 2 Notes

[1]A revised version of Chapter 2 has been published as Layman WS, McEwen DP, Beyer LA, Lalani SR, Fernbach SD, Oh E, Swaroop A, Hegg CC, Raphael Y, Martens JR, Martin DM. (2009). Defects in neural stem cell proliferation and olfaction in Chd7 deficient mice indicate a mechanism for hyposmia in human CHARGE syndrome. *Human Molecular Genetics*: **18**: 1909-1923.

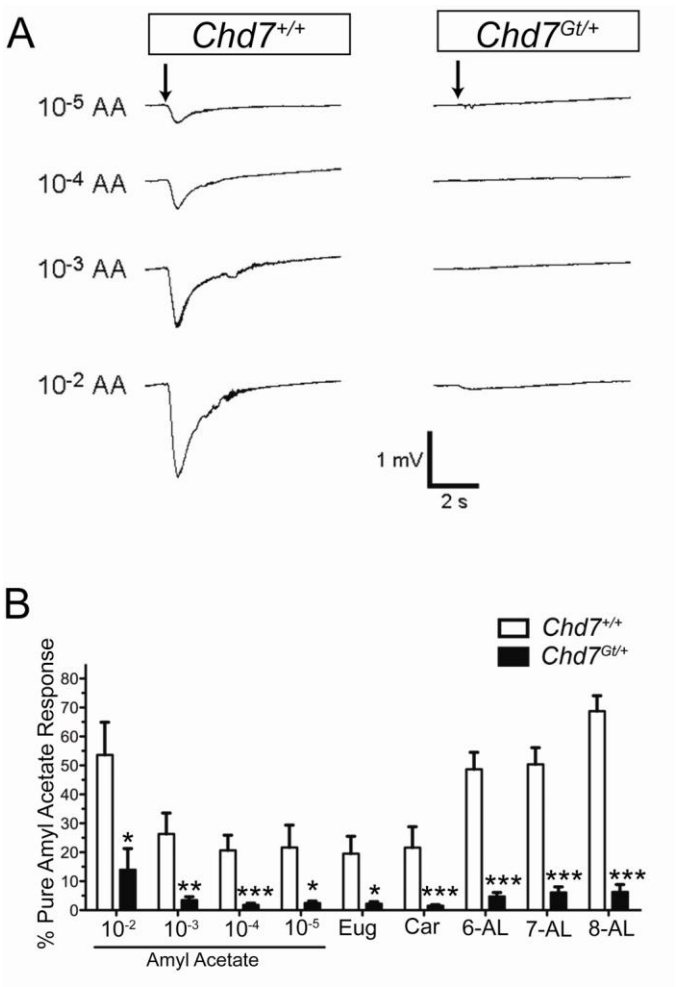

Figure 2.1 *Chd7*$^{Gt/+}$ mice have severely impaired olfaction. (A) Electro-olfactogram tracings from adult wild type and *Chd7*$^{Gt/+}$ mice. The olfactory epithelium from each mouse was exposed to four different concentrations of amyl acetate. (B) Histogram of electro-olfactogram responses from wild type (open bars; $N = 8$) and *Chd7*$^{Gt/+}$ (solid bars; $N = 7$) mice shows four different concentrations of amyl acetate and five additional odorants tested at 10^{-3} M. Each response was normalized and expressed as a percentage of a pure amyl acetate pulse given during the same trace. AA, amyl acetate; 8-AL, octanal; 7-AL, haptaldehyde; 6-AL, hexanal; Eug, eugenol; Car, carvone. * $P < 0.05$, ** $P < 0.005$, and *** $P < 0.001$ as determined by unpaired Student's *t* test.

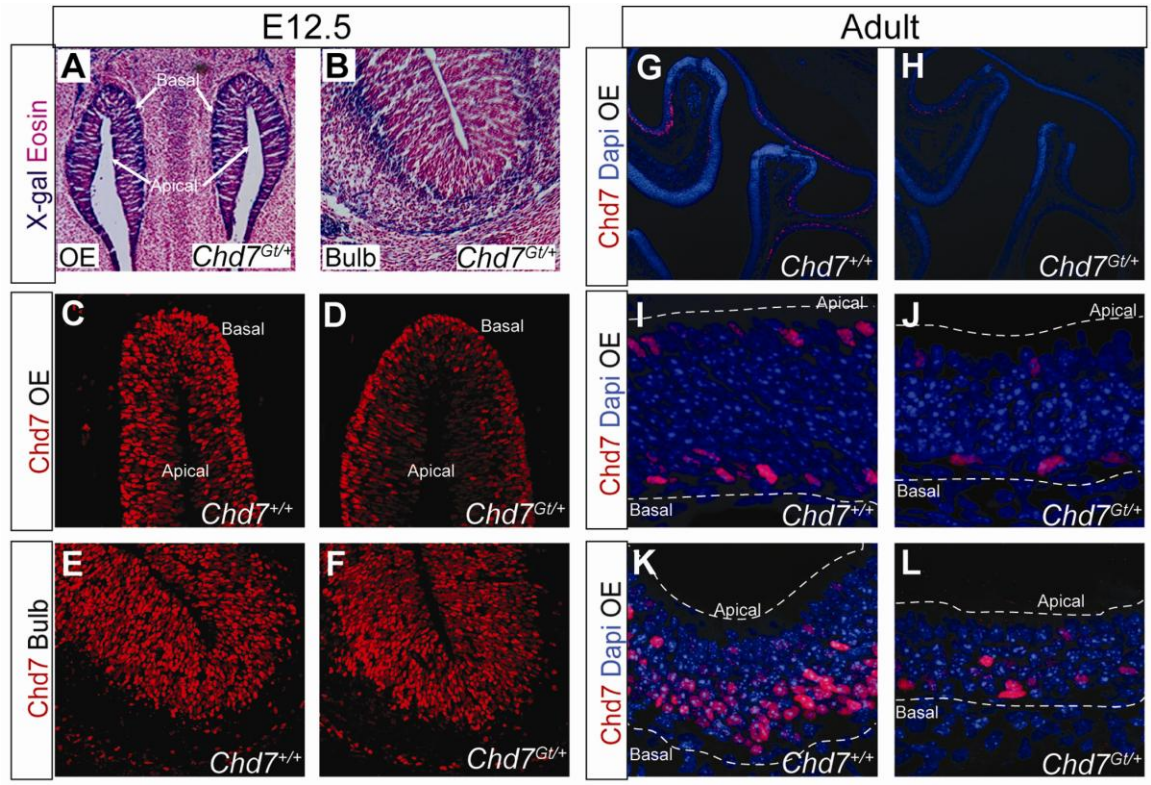

Figure 2.2 *Chd7* is expressed in developing and mature olfactory tissues. X-gal staining shows *Chd7* expression in the embryonic olfactory epithelium (A) and bulb (B). Immunofluorescence with anti-CHD7 shows *Chd7* expression in embryonic E12.5 olfactory epithelium (C, D) and bulb (E, F) and in the adult olfactory epithelium (G-L). *Chd7* expression in the adult olfactory epithelium is regionally variable (G, H), with most CHD7-positive cells present in the basal and apical regions of the olfactory epithelium (I, J). A few regions of the olfactory epithelium contain CHD7-postive cells which span the olfactory epithelium (basal to apical), typically in crypt regions where the epithelium undergoes acute turns in orientation (K, L). White dotted lines in I-L indicate apical and basal surfaces of the epithelium.

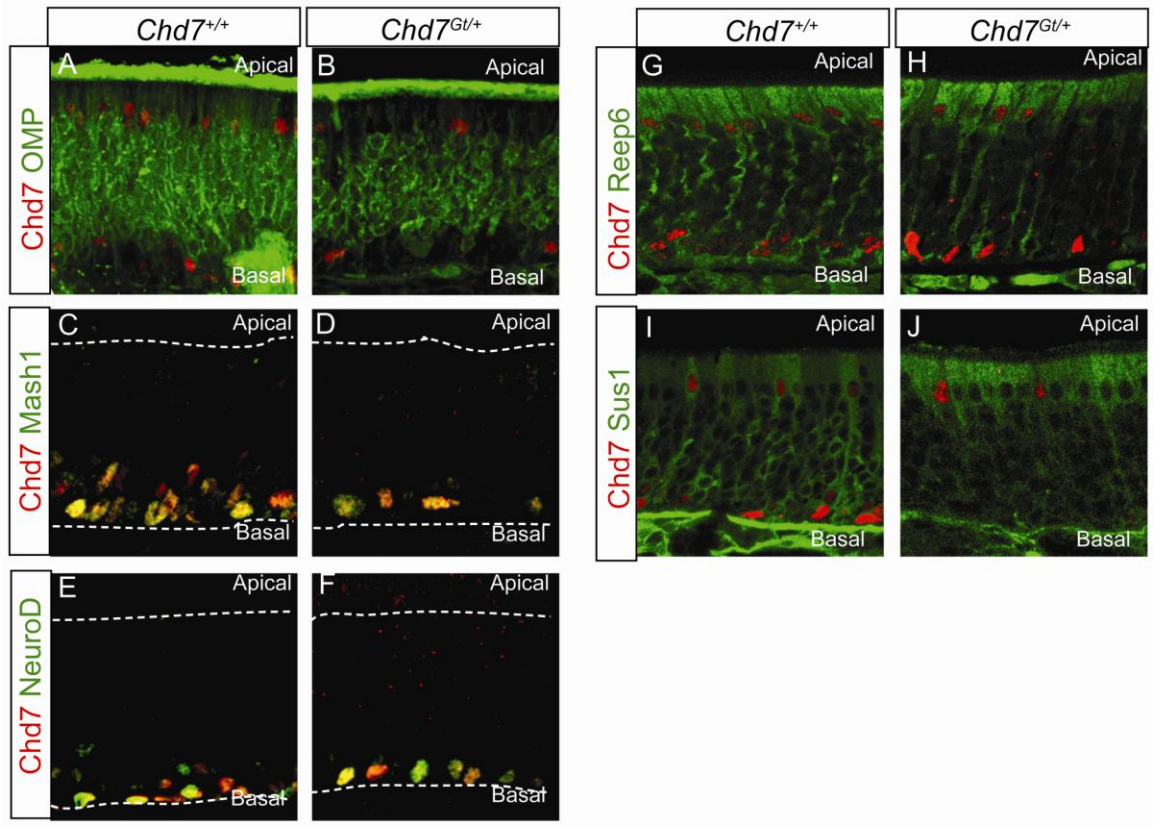

Figure 2.3 *Chd7* is expressed in basal stem cells in the mature olfactory epithelium. The adult olfactory epithelium from wild type and *Chd7*$^{Gt/+}$ mice is stained with anti-CHD7 and antibodies against OMP (A, B), Mash1 (C, D), NeuroD (E, F), Reep6 (G, H), and Sus1 (I, J). CHD7-positive cells in the apical and basal domains do not colocalize with anti-OMP (Fig. 3A, B). White dotted lines in C-F indicate the apical and basal surfaces of the epithelium. CHD7-positive cells express the pro-neuronal basal stem cell marker Mash1 and the immature olfactory sensory neuron marker NeuroD. CHD7-positive cells colocalize with nuclei of the sustentacular cell markers Reep6 and Sus1 (I, J). Arrow (I) indicates a CHD7-positive / Sus1-positive cell with a microvillar-like cell morphology.

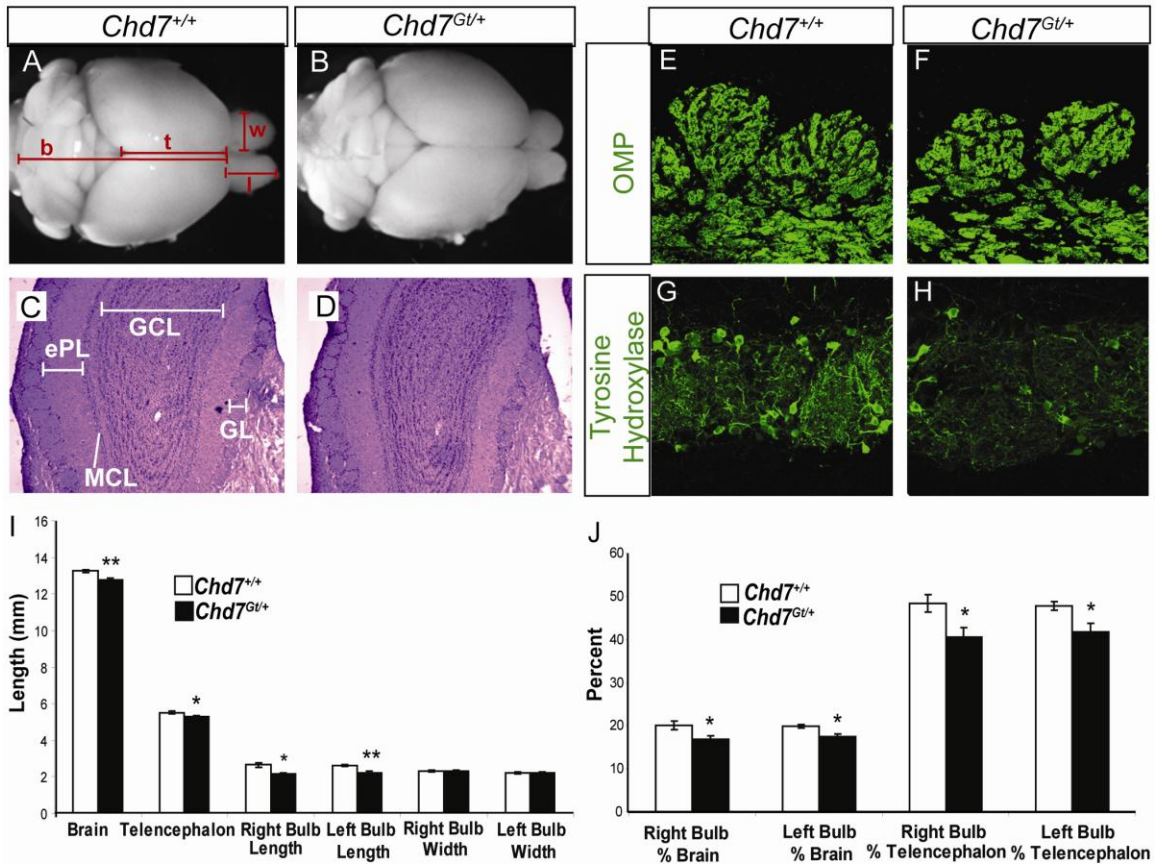

Figure 2.4 *Chd7* mutant mice have olfactory bulb hypoplasia. Brains were dissected and imaged from 6 week old $Chd7^{+/+}$ ($N = 5$) and $Chd7^{Gt/+}$ mice ($N = 5$) (A, B). Measurements were taken of the brain (b), telencephalon (t), olfactory bulb length (l), and olfactory bulb width (w). $Chd7^{Gt/+}$ mice have significantly smaller brains, telencephalons, and olfactory bulb lengths compared to wild type littermates (I). Significant differences in olfactory bulb length taken as a percent of the brain and telencephalon indicate that *Chd7* mutant mice (closed bars) have olfactory bulb hypoplasia compared to wild type littermates (open bars) (J). Cross-sections of the olfactory bulbs stained with hemotoxylin and eosin (C, D) show no difference in the layer composition of $Chd7^{Gt/+}$ olfactory bulbs. Anti-OMP in the olfactory bulb stains the glomeruli in both wild type and $Chd7^{Gt/+}$ mice (E, F). Dopaminergic interneurons surrounding the glomeruli express tyrosine hydroxylase (TH) in response to electrical activity from olfactory sensory neurons in wild type mice, whereas TH label is decreased in $Chd7^{Gt/+}$ mice (G, H). * $P < 0.05$ and ** $P < 0.01$ as determined by unpaired Student's t test. Abbreviations: GL (glomerular layer), ePL (external plexiform layer), MCL (mitral cell layer), and GCL (granule cell layer).

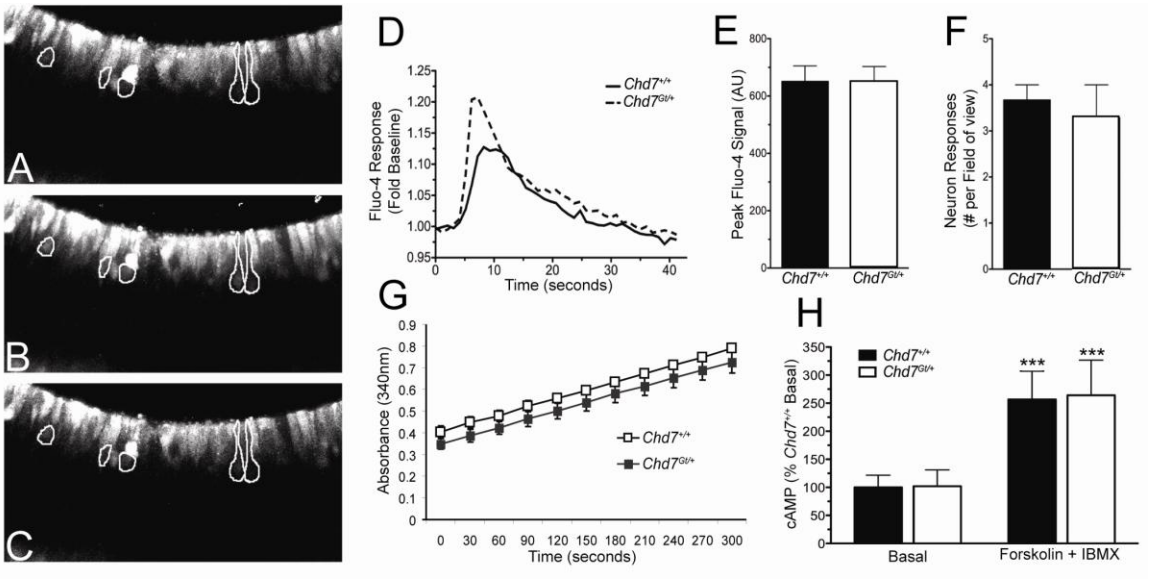

Figure 2.5 Olfactory sensory neurons and sustentacular cells are physiologically intact in early postnatal *Chd7*$^{Gt/+}$ mice. Odor-evoked calcium responses are similar in postnatal day 3 wild type (N = 4) and *Chd7*$^{Gt/+}$ (N = 4) mouse olfactory epithelial slices. Representative confocal images (A-C) from a single fluo-4 AM-loaded *Chd7*$^{Gt/+}$ mouse olfactory epithelial slice (A) before, (B) during, or (C) after odorant application. Representative responding neurons are outlined in A-C. Average time course data (D) were generated from recordings of 22 wild type and 23 *Chd7*$^{Gt/+}$ neurons imaged over 6 slices. No significant difference was observed between wild type and *Chd7*$^{Gt/+}$ mice as determined by an unpaired t test. Histogram representation of the average peak odor-evoked response (E-F) of the neurons measured in (D). Glutathione S transferase activity (G) was examined in six-week old wild type (closed circles, N = 3) and *Chd7*$^{Gt/+}$ (closed squares, N = 3) mice. A representative pair of six-week old wild type and *Chd7*$^{Gt/+}$ littermates showed no significant difference in sustentacular cell activity as determined by an unpaired t test. Adenylyl cyclase activity was examined in the presence or absence of 10 μM forskolin (H) in six-week old wild type (N = 8) and *Chd7*$^{Gt/+}$ (N = 8) littermate mice. No significant difference was observed in either the basal or forskolin-stimulated cyclase activity as determined by an unpaired t test. Data are presented as the mean value ± SEM from 3 separate experiments, where each condition was tested in duplicate. *** $P < 0.001$ as measured by one-way ANOVA analysis.

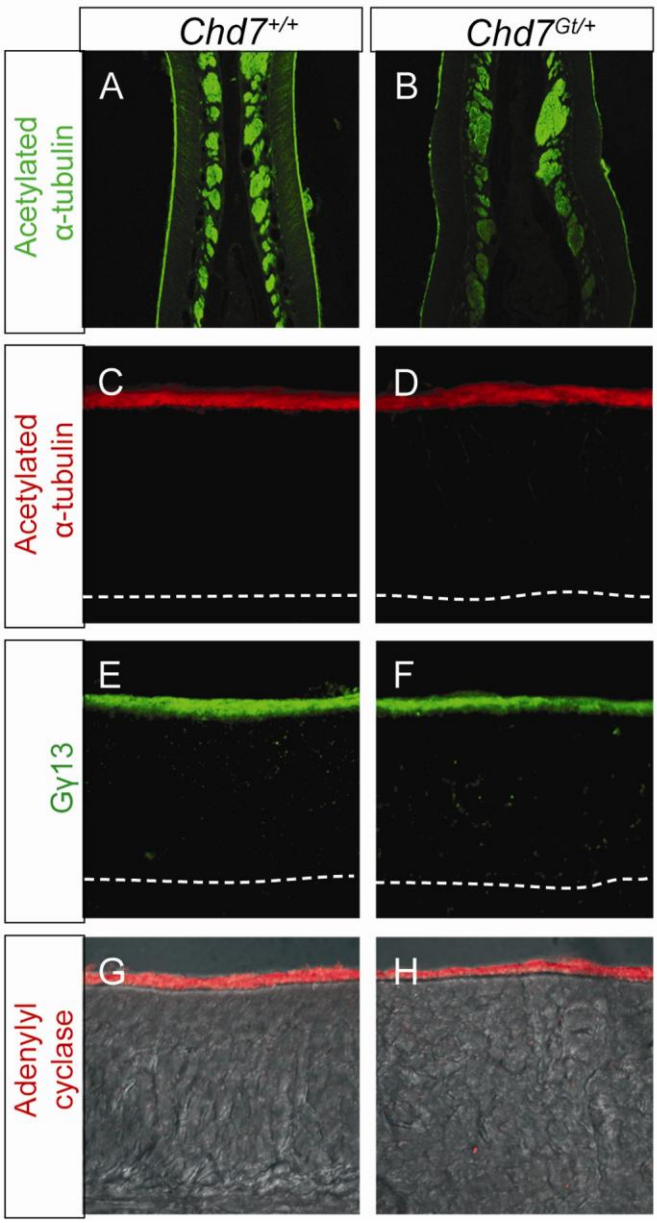

Figure 2.6 Components of the olfactory cilia are intact in *Chd7*$^{Gt/+}$ mice. Olfactory cilia proteins were labeled in wild type and *Chd7*$^{Gt/+}$ mice by immunofluorescence with anti-acetylated α-tubulin (A-D), anti-$G_{\gamma}13$ (E, F), and anti-adenylyl cyclase III (G, H). Regional decreases in immunofluorescence label were consistently observed in *Chd7*$^{Gt/+}$ mice for all cilia markers, as represented by acetylated α-tubulin label (A, B). White dotted lines in C-F indicate the basal surface of the epithelium. Immunofluorescence using antibodies against cilia proteins indicated that although regional decreases in label existed, all cilia components analyzed were present in *Chd7*$^{Gt/+}$ olfactory cilia compared to wild type littermates.

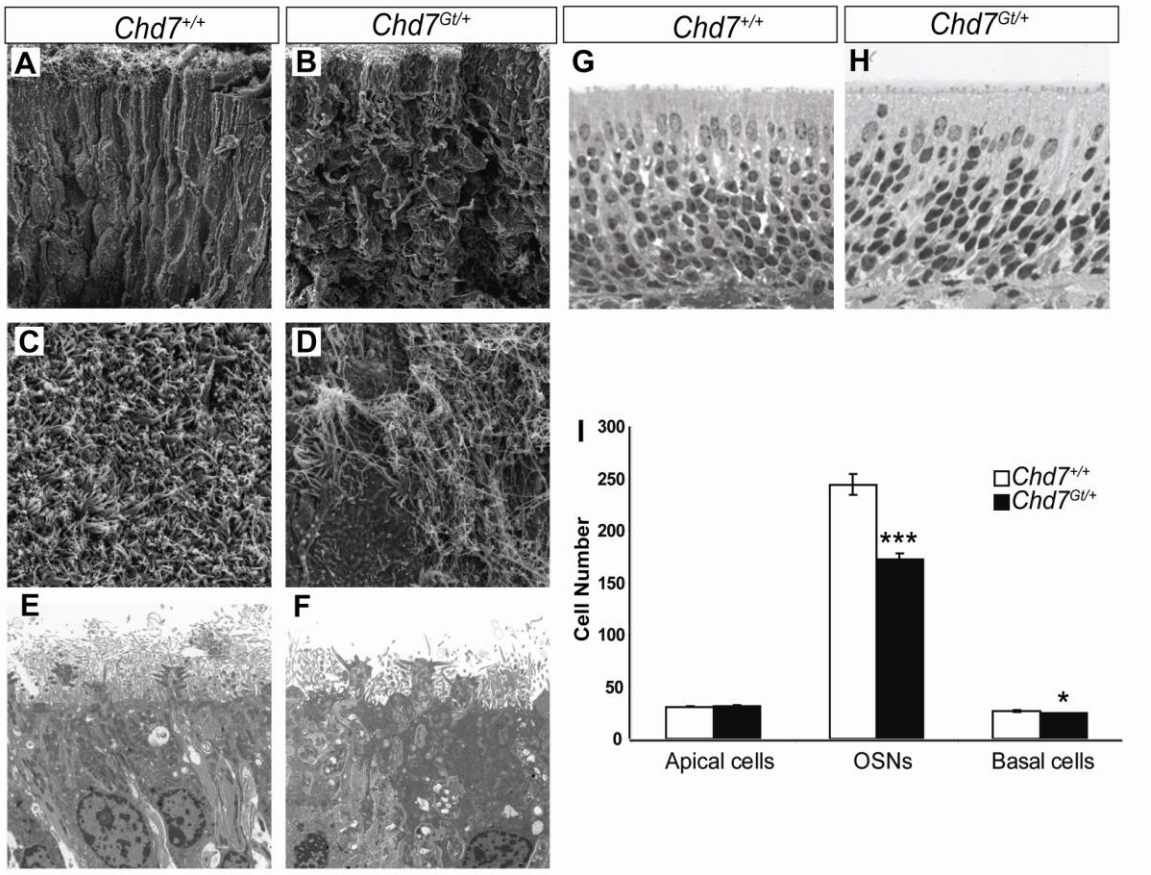

Figure 2.7 Olfactory sensory neurons in *Chd7*$^{Gt/+}$ mutant mice are disorganized and reduced in number. Scanning electron micrographs of the olfactory epithelium show loss of the orderly arrangement of olfactory sensory neurons in (B) *Chd7*$^{Gt/+}$ mice (N = 4) compared to (A) wild type littermates (N = 4). Olfactory cilia are present in wild type and *Chd7*$^{Gt/+}$ mice; however, *Chd7*$^{Gt/+}$ mice have variable distribution of cilia on the apical surface (C, D). Transmission electron micrographs from *Chd7*$^{Gt/+}$ mice (N = 3) compared to wild type littermates (N = 3) show that olfactory sensory neurons from *Chd7*$^{Gt/+}$ mice properly extend dendrites to the apical surface and have cilia which project along the nasal mucosa (E, F). Light microscopy of olfactory epithelial tissues processed for TEM (G, H) shows a reduction in olfactory sensory neurons. Cell counts of TEM tissue sections (I) show a significant reduction in *Chd7*$^{Gt/+}$ (closed bars) olfactory sensory neurons and basal cells compared to wild type (open bars) littermates * $P < 0.05$ and *** $P < 0.001$ as determined by unpaired Student's t test. Abbreviation: OSNs (olfactory sensory neurons).

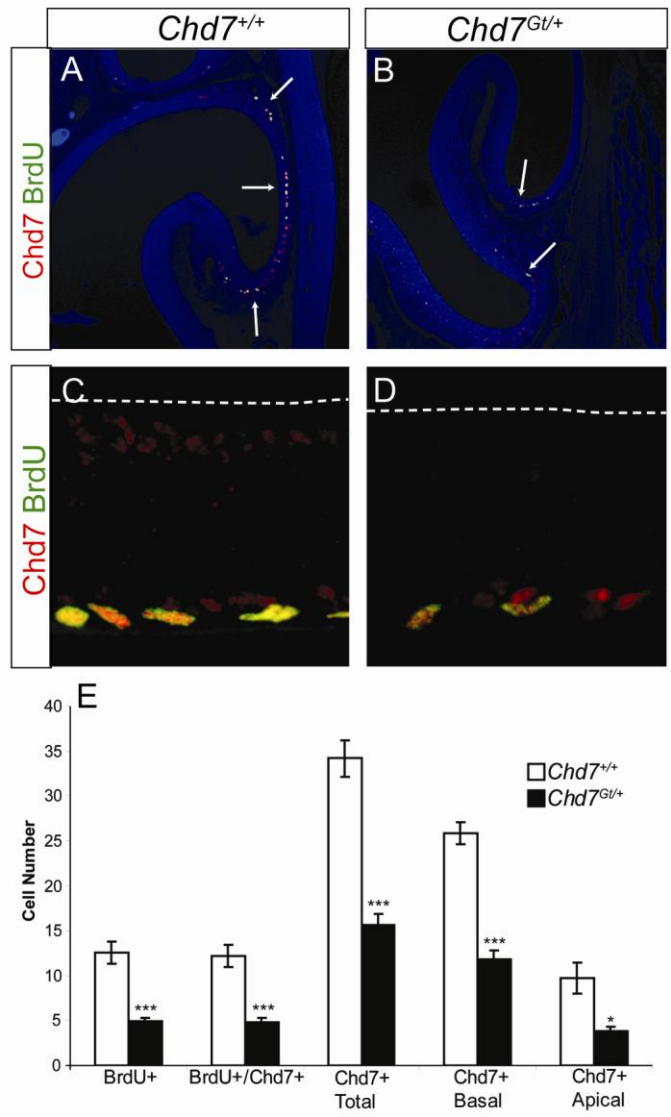

Figure 2.8 Olfactory epithelial basal cell proliferation is reduced in *Chd7*$^{Gt/+}$ mice. Adult wild type and *Chd7*$^{Gt/+}$ mice were exposed to BrdU 30 minutes prior to tissue collection, then processed for double immunofluorescence with anti-BrdU and anti-CHD7. Many CHD7-positive basal cells are actively dividing, based on co-localization between anti-CHD7 and anti-BrdU (A-D). *Chd7* is highly expressed in crypt regions (marked by arrows) which also appear to be regions of high proliferation in the olfactory epithelium (A, B). White dotted lines in C and D indicate the apical surface of the epithelium. Cell counts (wild type = open bars, *Chd7*$^{Gt/+}$ = closed bars) show a 50% reduction in the number of BrdU-positive cells in the *Chd7*$^{Gt/+}$ olfactory epithelium and a 50% reduction in the number of all CHD7-positive cells (basal and apical). * $P < 0.05$ and *** $P < 0.001$ as determined by unpaired Student's t test.

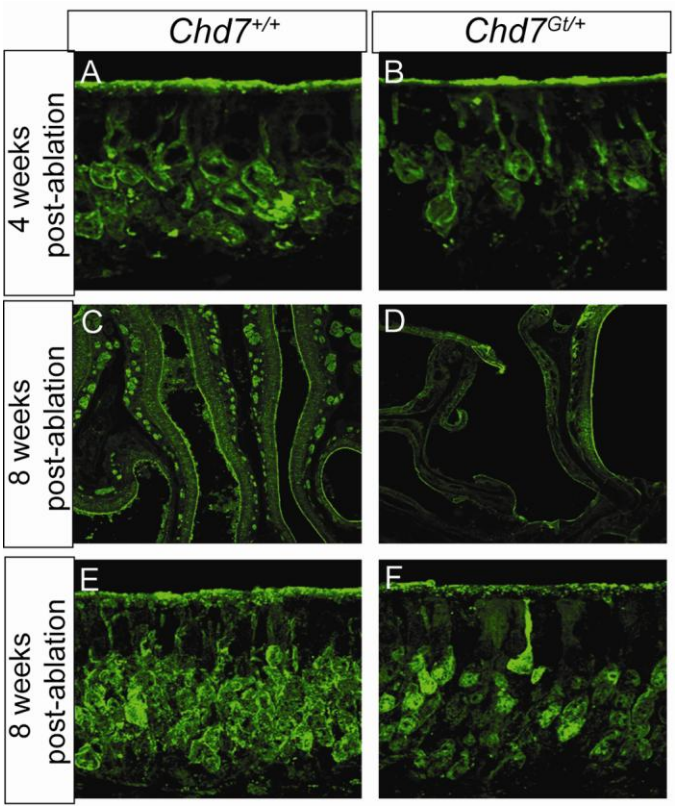

Figure 2.9 *Chd7*$^{Gt/+}$ mice exhibit altered regeneration of olfactory sensory neurons in the olfactory epithelium after chemical ablation. Six-week old wild type (N = 9) and *Chd7*$^{Gt/+}$ mice (N = 8) were given an intranasal infusion of 1% Triton-X 100 in saline then sacrificed 2, 4, or 8 weeks later. The olfactory epithelium at 4 weeks post-ablation (A, B) shows olfactory sensory neurons in both wild type (N = 4) and *Chd7*$^{Gt/+}$ (N = 4) littermates, with some disorganization and reduced OMP label. At 8 weeks post-ablation (C-F), wild type mice (N = 4) exhibit a normal appearing olfactory epithelium while *Chd7*$^{Gt/+}$ mice (N = 4) have regionally restricted OMP staining and OSN regeneration.

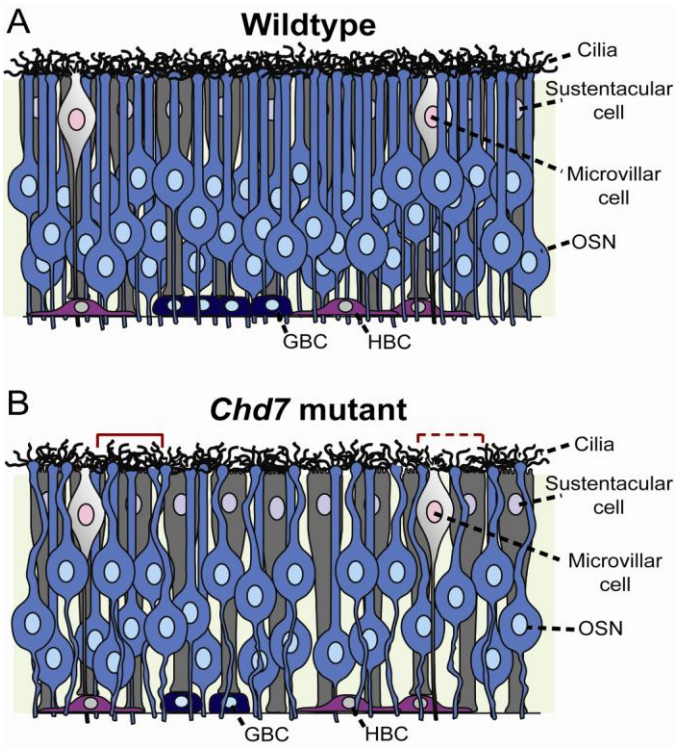

Figure 2.10 Diagram of the *Chd7* mutant mouse olfactory epithelium. Wild type (A) and *Chd7* mutant (B) mouse olfactory epithelium is depicted with all of the main cell types including olfactory sensory neurons (blue), sustentacular cells (dark gray), globose basal cells (GBCs; purple), horizontal basal cells (HBCs; pink), and microvillar cells (white). *Chd7* mutant mice have approximately 30% fewer olfactory sensory neurons and 50% fewer GBCs compared to wild type. Red bars indicate regions of normal cilia density (solid) and sparse cilia density (dashed). *Chd7* mutants have fewer olfactory sensory neurons, which causes gaps between the olfactory sensory neurons and a loss of support leading to a disorganized appearance. Abbreviation: OSNs (olfactory sensory neurons).

Patient #	B-SIT score	Exon	Mutation	De Novo vs. Familial
1	**3**	**2**	R312X	unknown
2	**1**	**11**	c.2836-15C>G	unknown
3	**5**	**12**	L1007P	unknown
4	**0**	**12**	T1027_P1029del	De Novo
5	**1**	**20**	R1557fsX1558	unknown
6	**8**	**33**	R2319S	Familial
7	**9**	**33**	R2319S	Familial
8	**11**	**33**	W2332X	De Novo

Table 2.1 Humans with CHD7 mutations and CHARGE syndrome have variable reductions in olfaction. Brief Smell Identification Tests (B-SIT) were performed on eight individuals with CHD7 mutations and a clinical phenotype of CHARGE. B-SIT scores of 9 or higher are considered normal.

References

1 Harris, J., Robert, E. and Kallen, B. (1997) Epidemiology of choanal atresia with special reference to the CHARGE association. *Pediatrics*, **99**, 363-367.

2 Issekutz, K.A., Graham, J.M., Jr., Prasad, C., Smith, I.M. and Blake, K.D. (2005) An epidemiological analysis of CHARGE syndrome: preliminary results from a Canadian study. *American journal of medical genetics*, **133**, 309-317.

3 Kallen, K., Robert, E., Mastroiacovo, P., Castilla, E.E. and Kallen, B. (1999) CHARGE Association in newborns: a registry-based study. *Teratology*, **60**, 334-343.

4 Hall, B.D. (1979) Choanal atresia and associated multiple anomalies. *The Journal of pediatrics*, **95**, 395-398.

5 Aramaki, M., Udaka, T., Kosaki, R., Makita, Y., Okamoto, N., Yoshihashi, H., Oki, H., Nanao, K., Moriyama, N., Oku, S. *et al.* (2006) Phenotypic spectrum of CHARGE syndrome with CHD7 mutations. *J Pediatr*, **148**, 410-414.

6 Jongmans, M.C., Admiraal, R.J., van der Donk, K.P., Vissers, L.E., Baas, A.F., Kapusta, L., van Hagen, J.M., Donnai, D., de Ravel, T.J., Veltman, J.A. *et al.* (2006) CHARGE syndrome: the phenotypic spectrum of mutations in the CHD7 gene. *J Med Genet*, **43**, 306-314.

7 Lalani, S.R., Safiullah, A.M., Fernbach, S.D., Harutyunyan, K.G., Thaller, C., Peterson, L.E., McPherson, J.D., Gibbs, R.A., White, L.D., Hefner, M. *et al.* (2006)

Spectrum of CHD7 Mutations in 110 Individuals with CHARGE Syndrome and Genotype-Phenotype Correlation. *American journal of human genetics*, **78**, 303-314.

8 Sanlaville, D., Etchevers, H.C., Gonzales, M., Martinovic, J., Clement-Ziza, M., Delezoide, A.L., Aubry, M.C., Pelet, A., Chemouny, S., Cruaud, C. *et al.* (2006) Phenotypic spectrum of CHARGE syndrome in fetuses with CHD7 truncating mutations correlates with expression during human development. *Journal of medical genetics*, **43**, 211-217.

9 Sanlaville, D. and Verloes, A. (2007) CHARGE syndrome: an update. *Eur J Hum Genet*, **15**, 389-399.

10 Vissers, L.E., van Ravenswaaij, C.M., Admiraal, R., Hurst, J.A., de Vries, B.B., Janssen, I.M., van der Vliet, W.A., Huys, E.H., de Jong, P.J., Hamel, B.C. *et al.* (2004) Mutations in a new member of the chromodomain gene family cause CHARGE syndrome. *Nature genetics*, **36**, 955-957.

11 Vuorela, P., Ala-Mello, S., Saloranta, C., Penttinen, M., Poyhonen, M., Huoponen, K., Borozdin, W., Bausch, B., Botzenhart, E.M., Wilhelm, C. *et al.* (2007) Molecular analysis of the CHD7 gene in CHARGE syndrome: identification of 22 novel mutations and evidence for a low contribution of large CHD7 deletions. *Genet Med*, **9**, 690-694.

12 Delahaye, A., Sznajer, Y., Lyonnet, S., Elmaleh-Berges, M., Delpierre, I., Audollent, S., Wiener-Vacher, S., Mansbach, A.L., Amiel, J., Baumann, C. *et al.* (2007)

Familial CHARGE syndrome because of CHD7 mutation: clinical intra- and interfamilial variability. *Clin Genet*, **72**, 112-121.

13 Jongmans, M.C., Hoefsloot, L.H., van der Donk, K.P., Admiraal, R.J., Magee, A., van de Laar, I., Hendriks, Y., Verheij, J.B., Walpole, I., Brunner, H.G. *et al.* (2008) Familial CHARGE syndrome and the CHD7 gene: a recurrent missense mutation, intrafamilial recurrence and variability. *Am J Med Genet A*, **146**, 43-50.

14 Vuorela, P.E., Penttinen, M.T., Hietala, M.H., Laine, J.O., Huoponen, K.A. and Kääriäinen, H.A. (2008) A familial CHARGE syndrome with a CHD7 nonsense mutation and new clinical features. *Clinical dysmorphology*, **17**, 249-253.

15 Asakura, Y., Toyota, Y., Muroya, K., Kurosawa, K., Fujita, K., Aida, N., Kawame, H., Kosaki, K. and Adachi, M. (2008) Endocrine and radiological studies in patients with molecularly confirmed CHARGE syndrome. *The Journal of clinical endocrinology and metabolism*, **93**, 920-924.

16 Azoulay, R., Fallet-Bianco, C., Garel, C., Grabar, S., Kalifa, G. and Adamsbaum, C. (2006) MRI of the olfactory bulbs and sulci in human fetuses. *Pediatric radiology*, **36**, 97-107.

17 Blustajn, J., Kirsch, C.F., Panigrahy, A. and Netchine, I. (2008) Olfactory anomalies in CHARGE syndrome: imaging findings of a potential major diagnostic criterion. *Ajnr*, **29**, 1266-1269.

18 Chalouhi, C., Faulcon, P., Le Bihan, C., Hertz-Pannier, L., Bonfils, P. and Abadie, V. (2005) Olfactory evaluation in children: application to the CHARGE syndrome. *Pediatrics*, **116**, e81-88.

19 Ogata, T., Fujiwara, I., Ogawa, E., Sato, N., Udaka, T. and Kosaki, K. (2006) Kallmann syndrome phenotype in a female patient with CHARGE syndrome and CHD7 mutation. *Endocrine journal*, **53**, 741-743.

20 Pinto, G., Abadie, V., Mesnage, R., Blustajn, J., Cabrol, S., Amiel, J., Hertz-Pannier, L., Bertrand, A.M., Lyonnet, S., Rappaport, R. *et al.* (2005) CHARGE syndrome includes hypogonadotropic hypogonadism and abnormal olfactory bulb development. *The Journal of clinical endocrinology and metabolism*, **90**, 5621-5626.

21 Bosman, E.A., Penn, A.C., Ambrose, J.C., Kettleborough, R., Stemple, D.L. and Steel, K.P. (2005) Multiple mutations in mouse Chd7 provide models for CHARGE syndrome. *Human molecular genetics*, **14**, 3463-3476.

22 Hurd, E.A., Capers, P.L., Blauwkamp, M.N., Adams, M.E., Raphael, Y., Poucher, H.K. and Martin, D.M. (2007) Loss of Chd7 function in gene-trapped reporter mice is embryonic lethal and associated with severe defects in multiple developing tissues. *Mamm Genome*, **18**, 94-104.

23 Shur, I. and Benayahu, D. (2005) Characterization and functional analysis of CReMM, a novel chromodomain helicase DNA-binding protein. *Journal of molecular biology*, **352**, 646-655.

24 Woodage, T., Basrai, M.A., Baxevanis, A.D., Hieter, P. and Collins, F.S. (1997) Characterization of the CHD family of proteins. *Proceedings of the National Academy of Sciences of the United States of America*, **94**, 11472-11477.

25 Becker, P.B. and Horz, W. (2002) ATP-dependent nucleosome remodeling. *Annual review of biochemistry*, **71**, 247-273.

26 Eberharter, A. and Becker, P.B. (2004) ATP-dependent nucleosome remodelling: factors and functions. *Journal of cell science*, **117**, 3707-3711.

27 Lusser, A. and Kadonaga, J.T. (2003) Chromatin remodeling by ATP-dependent molecular machines. *Bioessays*, **25**, 1192-1200.

28 Narlikar, G.J., Fan, H.Y. and Kingston, R.E. (2002) Cooperation between complexes that regulate chromatin structure and transcription. *Cell*, **108**, 475-487.

29 Smith, C.L. and Peterson, C.L. (2005) ATP-dependent chromatin remodeling. *Current topics in developmental biology*, **65**, 115-148.

30 Srinivasan, S., Dorighi, K.M. and Tamkun, J.W. (2008) Drosophila Kismet regulates histone H3 lysine 27 methylation and early elongation by RNA polymerase II. *PLoS genetics*, **4**, e1000217.

31 Takada, I., Mihara, M., Suzawa, M., Ohtake, F., Kobayashi, S., Igarashi, M., Youn, M.Y., Takeyama, K., Nakamura, T., Mezaki, Y. *et al.* (2007) A histone lysine

methyltransferase activated by non-canonical Wnt signalling suppresses PPAR-gamma transactivation. *Nature cell biology*, **9**, 1273-1285.

32 Kim, H.G., Kurth, I., Lan, F., Meliciani, I., Wenzel, W., Eom, S.H., Kang, G.B., Rosenberger, G., Tekin, M., Ozata, M. *et al.* (2008) Mutations in CHD7, encoding a chromatin-remodeling protein, cause idiopathic hypogonadotropic hypogonadism and Kallmann syndrome. *American journal of human genetics*, **83**, 511-519.

33 Murdoch, B. and Roskams, A.J. (2007) Olfactory epithelium progenitors: insights from transgenic mice and in vitro biology. *Journal of molecular histology*, **38**, 581-599.

34 Monti-Graziadei, G.A., Margolis, F.L., Harding, J.W. and Graziadei, P.P. (1977) Immunocytochemistry of the olfactory marker protein. *J Histochem Cytochem*, **25**, 1311-1316.

35 Saito, H., Kubota, M., Roberts, R.W., Chi, Q. and Matsunami, H. (2004) RTP family members induce functional expression of mammalian odorant receptors. *Cell*, **119**, 679-691.

36 Nadi, N.S., Head, R., Grillo, M., Hempstead, J., Grannot-Reisfeld, N. and Margolis, F.L. (1981) Chemical deafferentation of the olfactory bulb: plasticity of the levels of tyrosine hydroxylase, dopamine and norepinephrine. *Brain research*, **213**, 365-377.

37 Hegg, C.C. and Lucero, M.T. (2004) Dopamine reduces odor- and elevated-K(+)-induced calcium responses in mouse olfactory receptor neurons in situ. *Journal of neurophysiology*, **91**, 1492-1499.

38 Banger, K.K., Foster, J.R., Lock, E.A. and Reed, C.J. (1994) Immunohistochemical localisation of six glutathione S-transferases within the nasal cavity of the rat. *Archives of toxicology*, **69**, 91-98.

39 Krishna, N.S., Getchell, T.V. and Getchell, M.L. (1994) Differential expression of alpha, mu, and pi classes of glutathione S-transferases in chemosensory mucosae of rats during development. *Cell and tissue research*, **275**, 435-450.

40 McEwen, D.P., Koenekoop, R.K., Khanna, H., Jenkins, P.M., Lopez, I., Swaroop, A. and Martens, J.R. (2007) Hypomorphic CEP290/NPHP6 mutations result in anosmia caused by the selective loss of G proteins in cilia of olfactory sensory neurons. *Proceedings of the National Academy of Sciences of the United States of America*, **104**, 15917-15922.

41 Fath, M.A., Mullins, R.F., Searby, C., Nishimura, D.Y., Wei, J., Rahmouni, K., Davis, R.E., Tayeh, M.K., Andrews, M., Yang, B. *et al.* (2005) Mkks-null mice have a phenotype resembling Bardet-Biedl syndrome. *Human molecular genetics*, **14**, 1109-1118.

42 Kulaga, H.M., Leitch, C.C., Eichers, E.R., Badano, J.L., Lesemann, A., Hoskins, B.E., Lupski, J.R., Beales, P.L., Reed, R.R. and Katsanis, N. (2004) Loss of BBS proteins

causes anosmia in humans and defects in olfactory cilia structure and function in the mouse. *Nature genetics*, **36**, 994-998.

43 Reed, R.R. (1992) Signaling pathways in odorant detection. *Neuron*, **8**, 205-209.

44 Calof, A.L., Bonnin, A., Crocker, C., Kawauchi, S., Murray, R.C., Shou, J. and Wu, H.H. (2002) Progenitor cells of the olfactory receptor neuron lineage. *Microscopy research and technique*, **58**, 176-188.

45 Calof, A.L., Mumm, J.S., Rim, P.C. and Shou, J. (1998) The neuronal stem cell of the olfactory epithelium. *Journal of neurobiology*, **36**, 190-205.

46 Calof, A.L., Rim, P.C., Askins, K.J., Mumm, J.S., Gordon, M.K., Iannuzzelli, P. and Shou, J. (1998) Factors regulating neurogenesis and programmed cell death in mouse olfactory epithelium. *Annals of the New York Academy of Sciences*, **855**, 226-229.

47 Iwai, N., Zhou, Z., Roop, D.R. and Behringer, R.R. (2008) Horizontal basal cells are multipotent progenitors in normal and injured adult olfactory epithelium. *Stem cells (Dayton, Ohio)*, **26**, 1298-1306.

48 Nicolay, D.J., Doucette, J.R. and Nazarali, A.J. (2006) Transcriptional regulation of neurogenesis in the olfactory epithelium. *Cellular and molecular neurobiology*, **26**, 803-821.

49 Weiler, E. and Farbman, A.I. (1997) Proliferation in the rat olfactory epithelium: age-dependent changes. *J Neurosci*, **17**, 3610-3622.

50 Bagchi, A., Papazoglu, C., Wu, Y., Capurso, D., Brodt, M., Francis, D., Bredel, M., Vogel, H. and Mills, A.A. (2007) CHD5 is a tumor suppressor at human 1p36. *Cell*, **128**, 459-475.

51 Goehler, H., Lalowski, M., Stelzl, U., Waelter, S., Stroedicke, M., Worm, U., Droege, A., Lindenberg, K.S., Knoblich, M., Haenig, C. *et al.* (2004) A protein interaction network links GIT1, an enhancer of huntingtin aggregation, to Huntington's disease. *Molecular cell*, **15**, 853-865.

52 Minty, A., Dumont, X., Kaghad, M. and Caput, D. (2000) Covalent modification of p73alpha by SUMO-1. Two-hybrid screening with p73 identifies novel SUMO-1-interacting proteins and a SUMO-1 interaction motif. *The Journal of biological chemistry*, **275**, 36316-36323.

53 Schmidt, D.R. and Schreiber, S.L. (1999) Molecular association between ATR and two components of the nucleosome remodeling and deacetylating complex, HDAC2 and CHD4. *Biochemistry*, **38**, 14711-14717.

54 Stelzl, U., Worm, U., Lalowski, M., Haenig, C., Brembeck, F.H., Goehler, H., Stroedicke, M., Zenkner, M., Schoenherr, A., Koeppen, S. *et al.* (2005) A human protein-protein interaction network: a resource for annotating the proteome. *Cell*, **122**, 957-968.

55 Tai, H.H., Geisterfer, M., Bell, J.C., Moniwa, M., Davie, J.R., Boucher, L. and McBurney, M.W. (2003) CHD1 associates with NCoR and histone deacetylase as well as

with RNA splicing proteins. *Biochemical and biophysical research communications*, **308**, 170-176.

56 Tong, J.K., Hassig, C.A., Schnitzler, G.R., Kingston, R.E. and Schreiber, S.L. (1998) Chromatin deacetylation by an ATP-dependent nucleosome remodelling complex. *Nature*, **395**, 917-921.

57 Jepsen, K., Solum, D., Zhou, T., McEvilly, R.J., Kim, H.J., Glass, C.K., Hermanson, O. and Rosenfeld, M.G. (2007) SMRT-mediated repression of an H3K27 demethylase in progression from neural stem cell to neuron. *Nature*, **450**, 415-419.

58 Lunyak, V.V., Burgess, R., Prefontaine, G.G., Nelson, C., Sze, S.H., Chenoweth, J., Schwartz, P., Pevzner, P.A., Glass, C., Mandel, G. *et al.* (2002) Corepressor-dependent silencing of chromosomal regions encoding neuronal genes. *Science (New York, N.Y.)*, **298**, 1747-1752.

59 Schnetz MP, B.C., Shastri K, Balasubramanian D, Zentner G, , Balaji R, Z.X., Song L, Wang Z, LaFramboise T, Crawford GE, and PC, S. (2009) Genomic distribution of CHD7 on chromatin tracks H3K4 methylation patterns. *Genome research*, **in press**.

60 Omodei, D., Acampora, D., Mancuso, P., Prakash, N., Di Giovannantonio, L.G., Wurst, W. and Simeone, A. (2008) Anterior-posterior graded response to Otx2 controls proliferation and differentiation of dopaminergic progenitors in the ventral mesencephalon. *Development (Cambridge, England)*, **135**, 3459-3470.

61 Shou, J., Murray, R.C., Rim, P.C. and Calof, A.L. (2000) Opposing effects of bone morphogenetic proteins on neuron production and survival in the olfactory receptor neuron lineage. *Development (Cambridge, England)*, **127**, 5403-5413.

62 Shou, J., Rim, P.C. and Calof, A.L. (1999) BMPs inhibit neurogenesis by a mechanism involving degradation of a transcription factor. *Nature neuroscience*, **2**, 339-345.

63 Jongmans, M.C., van Ravenswaaij-Arts, C.M., Pitteloud, N., Ogata, T., Sato, N., Claahsen-van der Grinten, H.L., van der Donk, K., Seminara, S., Bergman, J.E., Brunner, H.G. *et al.* (2009) CHD7 mutations in patients initially diagnosed with Kallmann syndrome--the clinical overlap with CHARGE syndrome. *Clinical genetics*, **75**, 65-71.

64 Doty, R.L. (1997) Studies of human olfaction from the University of Pennsylvania Smell and Taste Center. *Chemical senses*, **22**, 565-586.

65 Double, K.L., Rowe, D.B., Hayes, M., Chan, D.K., Blackie, J., Corbett, A., Joffe, R., Fung, V.S., Morris, J. and Halliday, G.M. (2003) Identifying the pattern of olfactory deficits in Parkinson disease using the brief smell identification test. *Archives of neurology*, **60**, 545-549.

66 Kjelvik, G., Sando, S.B., Aasly, J., Engedal, K.A. and White, L.R. (2007) Use of the Brief Smell Identification Test for olfactory deficit in a Norwegian population with Alzheimer's disease. *International journal of geriatric psychiatry*, **22**, 1020-1024.

67 Salerno-Kennedy, R., Cusack, S. and Cashman, K.D. (2005) Olfactory function in people with genetic risk of dementia. *Irish journal of medical science*, **174**, 46-50.

68 Sclafani, A.M., Skidmore, J.M., Ramaprakash, H., Trumpp, A., Gage, P.J. and Martin, D.M. (2006) Nestin-Cre mediated deletion of Pitx2 in the mouse. *Genesis*, **44**, 336-344.

69 Osborne, M.P. and Comis, S.D. (1991) Preparation of inner ear sensory hair bundles for high resolution scanning electron microscopy. *Scanning microscopy*, **5**, 555-564.

70 Anderson, D.W., Probst, F.J., Belyantseva, I.A., Fridell, R.A., Beyer, L., Martin, D.M., Wu, D., Kachar, B., Friedman, T.B., Raphael, Y. *et al.* (2000) The motor and tail regions of myosin XV are critical for normal structure and function of auditory and vestibular hair cells. *Human molecular genetics*, **9**, 1729-1738.

71 Beyer, L.A., Odeh, H., Probst, F.J., Lambert, E.H., Dolan, D.F., Camper, S.A., Kohrman, D.C. and Raphael, Y. (2000) Hair cells in the inner ear of the pirouette and shaker 2 mutant mice. *Journal of neurocytology*, **29**, 227-240.

72 Raphael, Y., Kobayashi, K.N., Dootz, G.A., Beyer, L.A., Dolan, D.F. and Burmeister, M. (2001) Severe vestibular and auditory impairment in three alleles of Ames waltzer (av) mice. *Hearing research*, **151**, 237-249.

73 Washburn, K.B., Turner, T.J. and Talamo, B.R. (2002) Comparison of mechanical agitation and calcium shock methods for preparation of a membrane fraction enriched in olfactory cilia. *Chemical senses*, **27**, 635-642.

Chapter 3

Reproductive dysfunction and decreased GnRH neurogenesis in a mouse model of CHARGE syndrome[1]

Abstract

CHARGE is a multiple congenital anomaly disorder and a common cause of pubertal defects, olfactory dysfunction, growth delays, deaf-blindness, balance disorders, and congenital heart malformations. Mutations in *CHD7*, the gene encoding chromodomain helicase DNA binding protein 7, are present in 60-80% of individuals with CHARGE syndrome. Mutations in *CHD7* have also been reported in Kallmann syndrome (olfactory dysfunction, delayed puberty, and hypogonadotropic hypogonadism). CHD7 is a positive regulator of neural stem cell proliferation and olfactory sensory neuron formation in the olfactory epithelium, suggesting that loss of CHD7 might also disrupt development of other neural populations. Here we report that female $Chd7^{Gt/+}$ mice have delays in vaginal opening and estrus onset, and erratic estrus cycles. $Chd7^{Gt/+}$ mice also have decreased circulating levels of LH and FSH but apparently normal responsiveness to GnRH agonist and antagonist treatment. GnRH neurons in the adult $Chd7^{Gt/+}$ hypothalamus and embryonic nasal region are diminished, and there is decreased cellular proliferation in the embryonic olfactory placode. Expression levels of *GnRH1* and *Otx2* in the hypothalamus and *GnRHR* in the pituitary

are significantly reduced in adult *Chd7*$^{Gt/+}$ mice. Additionally, *Chd7* mutant embryos have CHD7 dosage dependent reductions in expression levels of *Fgfr1, Bmp4,* and *Otx2* in the olfactory placode. Together, these data suggest that CHD7 has critical roles in the development and maintenance of GnRH neurons for regulating puberty and reproduction.

Introduction

In humans, heterozygous mutations in *chromodomain helicase DNA binding protein 7* (*CHD7*) cause CHARGE syndrome, a clinically variable, multiple congenital anomaly condition with an estimated incidence of 1:8500-1:12,000 in newborns (1-3). CHARGE is characterized by ocular coloboma, heart defects, atresia of the choanae, retarded growth and development, genital hypoplasia, and ear abnormalities including deafness and vestibular disorders (4). Genital hypoplasia occurs in approximately 62% of CHARGE individuals with confirmed *CHD7* mutations, and gonadotropins (luteinizing hormone (LH) and follicle-stimulating hormone (FSH)) are deficient in 81% of males and 93% of females (5-12).

The gonadotropic hormones LH and FSH are generated and secreted from the pituitary in response to gonadotropin-releasing hormone (GnRH) from the median eminence (13-16). GnRH production is dependent upon multiple signaling mechanisms including sex-steroid feed-back regulation, kisspeptin-GPR54 signaling, and leptin signaling (14, 15, 17). Transcription of *GnRH1* requires the paired-like homeodomain transcription factor OTX2 (18-20). OTX2 is also required for neurogenesis in multiple tissues (21, 22). GnRH neurogenesis is partially regulated by FGF signaling, and

mutations in *FGF8* and *FGFR1* cause hypogonadotropic hypogonadism and olfactory dysfunction in humans and mice (23-28).

Mice with heterozygous loss of *Chd7* (*Chd7*$^{Gt/+}$) have olfactory defects (29) similar to those reported in CHARGE individuals, and are an excellent model for CHARGE syndrome. *Chd7* is highly expressed in the developing mouse and human olfactory epithelium (29-31), where GnRH neurons are born (32). In mice and humans, *Chd7* is expressed in the developing (30, 31) and mature hypothalamus, and in GnRH neuronal cell lines (8). CHD7 is hypothesized to influence gene expression by regulating access to chromatin through binding and unwinding chromatin (33-37), and CHD7 is likely to participate in multiple protein complexes that regulate transcription. Based on prior studies showing that CHD7 is critical for olfactory neural stem cell proliferation and regeneration of olfactory sensory neurons (29), we hypothesized that CHD7 may also regulate one or more aspects of GnRH neurogenesis. To test this, we analyzed *Chd7*$^{Gt/+}$ mice for pubertal development and underlying cellular mechanisms involved in hypogonadotropic hypogonadism.

Results

Analysis of puberty and estrus cycles

Endocrine defects including delayed puberty, hypogonadotropic hypogonadism, and genital hypoplasia have been reported in CHARGE individuals (5-11). Prior studies of the reproductive system in *Chd7*$^{Whi/+}$ mice, a model of CHARGE syndrome, reported an increased time to first litter and hypoplasia of the testes, clitoris, and uterus compared to wild type mice (38, 39). Based on these reproductive defects, we hypothesized that

mice deficient for *Chd7* might have underlying endocrine abnormalities. To test this, we analyzed female *Chd7*$^{Gt/+}$ mice which are heterozygous for a gene trapped loss of function *lacZ* reporter allele (30). Homozygous *Chd7*$^{Gt/Gt}$ embryos die by E11, presumably from cardiac or other internal organ defects (30). Recently weaned female wild type (*n = 5*) and *Chd7*$^{Gt/+}$ (*n = 6*) littermate mice were examined for vaginal opening and first estrus, two well established markers of rodent sexual maturity (Figure 3.1 A) (40). Vaginal opening was significantly delayed and occurs an average of 5 days later in *Chd7*$^{Gt/+}$ female mice (postnatal day 32) compared to wild type littermates (postnatal day 27) (Figure 3.1 A). Vaginal smears taken from both wild type and *Chd7*$^{Gt/+}$ littermate females showed that *Chd7*$^{Gt/+}$ female mice achieve first estrus on postnatal day 43, ten days later than their wild type littermates (postnatal day 33) (Figure 3.1 A).

Establishment of estrus cyclicity is another measure of reproductive health and development in mice, and the timing of cyclicity onset can be variable between inbred strains (40). Cyclicity in mice is defined by the sequential attainment of each stage of estrus during a 4-7 day period of time (40). To determine the onset of estrus cyclicity, vaginal smears were analyzed daily in female wild type (*n = 5*) and *Chd7*$^{Gt/+}$ (*n = 6*) mice for 3 months (Figure 3.1 B-D). In contrast to wild type littermates, female *Chd7*$^{Gt/+}$ mice have highly erratic estrus cycles, with no apparent pattern of timing or duration of cycle stages (Figure 3.1 B-D).

Body size can influence pubertal development in both humans and mice (40-45). For example, vaginal opening in wild type female mice is dependent upon attainment of a threshold body size (40). Both male and female *Chd7* deficient mice and humans with

CHARGE syndrome have postnatally acquired growth delays and reduced body size (12, 30, 39). We examined female wild type (*n = 5*) and *Chd7*$^{Gt/+}$ (*n = 6*) littermate mice for pubertal markers with respect to body size. Vaginal opening corresponds to attainment of a body size of approximately 15 grams in both wild type and *Chd7*$^{Gt/+}$ female littermates (Figure 3.1 E). However, wild type females have first estrus at approximately 18 grams, while *Chd7*$^{Gt/+}$ females have first estrus at approximately 15 grams.

Metabolic cues and nutritional state are also key elements involved in proper pubertal development (42-48). Defects in the leptin, insulin, GH, or IGF-1 signaling pathway have been reported to cause delayed puberty, hypogonadotropic hypogonadism and/or infertility (49-55). Levels of leptin, insulin, GH, and IGF-1 are also sensitive to nutritional state, with circulating levels that vary between 2- and 5-fold after fasting (56). To further explore factors that may influence pubertal development, female wild type (*n = 4*) and *Chd7*$^{Gt/+}$ (*n = 4*) littermate mice were analyzed for circulating levels of insulin and leptin (Figure 3.1 F). Insulin and leptin levels were not altered in *Chd7*$^{Gt/+}$ females compared to wild type (Figure 3.1 F). Additionally, circulating levels of growth hormone (GH) and insulin-like growth factor 1 (IGF1) were similar in wild type (*n = 4*) and *Chd7*$^{Gt/+}$ (*n = 4*) littermate females (Figure 3.1 G, H) and males (data not shown). Although we could detect no significant differences in insulin, leptin, GH, or IGF1, *Chd7*$^{Gt/+}$ mice (male and female) are significantly smaller than their wild type littermates (30). Our data cannot completely rule out a more subtle defect in metabolism or nutrition that may influence reproduction in *Chd7*$^{Gt/+}$ mice.

Chd7$^{Gt/+}$ mice have decreased levels of circulating gonadotropic hormones

CHARGE individuals are reported to have hypogonadotropic hypogonadism and variable response to GnRH stimulation (5-11). To test the integrity of the hypothalamic-pituitary axis, we assayed circulating levels of LH and FSH in 3-4 month old wild type (males *n = 4*, females *n = 5*) and *Chd7*$^{Gt/+}$ (males *n = 5*, females *n = 6*) sex-matched littermate mice (Figure 2 A, B). Circulating levels of female gonadotropic hormones fluctuate dependent upon stage of estrus (57); therefore, we collected serum from all females at late estrus. We found that *Chd7*$^{Gt/+}$ female mice have reduced levels of circulating LH (74% decrease) and FSH (83% decrease) in comparison to wild type littermates (Figure 3.2 A, B). *Chd7*$^{Gt/+}$ male mice also have reduced levels of circulating LH (86% decrease) whereas levels of FSH are normal (Figure 3.2 A, B). Interestingly, studies of *Fshβ*$^{-/-}$ mice reported that FSH is not required for male fertility but is required for female fertility (58, 59). In contrast, *Fshβ* mutations in human males cause azoospermia and infertility (60, 61). *Fshβ* is also expressed independent of GnRH signaling in an activin-dependent pathway (62, 63), and LH and FSH are differentially regulated by GnRH during development (64).

Chd7$^{Gt/+}$ mice respond normally to GnRH agonist stimulation

Hypogonadotropic hypogonadism can be caused by defects in the hypothalamus, the pituitary, or both. Mutations in the GnRH receptor gene, *GnRHR*, cause pituitary gonadotrope insensitivity to GnRH stimulation and subsequent hypogonadotropic hypogonadism (65, 66), whereas mutations in genes such as *GPR54* or *GnRH1* affect GnRH neuronal function at the level of the hypothalamus (67, 68). Mutations in genes

affecting GnRH neuronal function could therefore mask a normal ability of pituitary gonadotropes to respond to GnRH. To test this, we administered the GnRH agonist, leuprolide, to 3-4 month old wild type (males *n = 4*, females *n = 3*) and *Chd7*$^{Gt/+}$ (males *n = 4*, females *n = 4*) sex-matched, late estrus-matched (females) littermate mice. In mice, leuprolide causes a rapid (between 70 to 180 minutes) increase in production and circulation of LH and FSH (69, 70). Wild type and *Chd7*$^{Gt/+}$ mice had similar circulating levels of LH and FSH measured 2 hours following leuprolide administration (Figure 3.2 C, D). These observations are consistent with normal pituitary gonadotrope responsiveness to GnRH agonist in *Chd7*$^{Gt/+}$ mice.

Male *Chd7*$^{Gt/+}$ mice have normal baseline circulating levels of FSH (Figure 3.2 B). To determine whether pituitary gonadotropes in *Chd7*$^{Gt/+}$ males constitutively produce FSH independent of GnRH signal, we administered the GnRH antagonist antide to 3 month old male wild type (*n* = 4) and *Chd7*$^{Gt/+}$ (*n* = 4) littermate mice. In mice, antide causes a rapid (2 hours) decrease in the production and circulation of LH and FSH (71, 72). Wild type and *Chd7*$^{Gt/+}$ mice had no difference in circulating levels of FSH or LH 2 hours following antide administration (Figure 3.2 E, F). Additionally, no abnormalities in pituitary histology were found by hematoxylin and eosin staining of sections from E10.5, E14.5, E18.5, and adult *Chd7*$^{Gt/+}$ mice-data not shown and (30).

GnRH neurons are decreased in *Chd7* deficient mice

Reduced levels of circulating LH and FSH can reflect defects in GnRH neurons in the hypothalamus, as a result of reductions in GnRH neuronal number, defective migration to the hypothalamus, and/or aberrant hormone production and/or release (14).

To measure GnRH neurons in *Chd7*$^{Gt/+}$ mice, immunofluorescence was performed with anti-GnRH antibody on hypothalamic sections from 3-4 month old wild type (males *n = 4*, females *n = 4*) and *Chd7*$^{Gt/+}$ (males *n = 4*, females *n = 4*) sex-matched, late estrus-matched (females) littermates. A visually apparent decrease in GnRH immunofluorescence was found in the median eminence in both male and female *Chd7*$^{Gt/+}$ mice compared to wild type littermates (Figure 3.3 A, B). In contrast, there was no difference between wild type and *Chd7*$^{Gt/+}$ mice in immunofluorescence of arginine vasopressin (AVP)-positive fibers in the median eminence (Figure 3.3 C, D), providing evidence against a general defect in neural development or maintenance. Quantitation of anti-GnRH immunofluorescence in the median eminence using ImageJ software showed a 54% decrease in anti-GnRH immunofluorescence in *Chd7*$^{Gt/+}$ females and a 51% decrease in *Chd7*$^{Gt/+}$ males (Figure 3.3 K).

Reduced GnRH in the median eminence could be a result of fewer GnRH neurons in the hypothalamus or defects in GnRH neuronal function. Adult GnRH neurons have a rostral-caudal distribution that spans from the nasal region to the hypothalamus, but the vast majority of GnRH neurons reside in specific regions of the hypothalamus (73). To quantify GnRH neurons in the hypothalamus, immunofluorescence was performed with anti-GnRH antibody on hypothalamic sections from 3-4 month old wild type (males *n = 4*, females *n = 4*) and *Chd7*$^{Gt/+}$ sex-matched (males *n = 4*, females *n = 4*), late estrus-matched (for females) littermates. GnRH neuronal cell counts taken from the hypothalamus including the medial septal nucleus (MSN) (Figure 3 E, F) and preoptic area (POA) (Figure 3.3 G, H) showed a significant decrease (approximately 35%) in the number of GnRH-positive cell bodies in the hypothalamus of *Chd7*$^{Gt/+}$ females and

Chd7$^{Gt/+}$ males compared to wild type littermates (Figure 3.3 L). The average total number of GnRH-positive neurons counted in the hypothalamus is *Chd7*$^{Gt/+}$ females = 348 (*standard error = 21; P < 0.001*), *Chd7*$^{Gt/+}$ males = 361 (*standard error = 18; P < 0.001*), wild type females = 487 (*standard error = 26*), and wild type males = 473 (*standard error = 24*). To determine whether GnRH neurons exhibit migration abnormalities in *Chd7*$^{Gt/+}$ mice, immunofluorescence was performed with anti-GnRH antibody on both coronal and sagittal sections from 3-4 month old wild type (males *n = 4*, females *n = 4*) and *Chd7*$^{Gt/+}$ (males *n = 4*, females *n = 4*) sex-matched, late estrus-matched (females) littermates. GnRH neurons were distributed similarly throughout the rostral-caudal axis from the nasal region to the cerebellum in wild type and *Chd7*$^{Gt/+}$ mice. Thus, we did not identify a major defect in GnRH neuronal migration in *Chd7*$^{Gt/+}$ mice.

Chd7 is expressed in immortalized GnRH neuronal cell lines (8), but *Chd7* expression in GnRH neurons *in vivo* had not been previously examined. We analyzed adult *Chd7*$^{Gt/+}$ hypothalamic sections using anti-β-galactosidase and anti-GnRH and found that most GnRH-positive neurons were also positive for the β-galactosidase reporter (Figure 3.3 I, J). These data suggest that CHD7 may also regulate GnRH neuronal development or function.

Chd7$^{Gt/+}$ embryos have fewer GnRH neurons in the nasal region

The timing of GnRH neuron formation, their migratory paths, and molecules regulating this migration have been extensively studied (74). In mice, GnRH neurons arise from the E9.5-11.5 olfactory placode then migrate along olfactory tracts leading to

the forebrain (32). GnRH neurons reside in the nasal region until E13.5, at which time most GnRH neurons have migrated into the forebrain; GnRH neurons continue to migrate until E16.5 when they reach the hypothalamus and have assumed their adult-like distribution (32).

Hypogonadotropic hypogonadism is often associated with abnormalities in GnRH neurons, and can be caused by defects in neurogenesis, migration, or survival (75). Mouse models with mutations affecting genes such as *Pkr2*, *Epha5*, and *Nhlh2* are reported to have defects in GnRH neuronal migration and/or survival (76-78), while mutations in *Fgf8* and *Fgfr1* cause reduced neurogenesis (26-28). To determine whether GnRH neuronal numbers are altered in *Chd7*$^{Gt/+}$ embryos, GnRH-positive cells were counted in wild type (*n* = 4 each time point) and *Chd7*$^{Gt/+}$ (*n* = 4 each time point) littermate embryos at E11.5 and E12.5. We found approximately a 30% reduction in the number of GnRH neurons in the nasal region of *Chd7*$^{Gt/+}$ embryos at both E11.5 and E12.5 (Figure 3.4). The average total number of GnRH-positive neurons counted in the embryonic nasal region is E11.5 *Chd7*$^{Gt/+}$ = 565 (*standard error = 19; P < 0.001*), E12.5 *Chd7*$^{Gt/+}$ = 622 (*standard error = 32; P < 0.001*), E11.5 wild type = 793 (*standard error = 42*), and E12.5 wild type = 882 (*standard error = 40*). Decreased numbers of GnRH neurons in *Chd7*$^{Gt/+}$ embryos is consistent with reduced GnRH neurons in the hypothalamus of adult *Chd7*$^{Gt/+}$ mice.

Chd7$^{Gt/+}$ embryos have defects in cellular proliferation in the olfactory placode

Chd7 is highly expressed in the olfactory placode by E10.5 (30), and continues to be expressed in olfactory tissues throughout development and into adulthood (29). To

test cellular proliferation in the olfactory placode, immunofluorescence was performed with anti-CHD7 and the proliferation marker anti-phospho-histone H3 in wild type (n = 4), *Chd7*$^{Gt/+}$ (n = 4), and *Chd7*$^{Gt/Gt}$ (n = 3) littermate embryos at E10.5 (Figure 3.5 A-I). A 49% decrease in phospho-histone H3-positive cells was found in E10.5 *Chd7*$^{Gt/+}$ embryos compared to wild type (Figure 3.5 A-F, J). The vast majority (97%) of phospho-histone H3-positive cells in the olfactory placode were CHD7-positive, similar to previously published results showing CHD7 in 98% of proliferating cells in the adult olfactory epithelium (29). We found a 90% decrease in proliferation and reduced size of the olfactory placode in *Chd7*$^{Gt/Gt}$ embryos compared to wild type, and an 80% decrease in proliferation compared to *Chd7*$^{Gt/+}$ embryos (Figure 3.5 A-J). Together, these data indicate that *Chd7* deficiency negatively impacts cellular proliferation in the developing olfactory placode, consistent with fewer olfactory sensory neurons in the adult *Chd7*$^{Gt/+}$ olfactory epithelium (29) and fewer GnRH neurons available for migration into the hypothalamus.

Decreased numbers of adult GnRH neurons could also result from defects in cell survival (78). To test this, wild type (n = 4 each time point) and *Chd7*$^{Gt/+}$ (n = 4 each time point) littermate embryos at E10.5, E11.5, and E12.5 were analyzed for apoptosis by TUNEL assay. *Chd7*$^{Gt/+}$ embryos have significantly fewer TUNEL-positive cells in the nasal region compared to wild type embryos at all time points analyzed [E10.5 (21% decrease), E11.5 (11% decrease), and E12.5 (13% decrease)] (Figure 3.5 K). Fewer TUNEL-positive cells may be present due to an overall reduction in the number of cells in the nasal region of *Chd7*$^{Gt/+}$ embryos. Alternatively, *Chd7*$^{Gt/+}$ mice may have decreased susceptibility to apoptosis. The 49% decrease in cellular proliferation in the

E10.5 olfactory placode is greater than the 21% decrease in E10.5 TUNEL-positive cells in *Chd7*$^{Gt/+}$ embryos compared to wild type littermates. Wild type and *Chd7*$^{Gt/+}$ embryos at E10.5 appear to have normal invagination of the olfactory placode to form the olfactory pit (Figure 3.5 A-F). However, *Chd7*$^{Gt/Gt}$ embryos appear to lack olfactory pits, suggesting that invagination of the olfactory placode is disrupted (Figure 3.5 G-I). Altogether, our data suggest that defects in GnRH neurogenesis lead to reduced GnRH neurons in embryonic and adult *Chd7*$^{Gt/+}$ mice, and are not associated with increased cell death.

Reduced CHD7 dosage alters gene expression in olfactory placode, pituitary, and hypothalamus

CHD7 may regulate neural progenitors by directly influencing the expression of morphogens such as the bone morphogenetic proteins (BMPs) and fibroblast growth factors (FGFs). CHD7 may also regulate the expression and/or function of transcription factors involved in neurogenesis. *Chd7* is highly expressed throughout the entire olfactory placode, whereas the expression of morphogens is often regionally restricted within the olfactory placode (23, 79). To determine whether CHD7 regulates expression of *Fgfr1*, *Fgf8*, *Bmp4*, or *Otx2*, we analyzed microdissected olfactory placode from E10.5 wild type (n = 3), *Chd7*$^{Gt/+}$ (n = 3), and *Chd7*$^{Gt/Gt}$ (n = 4) littermate embryos using TaqMan gene expression assays. We found that *Chd7*$^{Gt/+}$ embryos have decreased expression of *Otx2* (fold change: -3.01 +/- 0.32), *Bmp4* (fold change: -2.61 +/- 0.15), and *Fgfr1* (fold change: -2.88 +/- 0.23) compared to wild type littermates (Figure 3.6 A). *Chd7*$^{Gt/Gt}$ embryos also have decreased expression of *Otx2* (fold change: -7.87 +/- 0.46),

Bmp4 (fold change: -7.91 +/- 0.37), and *Fgfr1* (fold change: -8.65 +/- 0.29) compared to wild type littermates (Figure 3.6 A). There was no significant difference in *Fgf8* expression in *Chd7*$^{Gt/+}$ or *Chd7*$^{Gt/Gt}$ embryos compared to wild type littermates (Figure 3.6 A). Potential changes in spatial distribution of gene expression within the *Chd7* mutant placode could not be determined from these studies.

To determine whether CHD7 regulates the expression of genes required for normal adult hypothalamic-pituitary signaling, we analyzed the expression of *GnRH1*, *Otx2*, *Kiss1*, and *GnRHR* using TaqMan gene expression assays. We analyzed RNA isolated from the hypothalamus and pituitary of 3-4 month old wild type (*n = 4*) and *Chd7*$^{Gt/+}$ (*n = 4*) littermate mice. We found decreased expression of *GnRHR* (fold change: -2.34 +/- 0.22) in *Chd7*$^{Gt/+}$ pituitary (Figure 3.6 B), consistent with decreased GnRH signal (80-82) rather than a direct effect of reduced *Chd7* dosage. We also found decreased expression of *GnRH1* (fold change: -3.61 +/- 0.63) and *Otx2* (fold change: -4.09 +/- 0.43) in *Chd7*$^{Gt/+}$ hypothalamus compared to wild type littermates (Figure 3.6 B). There was no significant difference in expression of *Kiss1* in the *Chd7*$^{Gt/+}$ hypothalamus compared to wild type littermates (Figure 3.6 B).

Discussion

We report here that *Chd7*$^{Gt/+}$ mice have delayed puberty, erratic estrus cycles, decreased levels of circulating gonadotropins, and reduced GnRH neurons in the hypothalamus. *Chd7*$^{Gt/+}$ embryos have fewer GnRH neurons and reduced cellular proliferation in the olfactory placode. Additionally, reduced CHD7 dosage impacts expression of genes involved in proliferation and/or neurogenesis (*Fgfr1*, *Bmp4*, and

Otx2) in the olfactory placode and GnRH signaling (*Otx2* and *GnRH1*) in the adult hypothalamus. Together, our data suggest that defects in neural progenitor proliferation in the developing olfactory epithelium may underlie the Kallmann-like features found in *Chd7*$^{Gt/+}$ mice and in *CHD7* mutation positive humans with CHARGE syndrome. These observations also provide evidence that CHD7 positively regulates cellular proliferation potentially by either directly or indirectly regulating transcription of *Fgfr1*, *Bmp4*, and *Otx2*. Combined with previous published results in the olfactory system (29) and the developing inner ear (83), our data imply a broad role for CHD7 in promoting neurogenesis in multiple tissues.

Although no binding site consensus sequences have been identified for CHD7, we compared our gene expression results to CHD7 CHiP-seq data (derived from embryonic stem cells) deposited in GEO by Schnetz et al (84). We found CHD7 binding sites at the medium threshold for *Otx2* (1 site inside the gene and 1 upstream close to the transcriptional start site), *Bmp4* (3 sites downstream of the gene), and *Fgfr1* (5 sites in the second intron and several sites both upstream and downstream of the gene). We also found a potential CHD7 binding site for *Fgf8* in the adjacent gene *Mgea5*, which could contain an enhancer region for *Fgf8*. There were no CHD7 binding sites at the low, medium, or high thresholds for *GnRH1*, *GnRHR*, or *Kiss1*. It is important to note that comparison of our data to that of prior ChIP-seq experiments is limited due to differences in cell types analyzed. Moreover, our results do not provide information on whether changes in gene expression result from direct or indirect effects of CHD7.

Roles for CHD7 in regulation of gene expression during tissue development and maintenance are emerging for multiple organs. In a study of neural crest formation in

Xenopus, CHD7 was implicated to regulate multipotent neural crest-like cells by binding to PBAF components including BRG1, BAF170, BAF155, BAF57, PB1, ARID2, and BRD7 (85). In mesenchymal stem cells, CHD7 regulates cell fate specification during osteoblast and adipocyte differentiation (86). CHD7 forms a complex with NLK, SETDB1, and PPAR-γ, and binds to methylated lysine 4 and lysine 9 residues on histone H3 at PPAR-γ target promoters, which suppresses ligand-induced transactivation of PPAR-γ target genes (86). Additionally, the *CHD7 Drosophila* orthologue, *Kismet*, is involved in transcriptional elongation by RNA polymerase II through recruitment of ASH1 and TRX, and may help maintain stem cell pluripotency by regulating methylation of histone H3 lysine 27 (87). These data provide evidence that the role of CHD7 in tissue development and maintenance is dependent upon coordination of multiple components. Our results showing that CHD7 affects GnRH neurogenesis and signaling, potentially by influencing transcriptional regulation of key target genes, add to this emerging evidence.

Previous reports of reproductive phenotypes in *Chd7* haploinsufficient mice using the $Chd7^{Whi}$ allele (which contains a nonsense mutation) (39) showed that $Chd7^{Whi/+}$ mice have genital hypoplasia, hypogonadism, and increased time to first litter (38). Similar to $Chd7^{Gt/+}$ mice, $Chd7^{Whi/+}$ mice were also reported to have reduced GnRH neurons in the adult hypothalamus (38). However, the mechanism underlying decreased GnRH neurons in $Chd7^{Whi/+}$ mice was not evaluated. Our data provides a potential cellular mechanism for the reduced gonadal size and decreased fertility associated with CHD7 haploinsufficiency. Compared to wild type littermates, $Chd7^{Gt/+}$ mice have reduced capacity for GnRH signal to pituitary gonadotropes, leading to less LH and FSH available to act on the gonads for sex-steroid production. Reductions in circulating LH and FSH

negatively affect both gonad size and fertility (88). Although our data do not exclude the possibility of a subtle defect in GnRH migration, reduced GnRH neurons in *Chd7*$^{Gt/+}$ mice are explained at least in part by defects in GnRH neurogenesis during development. Together, these data support our model for an underlying intrinsic cellular mechanism for hypogonadotropic hypogonadism in *Chd7* haploinsufficient mice.

Neural progenitors must be tightly regulated during development by factors that are likely to be temporally and spatially restricted (89). The neurogenic potential of progenitors is influenced by both BMP and FGF signaling in the central and peripheral nervous systems (90-94). The opposing effects of FGF and BMP signaling must be tightly regulated during olfactory development to obtain the proper proportions of olfactory sensory and olfactory respiratory cell types; notably, reductions in either FGF8 or BMP4 can cause decreased cellular proliferation in the olfactory placode (95). In addition, BMP4 and BMP7 have dosage and threshold dependent effects on neurogenesis in the olfactory epithelium (90-92, 96, 97). Although BMP activity is generally thought to inhibit neurogenesis, low doses of BMP4 are required for promoting neurogenesis in multiple tissues including the olfactory placode, hippocampus, and subventricular zone (95-100). Neurogenesis in the olfactory epithelium is also regulated by FGF8 and FGFR1, and mutations in *Fgf8* or *Fgfr1* in humans and mice cause reduced numbers of olfactory sensory neurons and GnRH neurons (23-28). FGF2 induces neurogenesis and increases cellular proliferation of progenitors in olfactory tissues (96), and FGF2 signals via FGFR1 to induce proliferation of olfactory bulb progenitors in the subventricular zone (101). Our data provide the first evidence that reduced CHD7 dosage results in

decreased expression of *Fgfr1* and *Bmp4*, and that CHD7 is required for proper cellular proliferation and genesis of GnRH neurons during development.

Proper CHD7 dosage is critical for development in humans and mice (30, 31, 39, 102). However, CHD7 function in adult tissues and post-mitotic cells has not been fully explored. Although adult *Chd7* expression in the brain is mostly restricted to proliferative regions, cells expressing *Chd7* are scattered throughout the adult mouse hypothalamus [data available on GENSAT website (http://www.gensat.org/index.html)]. *CHD7* is also expressed in GnRH neurons *in vivo* (Figure 3I, J) and in GnRH neuronal cell lines (8), but it is unknown whether CHD7 has a functional role in post-mitotic GnRH neurons. Our data provide the first evidence that CHD7 haploinsufficiency in mice results in decreased expression *GnRH1* and *Otx2* expression in the adult hypothalamus. These data are consistent with a recent report showing that loss of CHD7 in the developing mouse inner ear causes reduced expression of *Otx2* (83). Interestingly, humans with *OTX2* mutations have some clinical features similar to those seen in CHARGE, including pituitary hormone deficiency, short stature, and ocular colobomata (103, 104). Thus, fewer GnRH neurons in $Chd7^{Gt/+}$ mice and defects in GnRH signaling may be exacerbated by decreased expression of *GnRH1*. Together, these results provide evidence that CHD7 controls multiple facets of normal hypothalamic-pituitary signaling, by regulating GnRH neuronal cell number as well as expression of transcription factors and morphogens required for proper GnRH signaling.

Materials and Methods

Mice

Chd7$^{Gt/+}$ mice were generated and characterized as previously described (30). Mice were maintained by backcrossing with 129S1/Sv1mJ (Jackson Laboratory) mice to generation N6-N8. Mice are housed with a 10/14h dark/light cycle and fed ad libitum. Serum was collected in the afternoon between 2:00 and 3:00pm by cardiac exsanguinations after anaesthesia with 250 mg/kg body weight tribromoethanol. Timed pregnancies were established, and the morning of plug identification designated as E0.5. Embryos were collected after cervical dislocation and hysterectomy, and washed briefly in PBS. Amniotic sacs were collected and DNA isolated for PCR genotyping as described (30). All procedures were approved by The University of Michigan University Committee on Use and Care of Animals (UCUCA).

Vaginal Smears

Vaginal smears were taken at the same time daily over a three month period. One drop of water from a Pasteur pipette was gently expelled into the vagina and aspirated 4-6 times, and then transferred to a microscope slide. The smear was dried at room temperature and then fixed with 100% methanol. Fixed slides were stained for 30 minutes in 2% Giemsa (GibcoBRL, Grand Island, NY). Stained slides were then analyzed for stage of estrus cycle.

Immunofluorescence

Embryos were fixed in 4% paraformaldehyde for 30 minutes (E10.5) to 1.5 hrs (E12.5), then washed in PBS and dehydrated in an ethanol gradient. Embryos were subsequently embedded in paraffin and sectioned at 7 μm. Three to four month old *Chd7*$^{+/+}$ and *Chd7*$^{Gt/+}$ sex-matched littermate mice were anaesthetized with 250 mg/kg body weight tribromoethanol and perfusion fixed with 4% paraformaldehyde. Mice were then decapitated and heads placed in 4% paraformaldehyde overnight at 4°C. Heads were incubated in RDO Rapid Decalcifier (Apex Engineering, Aurora, IL) for 4-6 hours followed by 30% sucrose protection overnight at 4°C. Tissue was flash frozen in O.C.T. embedding medium (Tissue Tek, Torrance, CA) for sectioning at 14 μm. Following paraffin or cryosectioning, sections were processed for immunofluorescence with antibodies against CHD7 (1:1000; Abcam, Cambridge, MA), GnRH (1:150; Abcam (ab5617), Cambridge, MA), β-galactosidase (1:200; Vector Laboratories, Burlington, CA), arginine vasopressin (1:500; Abcam, Cambridge, MA), or phospho-histone H3 (1:200; Millipore, Temecula, CA). Secondary antibodies were used at 1:200 and were conjugated with Alexa 488, Alexa 555, or biotin with streptavidin-HRP (Vector Laboratories) and or biotinylated secondary antibodies conjugated with streptavidin-Alexa488 or streptavidin-Alexa555 (Molecular Probes, Eugene, OR and Invitrogen, Carlsbad, CA). Images were captured by single channel fluorescence microscopy on a Leica upright DMRB microscope and processed in Photoshop v.9.0 (San Jose, CA). NIH ImageJ software (Bethesda, MD) was used to analyze anti-GnRH fluorescence intensity over at least 30 images of the median eminence per animal. Fluorescence intensity was measured in restricted areas of the median eminence and background was subtracted to

obtain the final measurements. GnRH neuronal cell counts were performed by counting cell bodies only on at least four adults (4 pairs male and 4 pairs female) and four embryos of each genotype at each time point. A minimum of 30 sections per animal were used for all cell counts. Cell counts were analyzed for significance by Student's t-test using two-tailed unequal variance.

Mouse Insulin and Leptin ELISA Assay

Circulating serum levels of insulin and leptin were assayed by ELISA from three to four month old *Chd7*$^{+/+}$ and *Chd7*$^{Gt/+}$ stage of estrus cycle matched littermate mice. Insulin was measured using the Ultra Sensitive Mouse Insulin ELISA Kit (Crystal Chem, Downers Grove, IL). Leptin was measured using the Mouse Leptin ELISA Kit (Crystal Chem). Absorbance (A_{450}) for insulin and leptin was measured and analyzed using a standard curve. Differences in absorbance were analyzed for significance by Student's t-test using two-tailed unequal variance.

Mouse GH and IGF1 ELISA Assay

Circulating levels of growth hormone (GH) and insulin-like growth factor 1 (IGF1) were assayed by ELISA. GH was measured in serum collected from three to four month old *Chd7*$^{+/+}$ and *Chd7*$^{Gt/+}$ stage of estrus cycle matched littermate mice using the ELISA kit Cat# EZRMGH-45K (LINCO Research, St. Charles, Missouri). IGF1 was measured in serum using the ELISA Kit Cat# DSL-10-29200 (Diagnostic Systems Laboratories, Webster, Texas). Absorbance (A_{450}) for GH and IGF1 was measured and

analyzed using a standard curve. Differences in absorbance were analyzed for significance by Student's t-test using two-tailed unequal variance.

Mouse LH Sandwich Assay (MLHS)

Circulating levels of LH were assayed at the University of Virginia Center for Research in Reproduction Ligand Assay and Analysis Core using the following methods: LH was measured in serum by a sensitive two-site sandwich immunoassay (105, 106) using monoclonal antibodies against bovine LH (no. 581B7) and against the human LH-beta subunit (no. 5303: Medix Kauniainen, Finland) as previously described (106). The tracer antibody (no. 518B7) was kindly provided by Dr. Janet Roser (107), (Department of Animal Science, University of California, Davis) and iodinated by the chloramine T method and purified on Sephadex G-50 columns. The capture antibody (no. 5303) was biotinylated and immobilized on avidin-coated polystyrene beads (7mm; Epitope Diagnostics, Inc., San Diego, CA). Mouse LH reference prep (AFP5306A; provided by Dr. A.F. Parlow and the National Hormone and Peptide program) was used as standard. The mouse LH sandwich assay has a sensitivity of 0.07 ng/ml.

Mouse FSH Radioimmunoassay (RIA)

Circulating levels of FSH were assayed at the University of Virginia Center for Research in Reproduction Ligand Assay and Analysis Core using the following methods: FSH was assayed by RIA using reagents provided by Dr. A.F. Parlow and the National Hormone and Peptide Program, as previously described (108). Mouse FSH reference prep AFP5308D was used for assay standards and mouse FSH antiserum (guinea pig;

AFP-1760191) diluted to a final concentration of 1:400,000 was used as primary antibody. The secondary antibody was purchased from Equitech-Bio, Inc. and diluted to a final concentration of 1:25. The assay has a sensitivity of 2.0 ng/ml and less than 0.5% cross-reactivity with other pituitary hormones.

GnRH Agonist and Antagonist Assays

Three to four month old *Chd7*$^{+/+}$ and *Chd7*$^{Gt/+}$ sex-matched littermate mice were given a subcutaneous injection of either the GnRH agonist leuprolide (Sigma, St Louis, MO) or the GnRH antagonist antide (Sigma). Leuprolide was dissolved in 0.9% saline and administered at a dose of 1mg/kg body weight two hours prior to cardiac exsanguination (69, 70). Antide was dissolved in 20% propylene glycol and 0.9% saline and administered at a dose of 3.0mg/kg body weight two hours prior to cardiac exsanguination (71, 72). Serum was collected and analyzed by mouse LH sandwich assay and mouse FSH RIA.

Cellular Proliferation Assays

Wild type, *Chd7*$^{Gt/+}$, and *Chd7*$^{Gt/Gt}$ E10.5 embryos were processed as above for immunofluorescence. Serial adjacent sections were labeled with rabbit anti-H3 (1:200, Millipore, Temecula, MA) followed by incubation with anti-rabbit AlexaFluor488 conjugated secondary antibody (Invitrogen). A minimum of 30 sections per embryo were photographed by single channel fluorescence microscopy on a Leica upright DMRB microscope and processed for dual channel imaging with Adobe Photoshop software v9.0 (San Jose, CA). Cell counts were performed on at least four embryos of each genotype.

Statistical significance was determined using one-way ANOVA analysis with GraphPad Prism 5 software.

TUNEL Assays

Wild type and *Chd7*$^{Gt/+}$ E10.5, E11.5, and E12.5 embryos were processed as above for immunofluorescence. Serial adjacent sections were assayed for apoptosis using Fluorescein-FragEL DNA Fragmentation Detection Kit (Calbiochem, Darmstadt, Germany). A minimum of 30 sections per embryo were photographed by single channel fluorescence microscopy on a Leica upright DMRB microscope and processed for dual channel imaging with Adobe Photoshop software v9.0 (San Jose, CA). Cell counts were performed on at least four embryos of each genotype at each time point. Cell counts were analyzed for significance by Student's t-test using two-tailed unequal variance.

RNA Isolation and Real-Time PCR

Three to four month old *Chd7*$^{+/+}$ and *Chd7*$^{Gt/+}$ sex-matched littermate mice were euthanized by cervical dislocation and decapitated. The brain and pituitary were removed from the head. The hypothalamus was microdissected from whole brain and placed in ice cold TRIzol (Invitrogen) and mechanically homogenized prior to RNA isolation. Pituitary RNA was isolated using the RNAqueous-Micro RNA Isolation Kit (Ambion, Austin, TX). Wild type, *Chd7*$^{Gt/+}$, and *Chd7*$^{Gt/Gt}$ E10.5 embryos were harvested as described above. The olfactory placode was microdissected and RNA isolated using the RNAqueous-Micro RNA Isolation Kit (Ambion). Isolated RNA from adult and embryonic tissues was treated with DNase I prior to cDNA synthesis. cDNA

was generated using Superscript First-Strand cDNA Synthesis system for RT-PCR (Invitrogen) with random primers.

Relative expression levels were assayed utilizing TaqMan Gene Expression Master Mix and TaqMan probes (Applied Biosystems, Foster City, CA) for *GnRH1*, *GnRHR*, *Kiss1*, *Otx2*, *Bmp4*, *Fgfr1*, *Fgf8*, and *Gapdh*. Reactions were run in triplicate in an Applied Biosystems StepOne-Plus Real-Time PCR System. The level of *Gapdh* was used as an internal control. The difference in C_T between the assayed gene and *Gapdh* for any given sample was defined as $\Delta C_{T(X)}$. The difference in $\Delta C_{T(x)}$ between two samples was defined as $\Delta\Delta C_{T(X)}$, which represents a relative difference in expression of the assayed gene. The fold change of the assayed gene relative to *Gapdh* was defined as $2^{-\Delta\Delta CT}$ (109). DataAssist software (Applied Biosystems) was used for statistical analysis and to confirm $\Delta C_{T(X)}$ calculation.

Acknowledgements

The authors would like to thank Dr. Sally Camper for insightful discussions and critical reading of the manuscript. We also thank Gina Leinninger for help with ELISA assays and Joseph Micucci for help analyzing CHiP-seq data sets. This work was supported by the National Institutes of Health [F31DC010955-01 to W.S.L., R01DC009410 and an ARRA supplement to D.M.M.].

Chapter 3 Notes

[1]A revised version of Chapter 3 has been published as Layman WS, Hurd EA, Martin DM. (2011). Reproductive dysfunction caused by decreased GnRH neurogenesis in a mouse model of CHARGE syndrome. *Human Molecular Genetics*: in press.

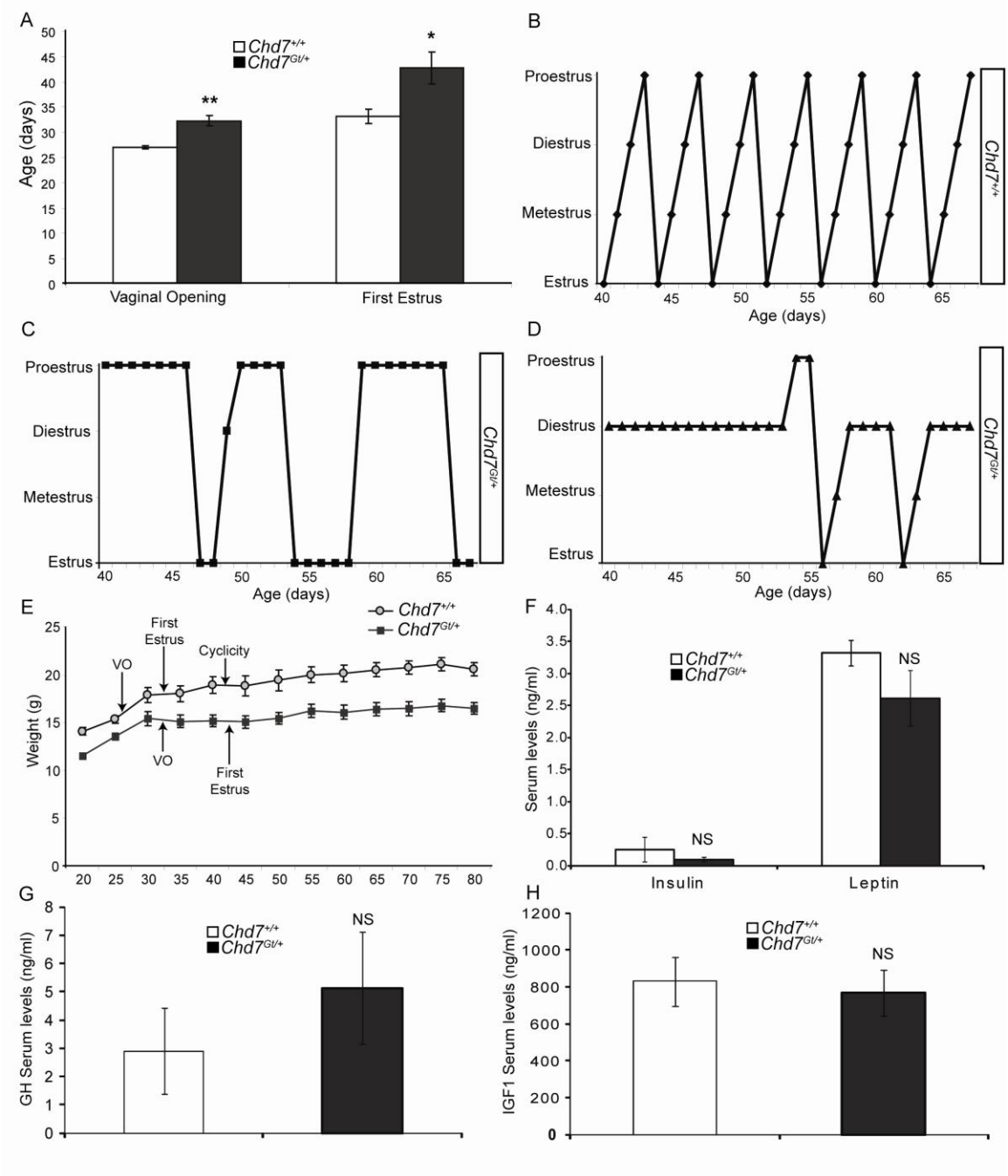

Figure 3.1 *Chd7*$^{Gt/+}$ females have delayed puberty and erratic estrus cycles. (A) Wild type and *Chd7*$^{Gt/+}$ female littermates were examined for vaginal opening and first estrus. (B) In wild type females, estrus cyclicity is obtained at postnatal day 39, nine days after first estrus. (C and D) *Chd7*$^{Gt/+}$ female littermates never achieve cyclicity and have erratic estrus cycles. (E) Pubertal markers (vaginal opening (VO), first estrus, and cyclicity) in relation to body size are depicted for wild type and *Chd7*$^{Gt/+}$ females. (F) Circulating levels of insulin and leptin are similar in wild type and *Chd7*$^{Gt/+}$ female littermate mice. (G and H) Circulating levels of growth hormone (GH) or insulin-like growth factor 1 (IGF1) are similar in wild type and *Chd7*$^{Gt/+}$ female littermate mice. * $P < 0.05$ ** $P < 0.01$ by unpaired Student's t test. NS= Not Significant.

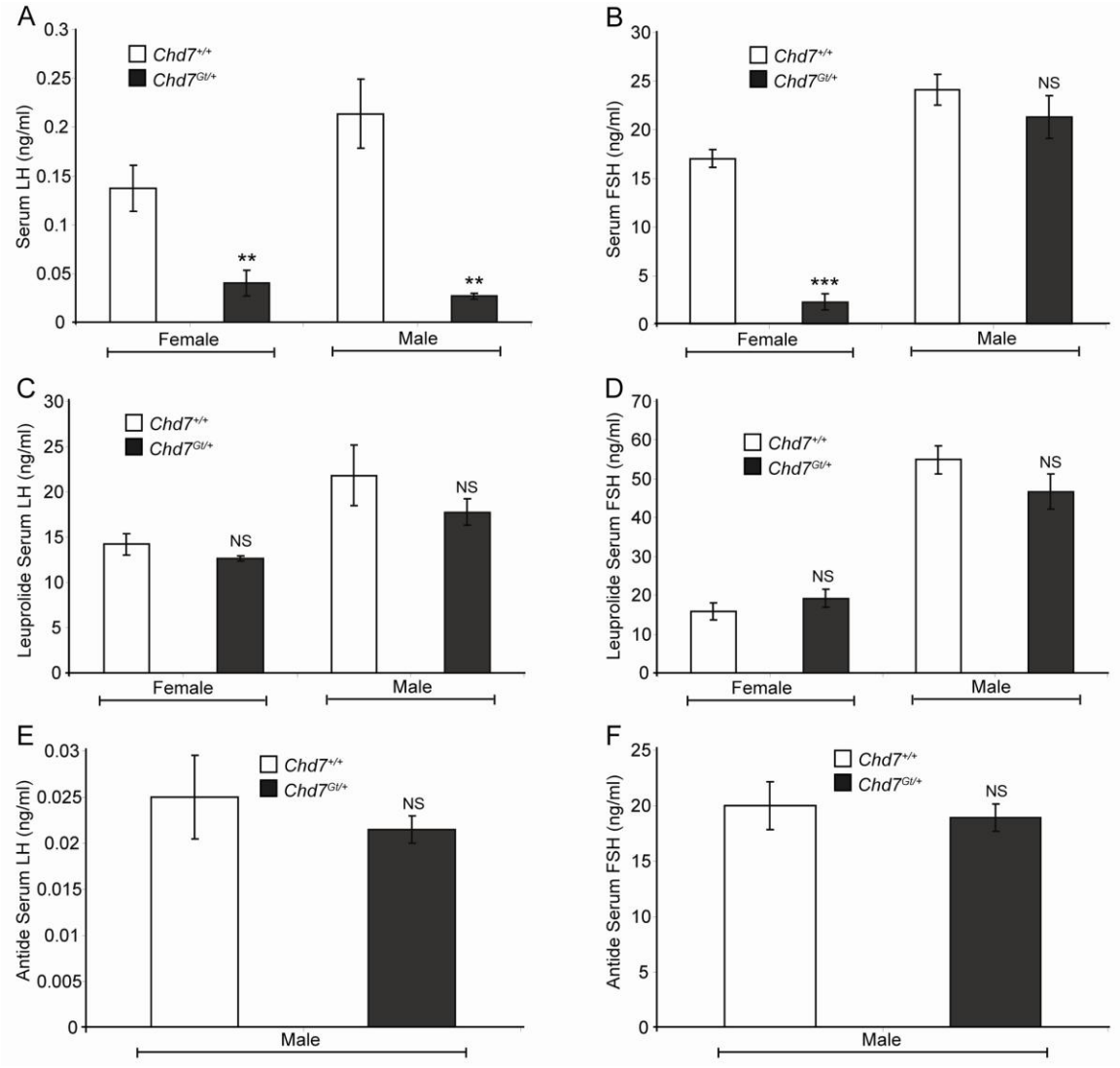

Figure 3.2 Circulating LH and FSH are decreased in *Chd7*$^{Gt/+}$ mice. (A) *Chd7*$^{Gt/+}$ mice analyzed for circulating LH have decreased serum levels compared to wild type littermates. The LH reportable range was 0.04 to 37.4 ng/ml. (B) *Chd7*$^{Gt/+}$ females have decreased levels of circulating FSH but *Chd7*$^{Gt/+}$ males have normal serum levels. The FSH reportable range was 2.3 to 20.0 ng/ml. (C and D) GnRH agonist, leuprolide, administered to wild type and *Chd7*$^{Gt/+}$ mice caused similar responses in the production and circulation of LH and FSH. The reportable range for LH was 0.04 to 37.4 ng/ml and for FSH was 6.7 to 75.0 ng/ml. (E and F) Wild type and *Chd7*$^{Gt/+}$ males were administered GnRH antagonist, antide. Wild type and *Chd7*$^{Gt/+}$ males have similar decreases in circulating levels of LH and FSH. The reportable range for LH was 0.04 to 37.4 ng/ml and for FSH was 6.7 to 75.0 ng/ml. * $P < 0.05$ ** $P < 0.01$ *** $P < 0.001$ by unpaired Student's t test. NS= Not Significant.

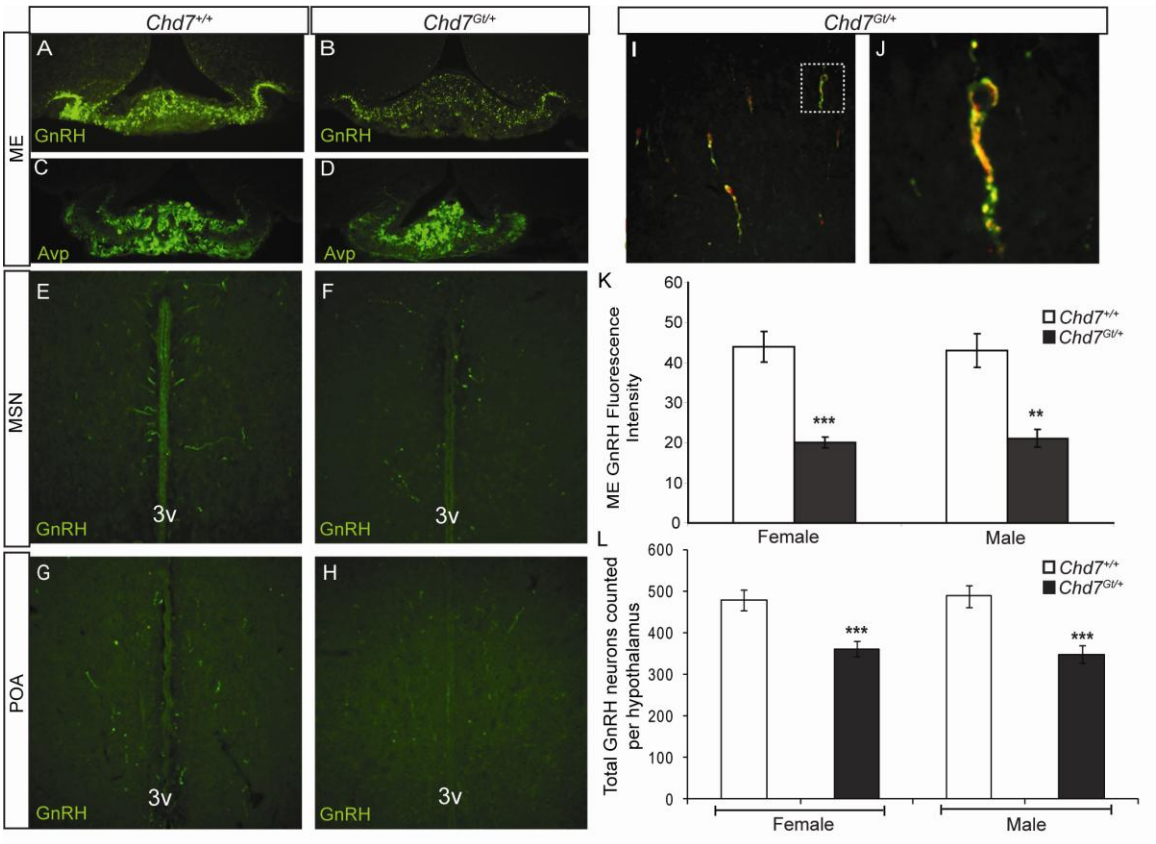

Figure 3.3 *Chd7*$^{Gt/+}$ mice have decreased GnRH neurons in the hypothalamus. (A and B) Immunofluorescence using anti-GnRH (green) revealed decreased GnRH immunofluorescence in the median eminence in *Chd7*$^{Gt/+}$ mice compared to wild type littermates. (C and D) Immunofluorescence using anti-arginine vasopressin (AVP) showed no difference in the median eminence in *Chd7*$^{Gt/+}$ mice compared to wild type littermates. (E-H) Immunofluorescence using anti-GnRH (green) showed decreased numbers of GnRH neurons in the medial septal nucleus (MSN) and preoptic area (POA) in *Chd7*$^{Gt/+}$ mice compared to wild type littermates. (I and J) *Chd7* is expressed in GnRH neurons *in vivo*. Immunofluorescence of *Chd7*$^{Gt/+}$ hypothalamic sections using anti-β-galactosidase (β-gal) and anti-GnRH showed that most GnRH-positive neurons in the hypothalamus are also positive for the β-galactosidase reporter for *Chd7* expression. White box in I indicates the co-labeled neuron magnified in J. (K) Quantitation of anti-GnRH immunofluorescence in the median eminence using ImageJ software showed significantly decreased GnRH in *Chd7*$^{Gt/+}$ mice compared to wild type. (L) Quantitation of GnRH neurons per hypothalamus showed decreased numbers of GnRH neurons in both male and female *Chd7*$^{Gt/+}$ mice compared to sex-matched wild type littermates. Sections are in the coronal plane. ** $P < 0.01$ *** $P < 0.001$ by unpaired Student's t test. 3v= third ventricle.

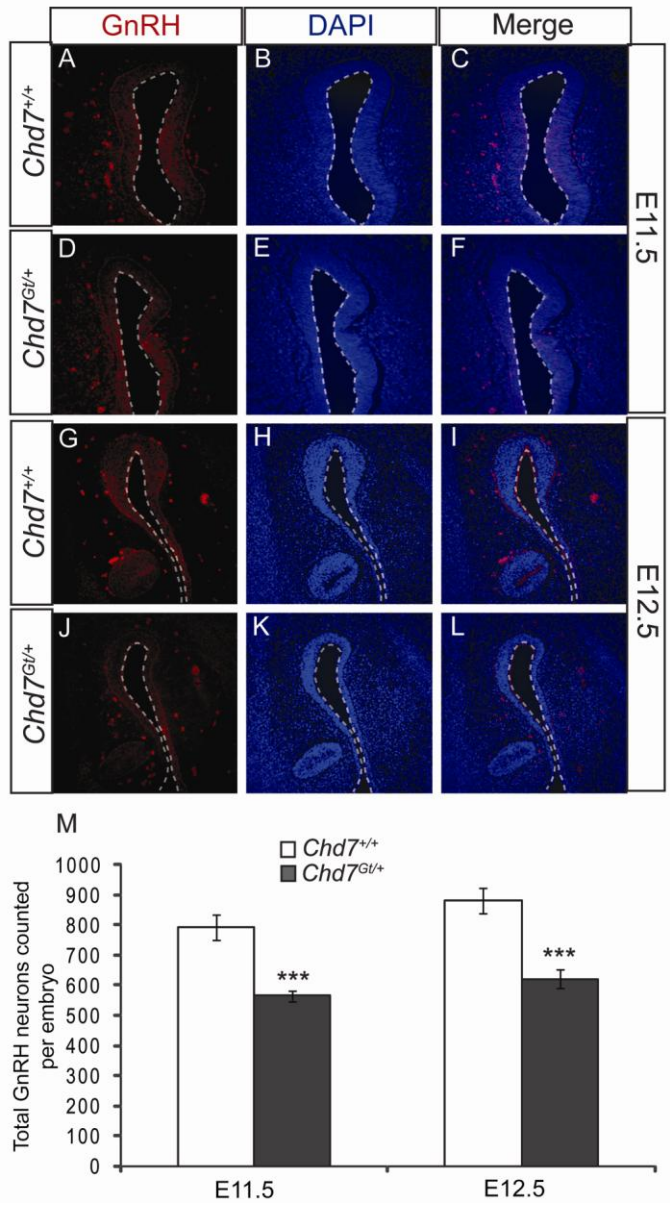

Figure 3.4 GnRH neurons are reduced in *Chd7*$^{Gt/+}$ embryos. (A-L) Immunofluorescence using antibody against GnRH (red) and counterstained with DAPI (blue) showed a decrease in anti-GnRH staining at E11.5 A-D and E12.5. (M) The total number of GnRH neurons per embryo was significantly decreased at each time point in *Chd7*$^{Gt/+}$ embryos compared to wild type littermates. Sections are in the transverse plane. *** $P < 0.001$ by unpaired Student's t test.

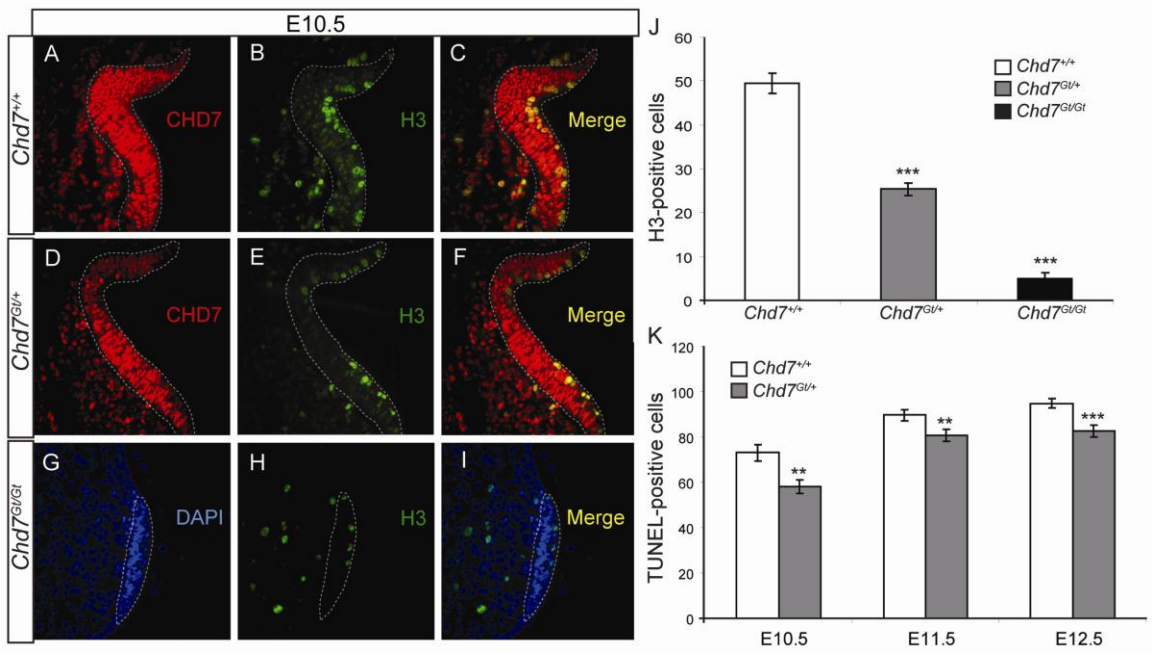

Figure 3.5 *Chd7*$^{Gt/+}$ embryos have reduced cellular proliferation in the olfactory placode. (A-F) Immunofluorescence of wild type and *Chd7*$^{Gt/+}$ at E10.5 using antibodies against CHD7 (red) and phospho-histone H3 (H3) (green). (G-I) Immunofluorescence of *Chd7*$^{Gt/Gt}$ embryos at E10.5 using antibodies against CHD7 (red) and phospho-histone H3 (H3) (green) counterstained with DAPI (blue). (J) Cell counts showed decreased cellular proliferation in the olfactory placode in *Chd7*$^{Gt/+}$ and *Chd7*$^{Gt/Gt}$ embryos compared to wild type littermates. (K) Cell counts showed a decrease in TUNEL-positive cells at E10.5, E11.5, and E12.5 in *Chd7*$^{Gt/+}$ embryos compared to wild type. Sections are in the transverse plane. ** $P < 0.01$ *** $P < 0.001$ by ANOVA (proliferation) and unpaired Student's t test (TUNEL).

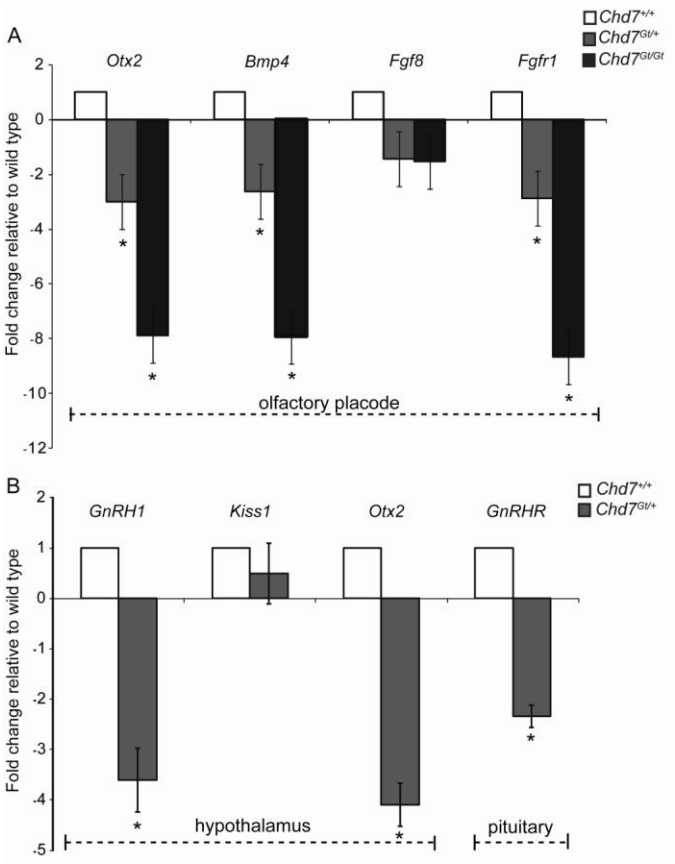

Figure 3.6 Reduced CHD7 dosage alters gene expression in olfactory placode, adult hypothalamus, and adult pituitary. TaqMan gene expression assays were done on microdissected tissues. (A) Expression of *Otx2*, *Bmp4*, and *Fgfr1* is decreased in E10.5 *Chd7*$^{Gt/+}$ and *Chd7*$^{Gt/Gt}$ olfactory placode compared to wild type littermates, whereas *Fgf8* expression is unchanged. (B) Expression of *Otx2* and *GnRH1* is decreased in *Chd7*$^{Gt/+}$ hypothalamus compared to wild type littermates, whereas *Kiss1* expression is unchanged. Expression of *GnRHR* is decreased in *Chd7*$^{Gt/+}$ pituitary compared to wild type littermates. *P<0.05 by DataAssist Software.

References

1 Harris, J., Robert, E. and Kallen, B. (1997) Epidemiology of choanal atresia with special reference to the CHARGE association. *Pediatrics*, **99**, 363-367.

2 Issekutz, K.A., Graham, J.M., Jr., Prasad, C., Smith, I.M. and Blake, K.D. (2005) An epidemiological analysis of CHARGE syndrome: preliminary results from a Canadian study. *Am J Med Genet A*, **133**, 309-317.

3 Kallen, K., Robert, E., Mastroiacovo, P., Castilla, E.E. and Kallen, B. (1999) CHARGE Association in newborns: a registry-based study. *Teratology*, **60**, 334-343.

4 Hall, B.D. (1979) Choanal atresia and associated multiple anomalies. *J Pediatr*, **95**, 395-398.

5 Asakura, Y., Toyota, Y., Muroya, K., Kurosawa, K., Fujita, K., Aida, N., Kawame, H., Kosaki, K. and Adachi, M. (2008) Endocrine and radiological studies in patients with molecularly confirmed CHARGE syndrome. *J Clin Endocrinol Metab*, **93**, 920-924.

6 Jongmans, M.C., Admiraal, R.J., van der Donk, K.P., Vissers, L.E., Baas, A.F., Kapusta, L., van Hagen, J.M., Donnai, D., de Ravel, T.J., Veltman, J.A. *et al.* (2006) CHARGE syndrome: the phenotypic spectrum of mutations in the CHD7 gene. *J Med Genet*, **43**, 306-314.

7 Jongmans, M.C., van Ravenswaaij-Arts, C.M., Pitteloud, N., Ogata, T., Sato, N., Claahsen-van der Grinten, H.L., van der Donk, K., Seminara, S., Bergman, J.E., Brunner, H.G. *et al.* (2009) CHD7 mutations in patients initially diagnosed with Kallmann syndrome--the clinical overlap with CHARGE syndrome. *Clin Genet*, **75**, 65-71.

8 Kim, H.G., Kurth, I., Lan, F., Meliciani, I., Wenzel, W., Eom, S.H., Kang, G.B., Rosenberger, G., Tekin, M., Ozata, M. *et al.* (2008) Mutations in CHD7, encoding a chromatin-remodeling protein, cause idiopathic hypogonadotropic hypogonadism and Kallmann syndrome. *Am J Hum Genet*, **83**, 511-519.

9 Lalani, S.R., Safiullah, A.M., Fernbach, S.D., Harutyunyan, K.G., Thaller, C., Peterson, L.E., McPherson, J.D., Gibbs, R.A., White, L.D., Hefner, M. *et al.* (2006) Spectrum of CHD7 Mutations in 110 Individuals with CHARGE Syndrome and Genotype-Phenotype Correlation. *Am J Hum Genet*, **78**, 303-314.

10 Ogata, T., Fujiwara, I., Ogawa, E., Sato, N., Udaka, T. and Kosaki, K. (2006) Kallmann syndrome phenotype in a female patient with CHARGE syndrome and CHD7 mutation. *Endocr J*, **53**, 741-743.

11 Pinto, G., Abadie, V., Mesnage, R., Blustajn, J., Cabrol, S., Amiel, J., Hertz-Pannier, L., Bertrand, A.M., Lyonnet, S., Rappaport, R. *et al.* (2005) CHARGE syndrome includes hypogonadotropic hypogonadism and abnormal olfactory bulb development. *J Clin Endocrinol Metab*, **90**, 5621-5626.

12 Zentner, G.E., Layman, W.S., Martin, D.M. and Scacheri, P.C. (2010) Molecular and phenotypic aspects of CHD7 mutation in CHARGE syndrome. *Am J Med Genet A*, **152A**, 674-686.

13 Camper, S., Suh, H., Raetzman, L., Douglas, K., Cushman, L., Nasonkin, I., Burrows, H., Gage, P. and Martin, D. (2002) Rossant, J. and Tam, P. (eds.), In *Mouse Development Patterning, Morphogenesis, and Organogenesis*. Academic Press, San Diego, pp. 499-518.

14 Krsmanovic, L.Z., Hu, L., Leung, P.K., Feng, H. and Catt, K.J. (2009) The hypothalamic GnRH pulse generator: multiple regulatory mechanisms. *Trends Endocrinol Metab*, **20**, 402-408.

15 Maffucci, J.A. and Gore, A.C. (2009) Chapter 2: hypothalamic neural systems controlling the female reproductive life cycle gonadotropin-releasing hormone, glutamate, and GABA. *Int Rev Cell Mol Biol*, **274**, 69-127.

16 Wray, S. (2002) Development of gonadotropin-releasing hormone-1 neurons. *Front Neuroendocrinol*, **23**, 292-316.

17 Chu, Z., Andrade, J., Shupnik, M.A. and Moenter, S.M. (2009) Differential regulation of gonadotropin-releasing hormone neuron activity and membrane properties by acutely applied estradiol: dependence on dose and estrogen receptor subtype. *J Neurosci*, **29**, 5616-5627.

18 Kelley, C.G., Lavorgna, G., Clark, M.E., Boncinelli, E. and Mellon, P.L. (2000) The Otx2 homeoprotein regulates expression from the gonadotropin-releasing hormone proximal promoter. *Mol Endocrinol*, **14**, 1246-1256.

19 Larder, R. and Mellon, P.L. (2009) Otx2 induction of the gonadotropin-releasing hormone promoter is modulated by direct interactions with Grg co-repressors. *J Biol Chem*, **284**, 16966-16978.

20 Dateki, S., Kosaka, K., Hasegawa, K., Tanaka, H., Azuma, N., Yokoya, S., Muroya, K., Adachi, M., Tajima, T., Motomura, K. *et al.* (2010) Heterozygous orthodenticle homeobox 2 mutations are associated with variable pituitary phenotype. *J Clin Endocrinol Metab*, **95**, 756-764.

21 Omodei, D., Acampora, D., Mancuso, P., Prakash, N., Di Giovannantonio, L.G., Wurst, W. and Simeone, A. (2008) Anterior-posterior graded response to Otx2 controls proliferation and differentiation of dopaminergic progenitors in the ventral mesencephalon. *Development*, **135**, 3459-3470.

22 Vernay, B., Koch, M., Vaccarino, F., Briscoe, J., Simeone, A., Kageyama, R. and Ang, S.L. (2005) Otx2 regulates subtype specification and neurogenesis in the midbrain. *J Neurosci*, **25**, 4856-4867.

23 Kawauchi, S., Shou, J., Santos, R., Hebert, J.M., McConnell, S.K., Mason, I. and Calof, A.L. (2005) Fgf8 expression defines a morphogenetic center required for olfactory neurogenesis and nasal cavity development in the mouse. *Development*, **132**, 5211-5223.

24 Hebert, J.M., Lin, M., Partanen, J., Rossant, J. and McConnell, S.K. (2003) FGF signaling through FGFR1 is required for olfactory bulb morphogenesis. *Development*, **130**, 1101-1111.

25 Hsu, P., Yu, F., Feron, F., Pickles, J.O., Sneesby, K. and Mackay-Sim, A. (2001) Basic fibroblast growth factor and fibroblast growth factor receptors in adult olfactory epithelium. *Brain Res*, **896**, 188-197.

26 Chung, W.C., Moyle, S.S. and Tsai, P.S. (2008) Fibroblast growth factor 8 signaling through fibroblast growth factor receptor 1 is required for the emergence of gonadotropin-releasing hormone neurons. *Endocrinology*, **149**, 4997-5003.

27 Falardeau, J., Chung, W.C., Beenken, A., Raivio, T., Plummer, L., Sidis, Y., Jacobson-Dickman, E.E., Eliseenkova, A.V., Ma, J., Dwyer, A. *et al.* (2008) Decreased FGF8 signaling causes deficiency of gonadotropin-releasing hormone in humans and mice. *J Clin Invest*, **118**, 2822-2831.

28 Tsai, P.S., Moenter, S.M., Postigo, H.R., El Majdoubi, M., Pak, T.R., Gill, J.C., Paruthiyil, S., Werner, S. and Weiner, R.I. (2005) Targeted expression of a dominant-negative fibroblast growth factor (FGF) receptor in gonadotropin-releasing hormone (GnRH) neurons reduces FGF responsiveness and the size of GnRH neuronal population. *Mol Endocrinol*, **19**, 225-236.

29 Layman, W.S., McEwen, D.P., Beyer, L.A., Lalani, S.R., Fernbach, S.D., Oh, E., Swaroop, A., Hegg, C.C., Raphael, Y., Martens, J.R. *et al.* (2009) Defects in neural stem

cell proliferation and olfaction in Chd7 deficient mice indicate a mechanism for hyposmia in human CHARGE syndrome. *Hum Mol Genet*, **18**, 1909-1923.

30 Hurd, E.A., Capers, P.L., Blauwkamp, M.N., Adams, M.E., Raphael, Y., Poucher, H.K. and Martin, D.M. (2007) Loss of Chd7 function in gene-trapped reporter mice is embryonic lethal and associated with severe defects in multiple developing tissues. *Mamm Genome*, **18**, 94-104.

31 Sanlaville, D., Etchevers, H.C., Gonzales, M., Martinovic, J., Clement-Ziza, M., Delezoide, A.L., Aubry, M.C., Pelet, A., Chemouny, S., Cruaud, C. *et al.* (2006) Phenotypic spectrum of CHARGE syndrome in fetuses with CHD7 truncating mutations correlates with expression during human development. *J Med Genet*, **43**, 211-217.

32 Wray, S., Grant, P. and Gainer, H. (1989) Evidence that cells expressing luteinizing hormone-releasing hormone mRNA in the mouse are derived from progenitor cells in the olfactory placode. *Proc Natl Acad Sci U S A*, **86**, 8132-8136.

33 Becker, P.B. and Horz, W. (2002) ATP-dependent nucleosome remodeling. *Annu Rev Biochem*, **71**, 247-273.

34 Eberharter, A. and Becker, P.B. (2004) ATP-dependent nucleosome remodelling: factors and functions. *J Cell Sci*, **117**, 3707-3711.

35 Lusser, A. and Kadonaga, J.T. (2003) Chromatin remodeling by ATP-dependent molecular machines. *Bioessays*, **25**, 1192-1200.

36 Narlikar, G.J., Fan, H.Y. and Kingston, R.E. (2002) Cooperation between complexes that regulate chromatin structure and transcription. *Cell*, **108**, 475-487.

37 Smith, C.L. and Peterson, C.L. (2005) ATP-dependent chromatin remodeling. *Curr Top Dev Biol*, **65**, 115-148.

38 Bergman, J.E., Bosman, E.A., van Ravenswaaij-Arts, C.M. and Steel, K.P. (2009) Study of smell and reproductive organs in a mouse model for CHARGE syndrome. *Eur J Hum Genet*.

39 Bosman, E.A., Penn, A.C., Ambrose, J.C., Kettleborough, R., Stemple, D.L. and Steel, K.P. (2005) Multiple mutations in mouse Chd7 provide models for CHARGE syndrome. *Hum Mol Genet*, **14**, 3463-3476.

40 Nelson, J.F., Karelus, K., Felicio, L.S. and Johnson, T.E. (1990) Genetic influences on the timing of puberty in mice. *Biol Reprod*, **42**, 649-655.

41 Lee, J.M., Appugliese, D., Kaciroti, N., Corwyn, R.F., Bradley, R.H. and Lumeng, J.C. (2007) Weight status in young girls and the onset of puberty. *Pediatrics*, **119**, e624-630.

42 Ahima, R.S., Dushay, J., Flier, S.N., Prabakaran, D. and Flier, J.S. (1997) Leptin accelerates the onset of puberty in normal female mice. *J Clin Invest*, **99**, 391-395.

43 Foster, D.L., Ebling, F.J., Micka, A.F., Vannerson, L.A., Bucholtz, D.C., Wood, R.I., Suttie, J.M. and Fenner, D.E. (1989) Metabolic interfaces between growth and

reproduction. I. Nutritional modulation of gonadotropin, prolactin, and growth hormone secretion in the growth-limited female lamb. *Endocrinology*, **125**, 342-350.

44 Frisch, R.E. and McArthur, J.W. (1974) Menstrual cycles: fatness as a determinant of minimum weight for height necessary for their maintenance or onset. *Science*, **185**, 949-951.

45 Kennedy, G.C. (1969) Interactions between feeding behavior and hormones during growth. *Ann N Y Acad Sci*, **157**, 1049-1061.

46 Budak, E., Fernandez Sanchez, M., Bellver, J., Cervero, A., Simon, C. and Pellicer, A. (2006) Interactions of the hormones leptin, ghrelin, adiponectin, resistin, and PYY3-36 with the reproductive system. *Fertil Steril*, **85**, 1563-1581.

47 Plum, L., Schubert, M. and Bruning, J.C. (2005) The role of insulin receptor signaling in the brain. *Trends Endocrinol Metab*, **16**, 59-65.

48 Schneider, J.E. (2004) Energy balance and reproduction. *Physiol Behav*, **81**, 289-317.

49 Bruning, J.C., Gautam, D., Burks, D.J., Gillette, J., Schubert, M., Orban, P.C., Klein, R., Krone, W., Muller-Wieland, D. and Kahn, C.R. (2000) Role of brain insulin receptor in control of body weight and reproduction. *Science*, **289**, 2122-2125.

50 Chehab, F.F., Lim, M.E. and Lu, R. (1996) Correction of the sterility defect in homozygous obese female mice by treatment with the human recombinant leptin. *Nat Genet*, **12**, 318-320.

51 He, D., Funabashi, T., Sano, A., Uemura, T., Minaguchi, H. and Kimura, F. (1999) Effects of glucose and related substrates on the recovery of the electrical activity of gonadotropin-releasing hormone pulse generator which is decreased by insulin-induced hypoglycemia in the estrogen-primed ovariectomized rat. *Brain Res*, **820**, 71-76.

52 Hiney, J.K., Srivastava, V., Nyberg, C.L., Ojeda, S.R. and Dees, W.L. (1996) Insulin-like growth factor I of peripheral origin acts centrally to accelerate the initiation of female puberty. *Endocrinology*, **137**, 3717-3728.

53 Longo, K.M., Sun, Y. and Gore, A.C. (1998) Insulin-like growth factor-I effects on gonadotropin-releasing hormone biosynthesis in GT1-7 cells. *Endocrinology*, **139**, 1125-1132.

54 Mounzih, K., Lu, R. and Chehab, F.F. (1997) Leptin treatment rescues the sterility of genetically obese ob/ob males. *Endocrinology*, **138**, 1190-1193.

55 Schneider, J.E. and Wade, G.N. (1989) Availability of metabolic fuels controls estrous cyclicity of Syrian hamsters. *Science*, **244**, 1326-1328.

56 Luque, R.M., Park, S. and Kineman, R.D. (2007) Severity of the catabolic condition differentially modulates hypothalamic expression of growth hormone-releasing

hormone in the fasted mouse: potential role of neuropeptide Y and corticotropin-releasing hormone. *Endocrinology*, **148**, 300-309.

57 Staley, K. and Scharfman, H. (2005) A woman's prerogative. *Nat Neurosci*, **8**, 697-699.

58 Kumar, T.R., Wang, Y., Lu, N. and Matzuk, M.M. (1997) Follicle stimulating hormone is required for ovarian follicle maturation but not male fertility. *Nat Genet*, **15**, 201-204.

59 Layman, L.C. and McDonough, P.G. (2000) Mutations of follicle stimulating hormone-beta and its receptor in human and mouse: genotype/phenotype. *Mol Cell Endocrinol*, **161**, 9-17.

60 Layman, L.C., Porto, A.L., Xie, J., da Motta, L.A., da Motta, L.D., Weiser, W. and Sluss, P.M. (2002) FSH beta gene mutations in a female with partial breast development and a male sibling with normal puberty and azoospermia. *J Clin Endocrinol Metab*, **87**, 3702-3707.

61 Phillip, M., Arbelle, J.E., Segev, Y. and Parvari, R. (1998) Male hypogonadism due to a mutation in the gene for the beta-subunit of follicle-stimulating hormone. *N Engl J Med*, **338**, 1729-1732.

62 Lamba, P., Santos, M.M., Philips, D.P. and Bernard, D.J. (2006) Acute regulation of murine follicle-stimulating hormone beta subunit transcription by activin A. *J Mol Endocrinol*, **36**, 201-220.

63 Weiss, J., Guendner, M.J., Halvorson, L.M. and Jameson, J.L. (1995) Transcriptional activation of the follicle-stimulating hormone beta-subunit gene by activin. *Endocrinology*, **136**, 1885-1891.

64 Wen, S., Ai, W., Alim, Z. and Boehm, U. (2010) Embryonic gonadotropin-releasing hormone signaling is necessary for maturation of the male reproductive axis. *Proc Natl Acad Sci U S A*.

65 Pask, A.J., Kanasaki, H., Kaiser, U.B., Conn, P.M., Janovick, J.A., Stockton, D.W., Hess, D.L., Justice, M.J. and Behringer, R.R. (2005) A novel mouse model of hypogonadotrophic hypogonadism: N-ethyl-N-nitrosourea-induced gonadotropin-releasing hormone receptor gene mutation. *Mol Endocrinol*, **19**, 972-981.

66 Wu, S., Wilson, M.D., Busby, E.R., Isaac, E.R. and Sherwood, N.M. (2010) Disruption of the single copy gonadotropin-releasing hormone receptor in mice by gene trap: severe reduction of reproductive organs and functions in developing and adult mice. *Endocrinology*, **151**, 1142-1152.

67 Messager, S., Chatzidaki, E.E., Ma, D., Hendrick, A.G., Zahn, D., Dixon, J., Thresher, R.R., Malinge, I., Lomet, D., Carlton, M.B. *et al.* (2005) Kisspeptin directly stimulates gonadotropin-releasing hormone release via G protein-coupled receptor 54. *Proc Natl Acad Sci U S A*, **102**, 1761-1766.

68 Gill, J.C., Wadas, B., Chen, P., Portillo, W., Reyna, A., Jorgensen, E., Mani, S., Schwarting, G.A., Moenter, S.M., Tobet, S. *et al.* (2008) The gonadotropin-releasing

hormone (GnRH) neuronal population is normal in size and distribution in GnRH-deficient and GnRH receptor-mutant hypogonadal mice. *Endocrinology*, **149**, 4596-4604.

69 Sofianos, Z.D., Katsila, T., Kostomitsopoulos, N., Balafas, V., Matsoukas, J., Tselios, T. and Tamvakopoulos, C. (2008) In vivo evaluation and in vitro metabolism of leuprolide in mice--mass spectrometry-based biomarker measurement for efficacy and toxicity. *J Mass Spectrom*, **43**, 1381-1392.

70 Yamazaki, I. and Okada, H. (1980) A radioimmunoassay for a highly active luteinizing hormone-releasing hormone analogue and relation between the serum level of the analogue and that of gonadotropin. *Endocrinol Jpn*, **27**, 593-605.

71 Danforth, D.R., Arbogast, L.K. and Friedman, C.I. (2005) Acute depletion of murine primordial follicle reserve by gonadotropin-releasing hormone antagonists. *Fertil Steril*, **83**, 1333-1338.

72 Ljungqvist, A., Feng, D.M., Hook, W., Shen, Z.X., Bowers, C. and Folkers, K. (1988) Antide and related antagonists of luteinizing hormone release with long action and oral activity. *Proc Natl Acad Sci U S A*, **85**, 8236-8240.

73 Bennett-Clarke, C. and Joseph, S.A. (1982) Immunocytochemical distribution of LHRH neurons and processes in the rat: hypothalamic and extrahypothalamic locations. *Cell Tissue Res*, **221**, 493-504.

74 Wierman, M.E., Kiseljak-Vassiliades, K. and Tobet, S. (2010) Gonadotropin-releasing hormone (GnRH) neuron migration: Initiation, maintenance and cessation as critical steps to ensure normal reproductive function. *Front Neuroendocrinology*.

75 Colledge, W.H., Mei, H. and Tassigny, X.D. (2010) Mouse models to study the central regulation of puberty. *Mol Cell Endocrinol*.

76 Matsumoto, S., Yamazaki, C., Masumoto, K.H., Nagano, M., Naito, M., Soga, T., Hiyama, H., Matsumoto, M., Takasaki, J., Kamohara, M. *et al.* (2006) Abnormal development of the olfactory bulb and reproductive system in mice lacking prokineticin receptor PKR2. *Proc Natl Acad Sci U S A*, **103**, 4140-4145.

77 Gamble, J.A., Karunadasa, D.K., Pape, J.R., Skynner, M.J., Todman, M.G., Bicknell, R.J., Allen, J.P. and Herbison, A.E. (2005) Disruption of ephrin signaling associates with disordered axophilic migration of the gonadotropin-releasing hormone neurons. *J Neurosci*, **25**, 3142-3150.

78 Cogliati, T., Delgado-Romero, P., Norwitz, E.R., Guduric-Fuchs, J., Kaiser, U.B., Wray, S. and Kirsch, I.R. (2007) Pubertal impairment in Nhlh2 null mice is associated with hypothalamic and pituitary deficiencies. *Mol Endocrinol*, **21**, 3013-3027.

79 Compagnucci, C., Fish, J.L., Schwark, M., Tarabykin, V. and Depew, M.J. (2011) Pax6 regulates craniofacial form through its control of an essential cephalic ectodermal patterning center. *Genesis*, **49**, 307-325.

80 Kaiser, U.B., Jakubowiak, A., Steinberger, A. and Chin, W.W. (1993) Regulation of rat pituitary gonadotropin-releasing hormone receptor mRNA levels in vivo and in vitro. *Endocrinology*, **133**, 931-934.

81 White, B.R., Duval, D.L., Mulvaney, J.M., Roberson, M.S. and Clay, C.M. (1999) Homologous regulation of the gonadotropin-releasing hormone receptor gene is partially mediated by protein kinase C activation of an activator protein-1 element. *Mol Endocrinol*, **13**, 566-577.

82 Yasin, M., Dalkin, A.C., Haisenleder, D.J., Kerrigan, J.R. and Marshall, J.C. (1995) Gonadotropin-releasing hormone (GnRH) pulse pattern regulates GnRH receptor gene expression: augmentation by estradiol. *Endocrinology*, **136**, 1559-1564.

83 Hurd, E.A., Poucher, H.K., Cheng, K., Raphael, Y. and Martin, D.M. (2010) The ATP-dependent chromatin remodeling enzyme CHD7 regulates pro-neural gene expression and neurogenesis in the inner ear. *Development*, **137**, 3139-3150.

84 Schnetz, M.P., Handoko, L., Akhtar-Zaidi, B., Bartels, C.F., Pereira, C.F., Fisher, A.G., Adams, D.J., Flicek, P., Crawford, G.E., Laframboise, T. *et al.* (2010) CHD7 targets active gene enhancer elements to modulate ES cell-specific gene expression. *PLoS Genet*, **6**, e1001023.

85 Bajpai, R., Chen, D.A., Rada-Iglesias, A., Zhang, J., Xiong, Y., Helms, J., Chang, C.P., Zhao, Y., Swigut, T. and Wysocka, J. (2010) CHD7 cooperates with PBAF to control multipotent neural crest formation. *Nature*, **463**, 958-962.

86 Takada, I., Mihara, M., Suzawa, M., Ohtake, F., Kobayashi, S., Igarashi, M., Youn, M.Y., Takeyama, K., Nakamura, T., Mezaki, Y. *et al.* (2007) A histone lysine methyltransferase activated by non-canonical Wnt signalling suppresses PPAR-gamma transactivation. *Nat Cell Biol*, **9**, 1273-1285.

87 Srinivasan, S., Dorighi, K.M. and Tamkun, J.W. (2008) Drosophila Kismet regulates histone H3 lysine 27 methylation and early elongation by RNA polymerase II. *PLoS Genet*, **4**, e1000217.

88 Cattanach, B.M., Iddon, C.A., Charlton, H.M., Chiappa, S.A. and Fink, G. (1977) Gonadotrophin-releasing hormone deficiency in a mutant mouse with hypogonadism. *Nature*, **269**, 338-340.

89 Ho, L. and Crabtree, G.R. (2010) Chromatin remodelling during development. *Nature*, **463**, 474-484.

90 Peretto, P., Cummings, D., Modena, C., Behrens, M., Venkatraman, G., Fasolo, A. and Margolis, F.L. (2002) BMP mRNA and protein expression in the developing mouse olfactory system. *J Comp Neurol*, **451**, 267-278.

91 Peretto, P., Dati, C., De Marchis, S., Kim, H.H., Ukhanova, M., Fasolo, A. and Margolis, F.L. (2004) Expression of the secreted factors noggin and bone morphogenetic proteins in the subependymal layer and olfactory bulb of the adult mouse brain. *Neuroscience*, **128**, 685-696.

92 Cate, H.S., Sabo, J.K., Merlo, D., Kemper, D., Aumann, T.D., Robinson, J., Merson, T.D., Emery, B., Perreau, V.M. and Kilpatrick, T.J. (2010) Modulation of bone morphogenic protein signalling alters numbers of astrocytes and oligodendroglia in the subventricular zone during cuprizone-induced demyelination. *J Neurochem*.

93 Kang, K. and Song, M.R. (2010) Diverse FGF receptor signaling controls astrocyte specification and proliferation. *Biochem Biophys Res Commun*.

94 Gonzalez-Quevedo, R., Lee, Y., Poss, K.D. and Wilkinson, D.G. (2010) Neuronal regulation of the spatial patterning of neurogenesis. *Dev Cell*, **18**, 136-147.

95 Maier, E., von Hofsten, J., Nord, H., Fernandes, M., Paek, H., Hebert, J.M. and Gunhaga, L. (2010) Opposing Fgf and Bmp activities regulate the specification of olfactory sensory and respiratory epithelial cell fates. *Development*, **137**, 1601-1611.

96 Shou, J., Murray, R.C., Rim, P.C. and Calof, A.L. (2000) Opposing effects of bone morphogenetic proteins on neuron production and survival in the olfactory receptor neuron lineage. *Development*, **127**, 5403-5413.

97 Shou, J., Rim, P.C. and Calof, A.L. (1999) BMPs inhibit neurogenesis by a mechanism involving degradation of a transcription factor. *Nat Neurosci*, **2**, 339-345.

98 Bonaguidi, M.A., Peng, C.Y., McGuire, T., Falciglia, G., Gobeske, K.T., Czeisler, C. and Kessler, J.A. (2008) Noggin expands neural stem cells in the adult hippocampus. *J Neurosci*, **28**, 9194-9204.

99 Calof, A.L., Bonnin, A., Crocker, C., Kawauchi, S., Murray, R.C., Shou, J. and Wu, H.H. (2002) Progenitor cells of the olfactory receptor neuron lineage. *Microsc Res Tech*, **58**, 176-188.

100 Colak, D., Mori, T., Brill, M.S., Pfeifer, A., Falk, S., Deng, C., Monteiro, R., Mummery, C., Sommer, L. and Gotz, M. (2008) Adult neurogenesis requires Smad4-mediated bone morphogenic protein signaling in stem cells. *J Neurosci*, **28**, 434-446.

101 Garcia-Gonzalez, D., Clemente, D., Coelho, M., Esteban, P.F., Soussi-Yanicostas, N. and de Castro, F. (2010) Dynamic roles of FGF-2 and Anosmin-1 in the migration of neuronal precursors from the subventricular zone during pre- and postnatal development. *Exp Neurol*, **222**, 285-295.

102 Vissers, L.E., van Ravenswaaij, C.M., Admiraal, R., Hurst, J.A., de Vries, B.B., Janssen, I.M., van der Vliet, W.A., Huys, E.H., de Jong, P.J., Hamel, B.C. *et al.* (2004) Mutations in a new member of the chromodomain gene family cause CHARGE syndrome. *Nat Genet*, **36**, 955-957.

103 Wyatt, A., Bakrania, P., Bunyan, D.J., Osborne, R.J., Crolla, J.A., Salt, A., Ayuso, C., Newbury-Ecob, R., Abou-Rayyah, Y., Collin, J.R. *et al.* (2008) Novel heterozygous OTX2 mutations and whole gene deletions in anophthalmia, microphthalmia and coloboma. *Hum Mutat*, **29**, E278-283.

104 Dateki, S., Fukami, M., Sato, N., Muroya, K., Adachi, M. and Ogata, T. (2008) OTX2 mutation in a patient with anophthalmia, short stature, and partial growth hormone

deficiency: functional studies using the IRBP, HESX1, and POU1F1 promoters. *J Clin Endocrinol Metab*, **93**, 3697-3702.

105 Fallest, P.C., Trader, G.L., Darrow, J.M. and Shupnik, M.A. (1995) Regulation of rat luteinizing hormone beta gene expression in transgenic mice by steroids and a gonadotropin-releasing hormone antagonist. *Biol Reprod*, **53**, 103-109.

106 Haavisto, A.M., Pettersson, K., Bergendahl, M., Perheentupa, A., Roser, J.F. and Huhtaniemi, I. (1993) A supersensitive immunofluorometric assay for rat luteinizing hormone. *Endocrinology*, **132**, 1687-1691.

107 Matteri, R.L., Roser, J.F., Baldwin, D.M., Lipovetsky, V. and Papkoff, H. (1987) Characterization of a monoclonal antibody which detects luteinizing hormone from diverse mammalian species. *Domest Anim Endocrinol*, **4**, 157-165.

108 Gay, V.L., Midgley, A.R., Jr. and Niswender, G.D. (1970) Patterns of gonadotrophin secretion associated with ovulation. *Fed Proc*, **29**, 1880-1887.

109 Livak, K.J. and Schmittgen, T.D. (2001) Analysis of relative gene expression data using real-time quantitative PCR and the 2(-Delta Delta C(T)) Method. *Methods*, **25**, 402-408.

Chapter 4

CHD7 deficient mice have defects in neural stem cell maintenance and cell fate

Introduction

CHD7 haploinsufficiency in humans causes CHARGE syndrome, a clinically variable, multiple congenital anomaly condition with an estimated incidence of 1:8500-1:12,000 (1-3). CHARGE is characterized by ocular coloboma, heart defects, atresia of the choanae, retarded growth and development, genital hypoplasia, and ear abnormalities including deafness and vestibular disorders (4). CHARGE individuals also have craniofacial abnormalities, hypogonadotropic hypogonadism, and olfactory dysfunction (4-11). Heterozygosity for nonsense, deletion, or missense *CHD7* mutations is estimated to occur in 60-80% of patients with CHARGE syndrome (5-11). These mutations are distributed throughout the coding sequence and do not appear to be correlated with specific aspects of the clinical phenotype (5-11). Most human *CHD7* mutations identified thus far are *de novo*; however, evidence for germline mosaicism has been suggested for families with multiple affected siblings (6, 12-14). Magnetic resonance imaging shows olfactory bulb defects ranging from hypoplasia to complete absence in all CHARGE individuals tested, and olfactory dysfunction in a majority of patients (15-20).

Chd7 is expressed in the developing and mature human and mouse subventricular zone and olfactory bulb (7, 8, 21-23). However, the cell type specific expression of *Chd7*

in these regions of the central nervous system is unknown. Since *Chd7* is expressed in the neural stem cell population in the olfactory epithelium (23), it is possible that *Chd7* is also expressed in the neural stem cells of the subventricular zone. *Chd7* is expressed in pro-neural and proliferating olfactory neural stem cells (23). *Chd7*$^{Gt/+}$ mice have a 50% reduction in olfactory neural stem cell proliferation and 30% fewer olfactory sensory neurons (23). Consistent with the human CHARGE phenotype, *Chd7*$^{Gt/+}$ mice also have olfactory bulb hypoplasia, which may be caused by defects in normal olfactory bulb regeneration (23). Since regeneration of the olfactory epithelium and olfactory bulb are required for normal odorant detection, haploinsufficiency for *Chd7* could contribute to defects in neural stem cells in the subventricular zone and subsequent olfactory bulb hypoplasia.

The interneuron populations in the olfactory bulb are continuously regenerated throughout the life of an organism from neural stem cells located in the subventricular zone (24-26). Neural stem cells in the subventricular zone proliferate, differentiate, and migrate along the rostral migratory stream (RMS) to the olfactory bulb. The olfactory bulb is primarily composed of three broad cell types including mitral cells, tufted cells, and interneurons (24-26). New neurons entering the olfactory bulb from the RMS are not randomly inserted into the olfactory bulb but are carefully integrated into the organized circuitry of the olfactory bulb as interneurons (24-26). Most (about 90%) of these newly generated neurons become granule cells, which are the most abundant interneuron cell type in the bulb (24, 26). Periglomerular cells comprise the second population of interneurons integrated from the RMS. Periglomerular cells are a diverse population of interneurons which include calretinin-containing, dopamine-containing, and calbindin-

containing neurons (24-28). Given the diversity of interneurons regenerated in the olfactory bulb by the neural stem cells of the subventricular zone, it is important to understand how loss of *Chd7* may impact these neural cell types.

Results

Chd7 is expressed in neural stem cells in the subventricular zone

Clinical data in humans with CHARGE have suggested a high prevalence of olfactory bulb defects, ranging from complete absence of the bulbs to mild hypoplasia or asymmetry (15-20). The subventricular zone contains a population of neural stem cells that give rise to the various interneuron populations in the olfactory bulb (25-27). Neural stem cell populations must be tightly regulated to maintain the proper proportions of neural stem cells, neuroblasts and differentiated interneurons (25-27). In order to identify CHD7-positive cell types within the adult subventricular zone, we used immunofluorescence with anti-CHD7 and cell type specific antibodies. Neural stem cells that function as primary precursors in the subventricular zone correspond to type B cells, a subpopulation of slowly dividing cells that are positive for the astrocyte marker glial fibrillary acidic protein (GFAP) (24, 26, 28). Type B cells produce type C cells which are GFAP-negative and Sox2-positive (24-26, 28). Type C cells divide rapidly and produce neuroblasts or type A cells (24-26, 28). Type A cells divide rapidly and migrate tangentially in chains along the RMS, which is lined by GFAP-positive astrocytes (24-26, 28). We found that most CHD7-positive cells in the subventricular zone were GFAP-negative but Sox2-positive in both wild type and $Chd7^{Gt/+}$ mice (Figure 4.1 A-C).

CHD7-positive cells were also located in the RMS in association with the GFAP-positive astrocytes which line the RMS in both wild type and *Chd7*$^{Gt/+}$ mice (Figure 4.1 D).

Cellular proliferation in the subventricular zone requires proper CHD7 dosage

Chd7 haploinsufficiency in mice causes a 50% decrease in neural stem cell proliferation in the adult and embryonic olfactory epithelium/placode (23). To determine whether CHD7 deficiency causes decreased cellular proliferation in the subventricular zone, we used a 30 minute BrdU incorporation assay to identify S-phase cells in the wild type and *Chd7*$^{Gt/+}$ subventricular zone (Figure 4.2 A and B). Quantification of BrdU-positive cells revealed a 46% reduction in proliferating cells in the subventricular zone in adult *Chd7*$^{Gt/+}$ mice compared to wild type littermates (Figure 4.2 C).

Interneuron populations in the olfactory bulb are CHD7-positive

Mitral and tufted cells of the olfactory bulb interact with a large population of local circuit interneurons that use γ-aminobutyric acid (GABA) as their main neurotransmitter (26). There are two principle types of these adult-born interneurons in the olfactory bulb: granule cells and periglomerular cells. These interneurons can be subdivided into calretinin-positive, tyrosine hydroxylase-positive, and calbindin-positive neurons (24-28). To determine the cell type specific expression of *Chd7* in the olfactory bulb, we used immunofluorescence with anti-CHD7 together with anti-calretinin, anti-tyrosine hydroxylase, and anti-calbindin. We found that CHD7-positive cells in the olfactory bulb co-localize with interneurons positive for GABA, calretinin, tyrosine

hydroxylase, and calbindin neurons in both wild type and *Chd7*$^{Gt/+}$ mice (Figure 4.3 A-D).

Chd7 conditional knockout embryos lack most olfactory tissues

Since *Chd7* null mice are embryonic lethal by E11 (22), we generated a *Chd7* conditional null allele, *Chd7*^{flox} (29). *Foxg1-Cre* is expressed in sensory neural tissues (olfactory epithelium) as well as in regions of the central nervous system including the subventricular zone by E8.5. *Chd7*$^{flox/Gt}$; *Foxg1-Cre* mice do not survive beyond postnatal day 1 (29). *Chd7*$^{flox/Gt}$; *Foxg1-Cre* pups are born with craniofacial dysmorphisms (Figure 4.4 C) and appear to have respiratory distress. Since newborn pups are obligate nose breathers, the respiratory distress may be due to craniofacial defects that affect air passage through the nose. Bisected heads from E12.5 and P0 *Chd7*$^{flox/Gt}$; *Foxg1-Cre* mice appear to have severely hypoplastic/absent olfactory turbinates and severely hypoplastic/absent olfactory bulbs compared to *Chd7*$^{flox/+}$ littermates (Figure 4.4 A-C). These data suggest that CHD7 is essential for normal olfactory epithelium and bulb development. However, the combined effect of tissue-specific loss of *Chd7* together with *Foxg1* haploinsufficiency may also contribute to this phenotype.

CHD7 deficient neurospheres have defects in neural stem cell self-renewal

The *in vitro* effect of *Chd7* tissue-specific loss was analyzed by generating neurosphere cultures derived from E14.5 embryonic telencephalon. *Chd7*$^{flox/Gt}$; *Foxg1-Cre* primary and secondary neurospheres were examined for frequency, size, and multipotency. We found that *Chd7*$^{flox/Gt}$; *Foxg1-Cre* telencephalon cells formed

mutipotent primary neurospheres at a significantly lower frequency than *Chd7*$^{flox/+}$ littermates (Figure 4.5 A), which suggests that there are significantly fewer neural stem cells in the *Chd7*$^{flox/Gt}$; *Foxg1-Cre* telencephalon. Additionally, *Chd7*$^{flox/Gt}$, *Chd7*$^{flox/+}$; *Foxg1-Cre*, and *Chd7*$^{flox/Gt}$; *Foxg1-Cre* telencephalon cells formed primary neurospheres that were significantly smaller than *Chd7*$^{flox/+}$ littermates (Figure 4.5 B). Secondary neurospheres formed by sub-cloning primary neurospheres also gave rise to fewer multipotent *Chd7*$^{flox/Gt}$; *Foxg1-Cre* neurospheres that were significantly smaller in size than *Chd7*$^{flox/+}$ littermates (Figure 4.5 C and D), indicating a defect in self-renewal. *Chd7*$^{flox/Gt}$ and *Chd7*$^{flox/+}$; *Foxg1-Cre* also formed significantly smaller multipotent secondary neurospheres but at a frequency similar to *Chd7*$^{flox/+}$ littermates (Figure 4.5 C and D). Consistent with the reduction in neurosphere size, *Chd7*$^{flox/Gt}$, *Chd7*$^{flox/+}$; *Foxg1-Cre*, *Chd7*$^{flox/Gt}$; *Foxg1-Cre* neurosphere colonies contained fewer cells than *Chd7*$^{flox/+}$ littermates (data not shown). These data together suggest that CHD7 deficiency reduces the self-renewal capacity of neural stem cells.

Loss of CHD7 leads to a cell fate switch

We recently showed that CHD7 positively regulates the expression of *Fgfr1* in the E10.5 olfactory placode (30). FGFR1 deficiency in subventricular zone neural stem cells causes decreased cellular proliferation and spontaneous cellular differentiation toward a glial cell fate (31). Adult *Chd7* conditional knockout mice were generated to test whether loss CHD7 causes a spontaneous shift in cellular differentiation toward a glial cell fate. *Ubc-creERT2* mice ubiquitously express *cre* in response to Tamoxifen administration (32). *Chd7*$^{flox/Gt}$; *Ubc-CreERT2* mice have a visually apparent increase in GFAP-positive

cells in the subventricular zone and olfactory bulb compared to *Chd7*$^{flox/+}$ littermates (Figure 4.6 A-F). The increase in GFAP-positive cells was also seen in the olfactory bulb surrounding the glomeruli in regions usually occupied by interneurons (Figure 4.6 E and F). These data suggest that loss of CHD7 in adult neural progenitors causes a spontaneous shift toward a glial cell fate.

Discussion

Here we provide evidence that CHD7 is required to maintain neural stem cell proliferation and self-renewal. We observed *Chd7* expression in the adult mouse subventricular zone, rostral migratory stream, and interneurons in the olfactory bulb. CHD7 co-localizes with Sox2-positive cells in the adult subventricular zone. *Chd7* continues to be expressed in migrating neuroblasts in the rostral migratory stream and in calbindin-positive, calretinin-postive, and tyrosine hydroxyase-positive interneuron populations in the olfactory bulb. *Chd7* deficient mice have a significant (46%) decrease in neural stem cell proliferation in the subventricular zone. Tissue-specific loss of CHD7 also results in a reduction in neural stem cell self-renewal. Additionally, conditional loss of CHD7 in adult neural progenitors causes a switch toward a glial cell fate. Taken together, these data indicate a critical role for CHD7 in neural stem cell maintenance and cell fate specification from developmental stages through adulthood.

Roles for CHD7 in regulation of gene expression during tissue development and maintenance are emerging for multiple organs. A recent study found that CHD7 binds to SOX2 in neural stem cells and helps regulate expression of genes that are mutated in human syndromes (33). In a study of neural crest formation in *Xenopus*, CHD7 was

implicated to regulate multipotent neural crest-like cells by binding to PBAF components including BRG1, BAF170, BAF155, BAF57, PB1, ARID2, and BRD7 (34). In mesenchymal stem cells, CHD7 regulates cell fate specification during osteoblast and adipocyte differentiation (35). CHD7 forms a complex with NLK, SETDB1, and PPAR-γ, and binds to methylated lysine 4 and lysine 9 residues on histone H3 at PPAR-γ target promoters, which suppresses ligand-induced transactivation of PPAR-γ target genes (35). Additionally, the *CHD7 Drosophila* orthologue, *Kismet*, is involved in transcriptional elongation by RNA polymerase II through recruitment of ASH1 and TRX, and may help maintain stem cell pluripotency by regulating methylation of histone H3 lysine 27 (36). Together, these data provide evidence that CHD7 functions to regulate gene expression through tissue-specific transcriptional complex formation with additional factors.

Neural stem cells and progenitors must be tightly regulated by factors that are likely to be temporally and spatially restricted (37). Previous reports have shown CHD7 regulates the expression of *Fgfr1* and *Bmp4* in the olfactory placode during development (30). Although BMP activity is generally thought to inhibit neurogenesis, low doses of BMP4 are required for promoting neurogenesis in multiple tissues including the subventricular zone, hippocampus, and the olfactory placode (38-43). FGF2 signals via FGFR1 to induce proliferation of neural stem cells in the subventricular zone (44). Loss of FGFR1 in neural stem cells from the subventricular zone results in decreased cellular proliferation and spontaneous cellular differentiation toward a glial cell fate (31). Our data are consistent with these previous reports, since conditional loss of CHD7 in adult neural progenitors appears to result in a spontaneous switch toward a glial cell fate.

Reductions in CHD7 dosage in neural stem cells may result in decreased *Bmp4* and *Fgfr1* expression causing decreased self-renewal and neurogenesis, and a switch in cell fate.

Adult *Chd7* expression in the mouse brain is mostly restricted to proliferative regions including the subventricular zone and dentate gyrus [data available on GENSAT website (http://www.gensat.org/index.html)]. However, CHD7 function in adult tissues has not been fully explored. Our data suggest that CHD7 promotes neural stem cell self-renewal and proliferation. Maintenance of neural stem cells is critical not only during development but also into adulthood. Defects in neural stem cell proliferation have been shown in humans and mouse models to cause defects in memory (Alzheimer's disease), impaired movement (Parkinson's disease), epilepsy and developmental delay (45-47). The *CHD7 Drosophila* orthologue, *Kismet*, has been shown to regulate memory and locomotion in adult *Drosophila* (48). CHARGE patients are reported to have developmental delay ranging from mild speech delay to severe mental impairment, epilepsy, arhinencephaly, and balance dysfunction (49). Several of the clinical features of CHARGE syndrome that affect the central nervous system may be explained by a defect in neural stem cell maintenance. Further research into the mechanisms underlying CHD7 function in neural stem cells will help elucidate how neural stem cells are regulated and maintained from development through adulthood.

Materials and Methods

Mice

Chd7$^{Gt/+}$ mice were generated by backcrossing with 129S1/Sv1mJ (Jackson Laboratory) mice to generation N7-N9 and genotyped using methods as previously

described (22). *Chd7*$^{flox/flox}$ mice were generated and genotyped using methods previously described (29). *Chd7*$^{flox/Gt}$ mice were mated with *Foxg1-Cre* mice. *Foxg1-Cre* mice were maintained on the Swiss Webster (Charles River Laboratories #F44281) background and genotyped for *Cre* as described (50). *Ubc-creERT2* mice were maintained on the $B6D_2F_1$/J background (Jackson Laboratory #100006). All procedures were approved by the University Committee on Use and Care for Animals at the University of Michigan.

Immunofluorescence

Six-eight week-old *Chd7*$^{+/+}$, *Chd7*$^{Gt/+}$, *Chd7*$^{flox/+}$, or *Chd7*$^{flox/Gt}$; *Ubc-CreERT2* sex-matched littermate mice were anaesthetized with 250 mg/kg body weight tribromoethanol and perfusion fixed with 4% paraformaldehyde. Mice were then decapitated, the brains were dissected from the head and placed in 4% paraformaldehyde overnight at 4°C, followed by 30% sucrose protection overnight at 4°C. Tissue was flash frozen in O.C.T. embedding medium (Tissue Tek, Torrance, CA) for sectioning. Following cryosectioning, 14 μm sections were processed for immunofluorescence with antibodies against CHD7 (1:1000; Abcam, Cambridge, MA), BrdU (1:100; Immunologicals Direct, Raleigh, NC), Tyrosine hydroxylase (1:150; Pel-Freez, Rogers, AR), Calbindin (1:1500; Sigma, St. Louis, MO), Calretinin (1:1000; Millipore, Temecula, CA), GFAP (1:500; Sigma), O4 antibody (1:800, Developmental Studies Hybridoma Bank, University of Iowa, Iowa City, IA), and Tuj1 (1:1000, Covance, Princeton, NJ). Secondary antibodies used at 1:200 were conjugated with Alexa 488, Alexa 555, or biotin with streptavidin-HRP (Vector Laboratories) and biotinylated

secondary antibodies conjugated with streptavidin-Alexa488 or streptavidin-Alexa555 Molecular Probes, Eugene, OR and Invitrogen, Carlsbad, CA). Images were captured by single channel fluorescence microscopy on a Leica upright DMRB microscope and processed in Photoshop v.9.0 (San Jose, CA).

Proliferation assays

Mice were injected intraperitoneally with 0.1 g/g body weight 5-bromo-2-deoxyuridine (BrdU) 30 minutes prior to sacrifice. Tissues were then processed for anti-BrdU and anti-CHD7 immunofluorescence as above. Secondary antibodies were conjugated with Alexa 488, Alexa 555, or biotin, as above. For quantitation of S-phase cells, images from the subventricular zone were analyzed in eight different mice ($N = 3$ wild type, $N = 3$ *Chd7*$^{Gt/+}$ sex-matched littermates). From each tissue section, 4-6 images were analyzed for number of BrdU-positive cells and the data tested for significance by t-test using two-tailed unequal variance.

Neurosphere cultures

Timed pregnancies were established and the morning of plug identification designated as E0.5. Embryos were harvested and amniotic sacs collected for PCR genotyping as described (22, 29). Microdissected E14.5 telencephalons were dissociated and plated as previously described (51). For the neurosphere formation assays (non-adherent cultures) we used ultra-low binding plates (Corning, Corning, NY). To test the self-renewal capacity of the neurospheres, individual neurospheres were selected, centrifuged at 210g for 4 min, and then mechanically dissociated and replated (51). We

quantified self-renewal as the number of secondary neurospheres generated per primary neurosphere as previously described (51). Cell suspensions were plated on adherent plates at clonal density, which means that cells were plated at a low density such that individual cells could form spatially distinct colonies (51). This allowed us to infer the developmental and proliferative potential of single cells on the basis of the types and numbers of cells that comprised each colony.

Tamoxifen administration

Tamoxifen (Sigma, cat # T5648-1g) was solubilized in sterilized corn oil (Sigma, cat # C8267-500ml) at a concentration of 20 mg/ml. A 0.2 mg/g body weight intraperitoneal injection was administered to 5 week old littermate mice once daily for 5 consecutive days. Mice were euthanized 3 weeks following the first Tamoxifen injection.

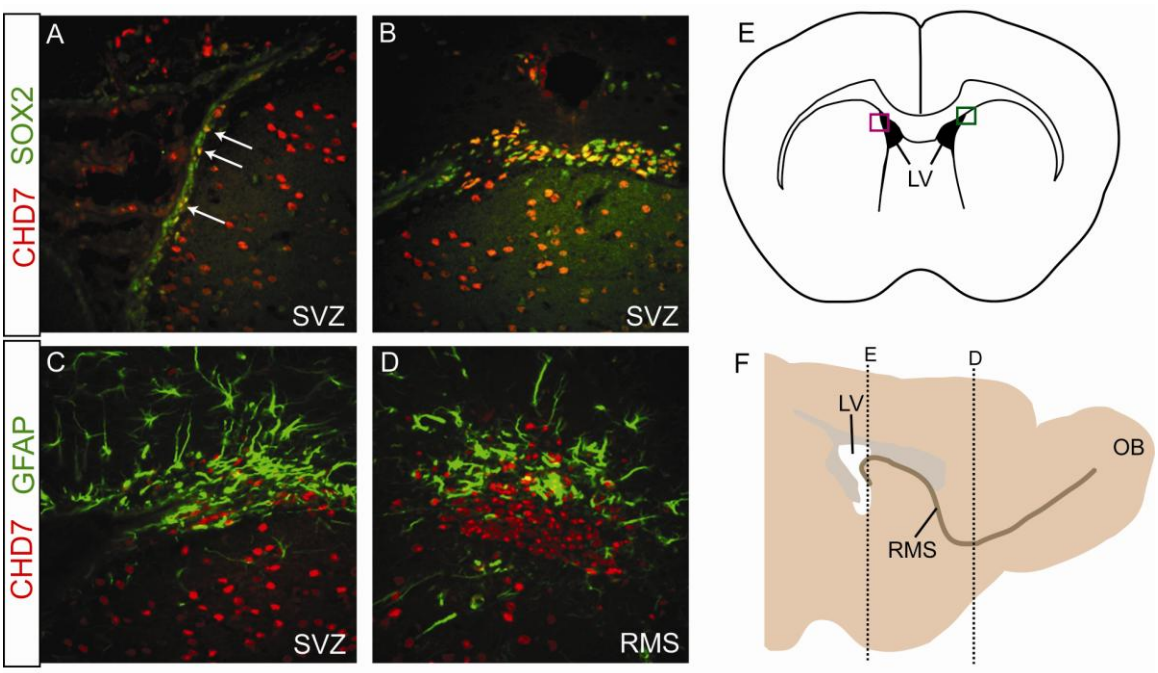

Figure 4.1 *Chd7* is expressed in neural stem cells in the subventricular zone. Immunofluorescence of adult wild type cryosections using anti-CHD7 (red) together with anti-SOX2 (green) or anti-GFAP (green). (A and B) Immunofluorescence showed that CHD7 co-localized with SOX2-positive cells in the SVZ. (C) The majority of CHD7-positive cells do not co-localize GFAP-positive cells in the SVZ. (D) CHD7-positive cells were found in the RMS surrounded by GFAP-positive cells which line the RMS. (E and F) Cartoons of a coronal adult brain section through the SVZ and a sagittal view of the RMS show the regions immunofluorescence images were obtained. (A) is the magenta box in (E). (B and C) are from the green box in (E). (D) is an image taken from the of section shown in (F).

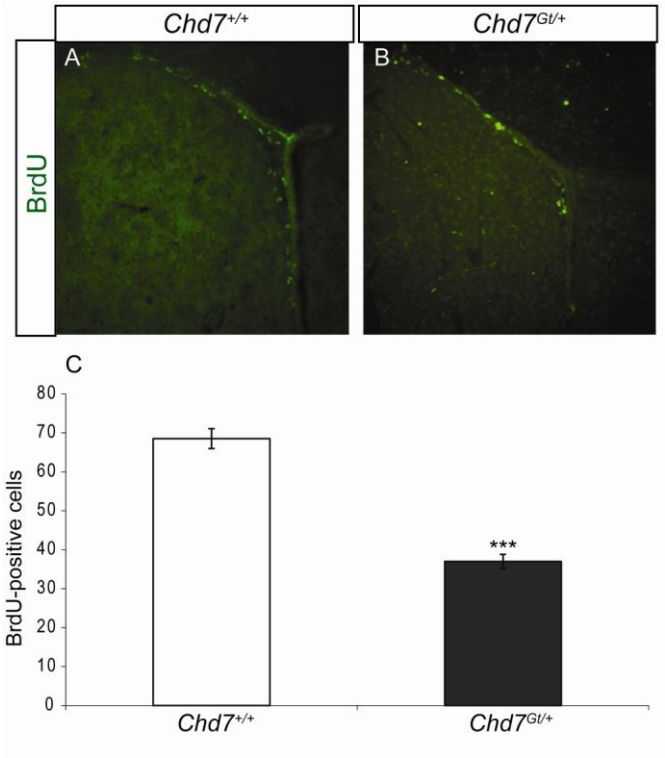

Figure 4.2 Cellular proliferation in the subventricular zone requires proper CHD7 dosage. Proliferation was examined using a 30 minute BrdU incorporation assay in conjunction with immunofluorescence using anti-BrdU on adult wild type and *Chd7*$^{Gt/+}$ littermate mice. (A and B) Immunofluorescence using anti-BrdU showed a decrease in BrdU-positive cells in the *Chd7*$^{Gt/+}$ SVZ compared to wild type littermates. (C) Quantification of the BrdU-positive cells showed a 47% decrease BrdU-positve cells in *Chd7*$^{Gt/+}$ mice compared to wild type littermates. ***P < 0.001 by unpaired Student's t test.

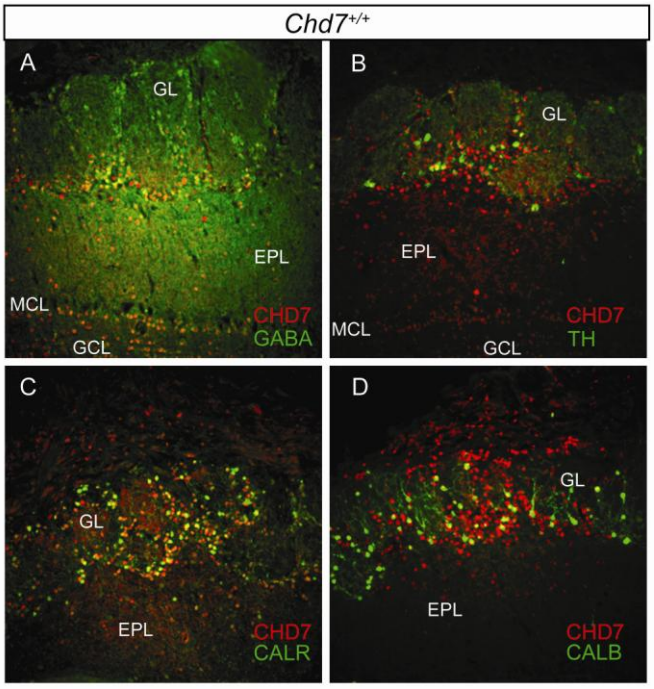

Figure 4.3 Interneuron populations in the olfactory bulb are CHD7-positive. Immunofluorescence of adult wild type mice using antibodies against CHD7, GABA, tyrosine hydroxylase (TH), calbindin (CALB), and calretinin (CALR). (A-D) CHD7-positive cells co-localize with GABA-positive, TH-positive, CALB-positive, and CALR-positive cells in the olfactory bulb. GL = glomerular layer, EPL = external plexiform layer, MCL = mitral cell layer, and GCL = granule cell layer.

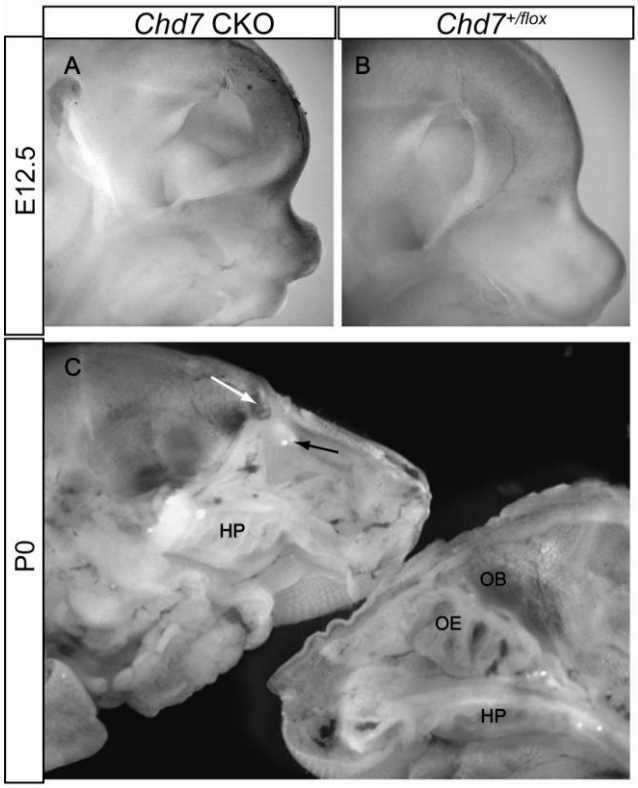

Figure 4.4 *Chd7* conditional knockout (CKO) mice have craniofacial dysmorphisms and lack most olfactory tissues. (A and B) *Chd7*$^{flox/Gt}$; *Foxg1-Cre* E12.5 embryos have forebrain hypoplasia and craniofacial dysmorphisms compared to *Chd7*$^{+/flox}$ littermates. (C) P0 *Chd7*$^{flox/Gt}$; *Foxg1-Cre* pups (left) have severely hypoplastic olfactory tissues and craniofacial dysmorphisms compared to *Chd7*$^{+/flox}$ littermates (right). White arrow indicates hypoplastic olfactory bulb. Black arrow indicates hypoplastic olfactory epithelium. HP = hard palate, OE = olfactory epithelium, and OB = olfactory bulb.

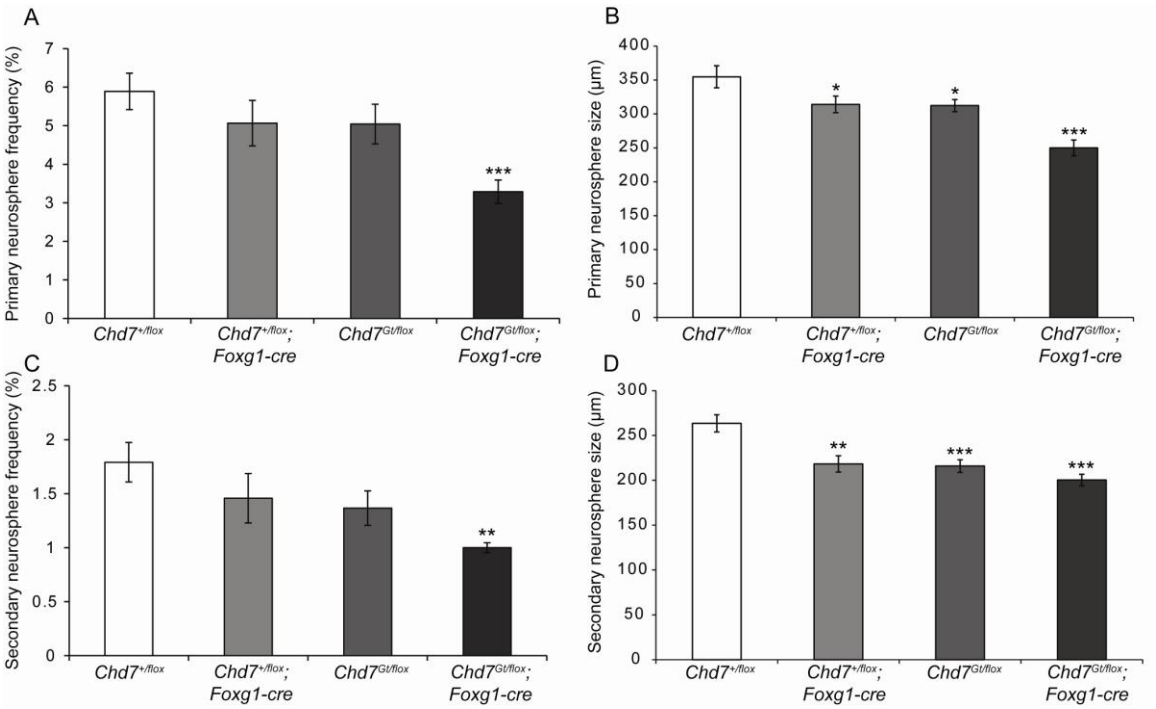

Figure 4.5 CHD7 deficient neurospheres have defects in neural stem cell self-renewal. E14.5 *Chd7*$^{flox/Gt}$; *Foxg1-Cre* primary and secondary neurospheres were examined for frequency, size, and multipotency. (A) *Chd7*$^{flox/Gt}$; *Foxg1-Cre* telencephalon cells formed mutipotent primary neurospheres at a significantly lower frequency than *Chd7*$^{flox/+}$. (B) *Chd7*$^{flox/Gt}$, *Chd7*$^{flox/+}$; *Foxg1-Cre*, and *Chd7*$^{flox/Gt}$; *Foxg1-Cre* telencephalon cells formed primary neurospheres that were significantly smaller than *Chd7*$^{flox/+}$ littermates. (C and D) Secondary neurospheres in *Chd7*$^{flox/Gt}$; *Foxg1-Cre* neurospheres were significantly smaller in size and at a reduced frequency compared to *Chd7*$^{flox/+}$ littermates. *Chd7*$^{flox/Gt}$ and *Chd7*$^{flox/+}$; *Foxg1-Cre* also formed significantly smaller secondary neurospheres but at frequency similar to *Chd7*$^{flox/+}$ littermates. * $P < 0.05$ ** $P < 0.01$ *** $P < 0.001$ by ANOVA.

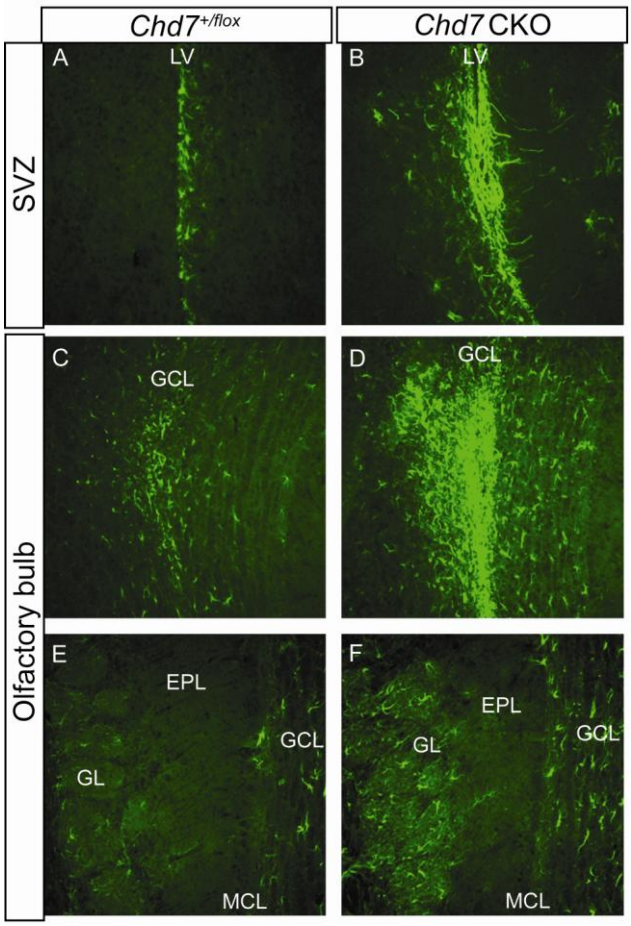

Figure 4.6 Loss of CHD7 results in increased GFAP-positive cells in the SVZ and olfactory bulb. Immunofluorescence of *Chd7*$^{flox/+}$ and *Chd7*$^{flox/Gt}$; *Ubc-CreERT2* littermate mice using anti-GFAP. (A-F) *Chd7*$^{flox/Gt}$; *Ubc-CreERT2* mice had a visually apparent increase in GFAP-positive cells in the subventricular zone and olfactory bulb compared to *Chd7*$^{flox/+}$ littermates. (E and F) The increase in GFAP-positive cells was also seen in the olfactory bulb surrounding the glomeruli in regions usually occupied by interneurons. GL = glomerular layer, EPL = external plexiform layer, MCL = mitral cell layer, and GCL = granule cell layer.

References

1 Harris, J., Robert, E. and Kallen, B. (1997) Epidemiology of choanal atresia with special reference to the CHARGE association. *Pediatrics*, **99**, 363-367.

2 Issekutz, K.A., Graham, J.M., Jr., Prasad, C., Smith, I.M. and Blake, K.D. (2005) An epidemiological analysis of CHARGE syndrome: preliminary results from a Canadian study. *Am J Med Genet A*, **133**, 309-317.

3 Kallen, K., Robert, E., Mastroiacovo, P., Castilla, E.E. and Kallen, B. (1999) CHARGE Association in newborns: a registry-based study. *Teratology*, **60**, 334-343.

4 Hall, B.D. (1979) Choanal atresia and associated multiple anomalies. *J Pediatr*, **95**, 395-398.

5 Aramaki, M., Udaka, T., Kosaki, R., Makita, Y., Okamoto, N., Yoshihashi, H., Oki, H., Nanao, K., Moriyama, N., Oku, S. *et al.* (2006) Phenotypic spectrum of CHARGE syndrome with CHD7 mutations. *J Pediatr*, **148**, 410-414.

6 Jongmans, M.C., Admiraal, R.J., van der Donk, K.P., Vissers, L.E., Baas, A.F., Kapusta, L., van Hagen, J.M., Donnai, D., de Ravel, T.J., Veltman, J.A. *et al.* (2006) CHARGE syndrome: the phenotypic spectrum of mutations in the CHD7 gene. *J Med Genet*, **43**, 306-314.

7 Lalani, S.R., Safiullah, A.M., Fernbach, S.D., Harutyunyan, K.G., Thaller, C., Peterson, L.E., McPherson, J.D., Gibbs, R.A., White, L.D., Hefner, M. *et al.* (2006)

Spectrum of CHD7 Mutations in 110 Individuals with CHARGE Syndrome and Genotype-Phenotype Correlation. *Am J Hum Genet*, **78**, 303-314.

8 Sanlaville, D., Etchevers, H.C., Gonzales, M., Martinovic, J., Clement-Ziza, M., Delezoide, A.L., Aubry, M.C., Pelet, A., Chemouny, S., Cruaud, C. *et al.* (2006) Phenotypic spectrum of CHARGE syndrome in fetuses with CHD7 truncating mutations correlates with expression during human development. *J Med Genet*, **43**, 211-217.

9 Sanlaville, D. and Verloes, A. (2007) CHARGE syndrome: an update. *Eur J Hum Genet*, **15**, 389-399.

10 Vissers, L.E., van Ravenswaaij, C.M., Admiraal, R., Hurst, J.A., de Vries, B.B., Janssen, I.M., van der Vliet, W.A., Huys, E.H., de Jong, P.J., Hamel, B.C. *et al.* (2004) Mutations in a new member of the chromodomain gene family cause CHARGE syndrome. *Nat Genet*, **36**, 955-957.

11 Vuorela, P., Ala-Mello, S., Saloranta, C., Penttinen, M., Poyhonen, M., Huoponen, K., Borozdin, W., Bausch, B., Botzenhart, E.M., Wilhelm, C. *et al.* (2007) Molecular analysis of the CHD7 gene in CHARGE syndrome: identification of 22 novel mutations and evidence for a low contribution of large CHD7 deletions. *Genet Med*, **9**, 690-694.

12 Delahaye, A., Sznajer, Y., Lyonnet, S., Elmaleh-Berges, M., Delpierre, I., Audollent, S., Wiener-Vacher, S., Mansbach, A.L., Amiel, J., Baumann, C. *et al.* (2007)

Familial CHARGE syndrome because of CHD7 mutation: clinical intra- and interfamilial variability. *Clin Genet*, **72**, 112-121.

13 Jongmans, M.C., Hoefsloot, L.H., van der Donk, K.P., Admiraal, R.J., Magee, A., van de Laar, I., Hendriks, Y., Verheij, J.B., Walpole, I., Brunner, H.G. *et al.* (2008) Familial CHARGE syndrome and the CHD7 gene: a recurrent missense mutation, intrafamilial recurrence and variability. *Am J Med Genet A*, **146**, 43-50.

14 Vuorela, P.E., Penttinen, M.T., Hietala, M.H., Laine, J.O., Huoponen, K.A. and Kääriäinen, H.A. (2008) A familial CHARGE syndrome with a CHD7 nonsense mutation and new clinical features. *Clinical dysmorphology*, **17**, 249-253.

15 Asakura, Y., Toyota, Y., Muroya, K., Kurosawa, K., Fujita, K., Aida, N., Kawame, H., Kosaki, K. and Adachi, M. (2008) Endocrine and radiological studies in patients with molecularly confirmed CHARGE syndrome. *J Clin Endocrinol Metab*, **93**, 920-924.

16 Azoulay, R., Fallet-Bianco, C., Garel, C., Grabar, S., Kalifa, G. and Adamsbaum, C. (2006) MRI of the olfactory bulbs and sulci in human fetuses. *Pediatr Radiol*, **36**, 97-107.

17 Blustajn, J., Kirsch, C.F., Panigrahy, A. and Netchine, I. (2008) Olfactory anomalies in CHARGE syndrome: imaging findings of a potential major diagnostic criterion. *AJNR Am J Neuroradiol*, **29**, 1266-1269.

18 Chalouhi, C., Faulcon, P., Le Bihan, C., Hertz-Pannier, L., Bonfils, P. and Abadie, V. (2005) Olfactory evaluation in children: application to the CHARGE syndrome. *Pediatrics*, **116**, e81-88.

19 Ogata, T., Fujiwara, I., Ogawa, E., Sato, N., Udaka, T. and Kosaki, K. (2006) Kallmann syndrome phenotype in a female patient with CHARGE syndrome and CHD7 mutation. *Endocr J*, **53**, 741-743.

20 Pinto, G., Abadie, V., Mesnage, R., Blustajn, J., Cabrol, S., Amiel, J., Hertz-Pannier, L., Bertrand, A.M., Lyonnet, S., Rappaport, R. *et al.* (2005) CHARGE syndrome includes hypogonadotropic hypogonadism and abnormal olfactory bulb development. *J Clin Endocrinol Metab*, **90**, 5621-5626.

21 Bosman, E.A., Penn, A.C., Ambrose, J.C., Kettleborough, R., Stemple, D.L. and Steel, K.P. (2005) Multiple mutations in mouse Chd7 provide models for CHARGE syndrome. *Hum Mol Genet*, **14**, 3463-3476.

22 Hurd, E.A., Capers, P.L., Blauwkamp, M.N., Adams, M.E., Raphael, Y., Poucher, H.K. and Martin, D.M. (2007) Loss of Chd7 function in gene-trapped reporter mice is embryonic lethal and associated with severe defects in multiple developing tissues. *Mamm Genome*, **18**, 94-104.

23 Layman, W.S., McEwen, D.P., Beyer, L.A., Lalani, S.R., Fernbach, S.D., Oh, E., Swaroop, A., Hegg, C.C., Raphael, Y., Martens, J.R. *et al.* (2009) Defects in neural stem

cell proliferation and olfaction in Chd7 deficient mice indicate a mechanism for hyposmia in human CHARGE syndrome. *Hum Mol Genet*, **18**, 1909-1923.

24 Alvarez-Buylla, A. and Lim, D.A. (2004) For the long run: maintaining germinal niches in the adult brain. *Neuron*, **41**, 683-686.

25 Lim, D.A. and Alvarez-Buylla, A. (1999) Interaction between astrocytes and adult subventricular zone precursors stimulates neurogenesis. *Proc Natl Acad Sci U S A*, **96**, 7526-7531.

26 Lledo, P.M., Merkle, F.T. and Alvarez-Buylla, A. (2008) Origin and function of olfactory bulb interneuron diversity. *Trends Neurosci*, **31**, 392-400.

27 Cummings, D.M. and Belluscio, L. (2008) Charting plasticity in the regenerating maps of the mammalian olfactory bulb. *Neuroscientist*, **14**, 251-263.

28 Doetsch, F., Caille, I., Lim, D.A., Garcia-Verdugo, J.M. and Alvarez-Buylla, A. (1999) Subventricular zone astrocytes are neural stem cells in the adult mammalian brain. *Cell*, **97**, 703-716.

29 Hurd, E.A., Poucher, H.K., Cheng, K., Raphael, Y. and Martin, D.M. (2010) The ATP-dependent chromatin remodeling enzyme CHD7 regulates pro-neural gene expression and neurogenesis in the inner ear. *Development*, **137**, 3139-3150.

30 Layman, W.S., Hurd, E.A. and Martin, D.M. (2011) Reproductive dysfunction and decreased GnRH neurogenesis in a mouse model of CHARGE syndrome. *Hum Mol Genet*, **in press**.

31 Ma, D.K., Ponnusamy, K., Song, M.R., Ming, G.L. and Song, H. (2009) Molecular genetic analysis of FGFR1 signalling reveals distinct roles of MAPK and PLCgamma1 activation for self-renewal of adult neural stem cells. *Mol Brain*, **2**, 16.

32 Ruzankina, Y., Pinzon-Guzman, C., Asare, A., Ong, T., Pontano, L., Cotsarelis, G., Zediak, V.P., Velez, M., Bhandoola, A. and Brown, E.J. (2007) Deletion of the developmentally essential gene ATR in adult mice leads to age-related phenotypes and stem cell loss. *Cell Stem Cell*, **1**, 113-126.

33 Engelen, E., Akinci, U., Bryne, J.C., Hou, J., Gontan, C., Moen, M., Szumska, D., Kockx, C., van Ijcken, W., Dekkers, D.H. *et al.* (2011) Sox2 cooperates with Chd7 to regulate genes that are mutated in human syndromes. *Nat Genet*.

34 Bajpai, R., Chen, D.A., Rada-Iglesias, A., Zhang, J., Xiong, Y., Helms, J., Chang, C.P., Zhao, Y., Swigut, T. and Wysocka, J. (2010) CHD7 cooperates with PBAF to control multipotent neural crest formation. *Nature*, **463**, 958-962.

35 Takada, I., Mihara, M., Suzawa, M., Ohtake, F., Kobayashi, S., Igarashi, M., Youn, M.Y., Takeyama, K., Nakamura, T., Mezaki, Y. *et al.* (2007) A histone lysine methyltransferase activated by non-canonical Wnt signalling suppresses PPAR-gamma transactivation. *Nat Cell Biol*, **9**, 1273-1285.

36 Srinivasan, S., Dorighi, K.M. and Tamkun, J.W. (2008) Drosophila Kismet regulates histone H3 lysine 27 methylation and early elongation by RNA polymerase II. *PLoS Genet*, **4**, e1000217.

37 Ho, L. and Crabtree, G.R. (2010) Chromatin remodelling during development. *Nature*, **463**, 474-484.

38 Bonaguidi, M.A., Peng, C.Y., McGuire, T., Falciglia, G., Gobeske, K.T., Czeisler, C. and Kessler, J.A. (2008) Noggin expands neural stem cells in the adult hippocampus. *J Neurosci*, **28**, 9194-9204.

39 Calof, A.L., Bonnin, A., Crocker, C., Kawauchi, S., Murray, R.C., Shou, J. and Wu, H.H. (2002) Progenitor cells of the olfactory receptor neuron lineage. *Microsc Res Tech*, **58**, 176-188.

40 Colak, D., Mori, T., Brill, M.S., Pfeifer, A., Falk, S., Deng, C., Monteiro, R., Mummery, C., Sommer, L. and Gotz, M. (2008) Adult neurogenesis requires Smad4-mediated bone morphogenic protein signaling in stem cells. *J Neurosci*, **28**, 434-446.

41 Maier, E., von Hofsten, J., Nord, H., Fernandes, M., Paek, H., Hebert, J.M. and Gunhaga, L. (2010) Opposing Fgf and Bmp activities regulate the specification of olfactory sensory and respiratory epithelial cell fates. *Development*, **137**, 1601-1611.

42 Shou, J., Murray, R.C., Rim, P.C. and Calof, A.L. (2000) Opposing effects of bone morphogenetic proteins on neuron production and survival in the olfactory receptor neuron lineage. *Development*, **127**, 5403-5413.

43 Shou, J., Rim, P.C. and Calof, A.L. (1999) BMPs inhibit neurogenesis by a mechanism involving degradation of a transcription factor. *Nat Neurosci*, **2**, 339-345.

44 Garcia-Gonzalez, D., Clemente, D., Coelho, M., Esteban, P.F., Soussi-Yanicostas, N. and de Castro, F. (2010) Dynamic roles of FGF-2 and Anosmin-1 in the migration of neuronal precursors from the subventricular zone during pre- and postnatal development. *Exp Neurol*, **222**, 285-295.

45 Guo, W., Allan, A.M., Zong, R., Zhang, L., Johnson, E.B., Schaller, E.G., Murthy, A.C., Goggin, S.L., Eisch, A.J., Oostra, B.A. *et al.* (2011) Ablation of Fmrp in adult neural stem cells disrupts hippocampus-dependent learning. *Nat Med*, **17**, 559-565.

46 Hagstrom, S.A., Pauer, G.J., Reid, J., Simpson, E., Crowe, S., Maumenee, I.H. and Traboulsi, E.I. (2005) SOX2 mutation causes anophthalmia, hearing loss, and brain anomalies. *Am J Med Genet A*, **138A**, 95-98.

47 Sierra, A., Encinas, J.M. and Maletic-Savatic, M. (2011) Adult human neurogenesis: from microscopy to magnetic resonance imaging. *Front Neurosci*, **5**, 47.

48 Melicharek, D.J., Ramirez, L.C., Singh, S., Thompson, R. and Marenda, D.R. (2010) Kismet/CHD7 regulates axon morphology, memory and locomotion in a Drosophila model of CHARGE syndrome. *Hum Mol Genet*, **19**, 4253-4264.

49 Zentner, G.E., Layman, W.S., Martin, D.M. and Scacheri, P.C. (2010) Molecular and phenotypic aspects of CHD7 mutation in CHARGE syndrome. *Am J Med Genet A*, **152A**, 674-686.

50 Hebert, J.M. and McConnell, S.K. (2000) Targeting of cre to the Foxg1 (BF-1) locus mediates loxP recombination in the telencephalon and other developing head structures. *Dev Biol*, **222**, 296-306.

51 Molofsky, A.V., Pardal, R., Iwashita, T., Park, I.K., Clarke, M.F. and Morrison, S.J. (2003) Bmi-1 dependence distinguishes neural stem cell self-renewal from progenitor proliferation. *Nature*, **425**, 962-967.

Chapter 5

Conclusion

The focus of my thesis work has been to understand the role of CHD7 in neural development and maintenance. Specifically, I have focused on the Kallmann-like features associated with CHD7 deficiency in a mouse model of human CHARGE syndrome. Overall, my work has shown that defects in neural progenitor proliferation and neurogenesis contribute to the Kallmann-like features associated with CHD7 deficiency. However, the presence of CHD7 in multiple tissue types and the variability in clinical features indicate that CHD7 has pleiotropic roles that cannot be simply explained by defects in neural progenitor proliferation and neurogenesis.

CHD7 in olfactory tissues

The results of this dissertation have contributed to our understanding of the olfactory impairment that is associated with CHARGE syndrome. CHD7 is required for proper development and maintenance of olfactory tissues. *Chd7* is expressed in developing and mature olfactory tissues, including the olfactory epithelium and olfactory bulb in humans and mice. In mice, *Chd7* is expressed in neural progenitors of both the olfactory epithelium and olfactory bulb, and appears to regulate proliferation and

neurogenesis in these tissues. *Chd7* haploinsufficiency causes decreased cellular proliferation and neurogenesis, resulting in a reduced capacity for neural regeneration. Additionally, tissue-specific loss of CHD7 results in a reduced capacity for neural stem cell self-renewal and conditional loss of CHD7 causes an increase in GFAP-positive cells in the SVZ and olfactory bulb.

Olfactory impairment associated with CHD7 deficiency in mice as assessed by electro-olfactogram is correlated with decreases in cellular proliferation and reduced olfactory sensory neurons in the adult olfactory epithelium. However, a reduction in the number of olfactory sensory neurons had not been previously shown to cause olfactory impairment. We have shown that individual olfactory sensory neurons in *Chd7*$^{Gt/+}$ P3 pups have normal calcium signaling in response to odorant, suggesting that *Chd7* haploinsufficiency does not affect the ability of each individual olfactory sensory neuron to respond to odorants. This further suggests that *Chd7*$^{Gt/+}$ mice are unable to properly propagate the olfactory signal from the olfactory sensory neurons to the olfactory bulb. Signal propagation from the olfactory sensory neurons to the olfactory bulb requires multiple components to act in coordination. Calcium channels located in sustentacular cells and olfactory sensory neuron dendrites and axons each have a role in olfactory signal propagation (1-3). CHD7 is present in some sustentacular cells but it's role in these cells is unknown. CHD7 may be required in sustentacular cells for signal propagation by regulating genes involved in calcium signaling or calcium channels. However, gap junctions between cells of the olfactory epithelium are also required for odorant sensitivity and perception (4). Gap junctions are specialized intercellular channels that are comprised of two connexins which connect across the intercellular

space (4). Since *Chd7*$^{Gt/+}$ mice have decreased numbers of olfactory sensory neurons that appear disorganized, it is possible that gap junctions are not properly formed in these mice, which may cause to an inability to propagate the olfactory signal to the olfactory bulb. In addition, CHD7 may regulate the expression of connexins within immature olfactory neural progenitors or in sustentacular cells. Although olfactory impairment is prevalent in humans and mice with CHD7 deficiency, the primary cause underlying the olfactory dysfunction is not fully understood.

CHD7 haploinsufficiency in humans causes olfactory bulb hypoplasia and/or aplasia. Prior to our work, olfactory impairment in CHARGE individuals was thought to be caused primarily by defects associated with the olfactory bulb. Our data were the first to analyze olfactory function independent of the olfactory bulb and behavioral issues associated with CHD7 deficiency. *Chd7*$^{Gt/+}$ mice have olfactory bulb hypoplasia that may also contribute to olfactory impairment. Although the olfactory sensory neurons in *Chd7*$^{Gt/+}$ mice project axons to the olfactory bulb glomeruli, it is unknown whether the axons project properly to the appropriate glomerulus. If olfactory sensory neuron axons do not project to the glomeruli properly, then amplification of the olfactory signal by multiple individual olfactory sensory neurons transmitting a signal to the same glomerulus is lost (5, 6). CHD7 may regulate genes associated with axon guidance and adhesion molecules necessary for generating the olfactory map in the olfactory bulb. Inhibitory inputs by interneuron populations in the olfactory bulb also play a key role in the local circuitry in the olfactory bulb. Studies suggest that interneuron populations have a vital role in both neural plasticity and modification of postsynaptic target firing patterns (7, 8). CHD7 is present in the adult interneuron populations of the olfactory

bulb, and it will be important to understand how CHD7 deficiency influences these interneuron populations and what impact CHD7 deficiency has on olfactory plasticity in the olfactory bulb over time.

Significance and future directions

The studies presented here describe a role for CHD7 in development and maintenance of olfactory tissues. CHD7 is a chromodomain protein that is thought to regulate transcription factor access to target genes by altering nucleosome structure. Chromatin structure has a vital role in gene regulation, via its effects on cellular proliferation and maintenance of the differentiated state. Recent studies have begun to clarify a role for CHD7 in regulating gene expression during tissue development and maintenance. CHD7 has been shown by ChIP-chip to bind to chromatin in a cell type specific manner via methylated histone H3 lysine 4 in enhancer regions of numerous genes. This has been demonstrated in human colorectal carcinoma cells, human neuroblastoma cells, and mouse embryonic stem cells before and after differentiation, further supporting the idea that CHD7 may have temporal and tissue-specific functions (9). CHD7 was shown by ChIP-seq to bind to enhancer and promoter regions of more than 10,000 genes in mouse embryonic stem (ES) cells (10). CHD7 was shown to localize with ES cell master regulators SOX2, OCT4, and NANOG (10). CHD7 was also reported to form a complex with SOX2 in ES-cell derived neural stem cells (11). SOX2 is a HMG-box transcription factor that is required for the *in vivo* maintenance of both mouse ES cells and neural stem cells (12). Our data revealed that CHD7 co-localizes *in vivo* with SOX2 in neural stem cells of the adult mouse SVZ. Further exploration into

the relationship between CHD7 and SOX2 is vital to understanding the functional role of CHD7 in neural stem cells.

Chd7 is expressed in 98% of proliferating neural progenitors in the adult mouse olfactory epithelium. In mice, *Chd7* haploinsufficiency causes approximately a 50% reduction in the number of proliferating neural progenitors in both the olfactory epithelium and SVZ. However, the mechanism underlying this observation is not known. Neural stem cells are reliant upon both symmetric (self-renewal) and asymmetric (division to produce a more differentiated cell) cell division to regulate and maintain the proper proportions of neural stem cells, progenitors, and differentiated cell types (13-15). Since CHD7 is present in most proliferating neural progenitors, CHD7 could regulate the expression of genes essential for initiating cell division and/or cell cycle progression. Understanding whether CHD7 functions prior to initiation of cell division or whether CHD7 functions only during cell cycle progression will help provide a basis for uncovering the role of CHD7 in proliferating neural progenitors.

Our data in the embryonic mouse olfactory placode showed that loss of proper CHD7 dosage affects the expression of genes such as *Fgfr1* and *Bmp4* (16). FGFR1 and BMP4 have distinct roles in cellular proliferation and cellular differentiation in neurogenic domains (17-25). The opposing effects of FGF and BMP signaling must be tightly regulated during olfactory development to obtain the proper proportions of olfactory sensory and olfactory respiratory cell types (26). The adult olfactory epithelium requires CHD7 for normal olfactory sensory neuron regeneration (27). However, it is unknown whether CHD7 continues to regulate the expression of *Fgfr1* and *Bmp4* throughout adulthood in olfactory tissues. Loss of FGFR1 in neural stem cells from the

subventricular zone results in decreased cellular proliferation and spontaneous cellular differentiation toward a glial cell fate (28). We showed that conditional loss of CHD7 in adult mice caused a spontaneous shift toward a glial cell fate in the SVZ and olfactory bulb. These data together suggest that CHD7 may continue to regulate the expression of morphogenic genes such as *Fgfr1* and *Bmp4*.

CHD7 and reproductive dysfunction

The data presented in this dissertation have contributed to better understanding the mechanisms underlying CHD7 function in pubertal development and reproduction. *Chd7* haploinsufficiency in mice causes pubertal delay, hypogonadotropic hypogonadism, and decreased GnRH neurogenesis (16). Decreased GnRH neurogenesis results from reduced cellular proliferation in the olfactory placode during development. Reduced cellular proliferation in the *Chd7* mutant olfactory placode is likely due to decreased expression of *Fgfr1*, *Bmp4*, and *Otx2*. Additionally, expression levels of *Otx2* and *GnRH1* are significantly reduced in adult $Chd7^{Gt/+}$ mice compared to wild type littermates. Together, these data suggest that CHD7 has a role in both the genesis and function of GnRH neurons.

GnRH neurons are derived from neural progenitors in the olfactory placode (29-31). It is currently unknown whether neural progenitors for GnRH neurons are different from neural progenitors for olfactory sensory neurons. Extensive work has been done in the olfactory placode in identification of GnRH specific neural progenitors (29-34). However, these studies have been unable to identify markers that are specific for GnRH neural precursors, which suggest that neural progenitors in the olfactory placode may

have the capacity to become GnRH neurons, olfactory sensory neurons, or olfactory ensheathing cells. CHD7 deficiency causes decreased numbers of GnRH neurons and olfactory sensory neurons, which suggests that CHD7 is essential for the maintenance of neural progenitors and neurogenesis in the olfactory placode and epithelium. Although olfaction and reproduction may appear to be unrelated, our data clearly show how defects in olfactory tissues can have lifelong effects on both olfaction and reproduction in humans and mice.

Significance and future directions

Studies presented here have provided insight into CHD7 mediated reproductive development and function. Our data provide evidence that *Chd7* haploinsufficiency in mice causes delayed pubertal development and decreased levels of LH and FSH. However, the role of CHD7 in the pituitary has not been fully characterized. *Chd7* is highly expressed in the embryonic and adult pituitary (data not shown). No gross morphological abnormalities exist in the $Chd7^{Gt/+}$ pituitary, and response to GnRH agonist and antagonist is normal. Although the pituitary appears normal in $Chd7^{Gt/+}$ mice, the anterior pituitary contains several cell type that include somatotrophs that produce GH, lactotrophs producing prolactin, gonadotrophs that secrete both LH and FSH, thyrotrophs producing TSH, corticotrophs that express proopiomelanocortin (POMC) and cleave it to produce ACTH, and nonsecreting cells (35). The anterior pituitary in rodents continues to grow and mature substantially during the first postnatal weeks of life (36). Debate also exists in the literature in regards to the existence of a stem cell population in the adult rodent pituitary (37). Previous reports have identified a

SOX2-positive cell population located around the lumen in the marginal zone of the pituitary between the anterior and the intermediate lobes and scattered in small clusters inside the pituitary gland in mice (38). These SOX2-positive cells were shown to have the characteristics of progenitors and stem cells (38). Since CHD7 has been shown to complex with SOX2, CHD7 and SOX2 may function to help maintain the proper proportions of the different hormone producing cell types in the embryonic and adult pituitary.

Chd7 continues to be expressed in adult GnRH neurons and CHD7 deficiency causes decreased expression of *Otx2* and *GnRH1* (16). However, the decrease in *GnRH1* expression in adult *Chd7*$^{Gt/+}$ hypothalamus may be multifactorial because many CHD7-positive cells in the hypothalamus are GnRH-negative. Interestingly, BMP4 signaling is required for *GnRH1* expression in mature GnRH cell lines (GT1-7) (39), and for gonadotropin expression in mouse LβT2 gonadotrophs (40). We have shown that CHD7 regulates the expression of *Bmp4* in the mouse olfactory placode (16) and developing inner ear (data not shown). Loss of proper BMP4 signal in the *Chd7*$^{Gt/+}$ hypothalamus and pituitary may contribute to decreases in *GnRH1* expression in the hypothalamus, GnRH in the median eminence, and circulating LH and FSH from the pituitary. Further investigation is needed to understand the potentially multifaceted regulation by CHD7 of the hypothalamic-pituitary axis and the reproductive dysfunction associated with loss of CHD7.

Summary

Studies reported in this dissertation highlight an increased understanding of the functional role of CHD7 in developing and mature olfactory and endocrine related tissues. However, it is unclear whether humans and mice with CHD7 deficiency have similar defects in the maintenance of the neural progenitor pool and neurogenesis. Humans and mice with CHD7 deficiency have Kallmann-like features which include olfactory impairment and reproductive dysfunction. In a study that examined Kallmann-like features in human fetuses, CHARGE fetuses were found to have GnRH neurons only in the frontonasal region but not in the hypothalamus, which suggests that the GnRH neurons fail to migrate properly into the forebrain through the cribriform plate (41). Notably, CHARGE fetuses appear to have premature termination of the olfactory sensory neuron axons prior to their penetration of the cribriform plate and extension into the forebrain (41). GnRH neurons are unable to penetrate the cribform plate independently and are fully dependent upon the olfactory sensory neuron axons to penetrate through the cribriform plate to access the forebrain (29-31, 34). The GnRH neuronal migration defect found in CHARGE fetuses is likely caused by a defect in the ability of olfactory sensory neurons to penetrate the cribriform plate. This may be due to defects in axonal guidance or simply because a threshold number of olfactory sensory neurons are required for penetration of the cribriform plate. Humans possess a poorly developed olfactory sense in comparison to mice (42, 43), and subtle defects in cribriform plate penetration into the forebrain may be more apparent in humans than in mice.

It is increasingly clear that the pleiotropic roles for CHD7 in the development and maintenance of neural tissues are due to temporal and tissue specific transcriptional

complex formation. We have shown that CHD7 regulates the expression of *Otx2*, a paired-like homeodomain transcription factor (44-48), in the developing olfactory placode (16) and inner ear (49). However, *Otx2* is not expressed in adult SVZ [data available on GENSAT website (http://www.gensat.org/index.html)] whereas *Chd7* is expressed in the adult SVZ. Although CHD7 mediated expression of target genes such as *Otx2* exists in multiple tissue types, this is not true of all tissues affected by CHD7 deficiency. Thus, caution must be taken in selecting and verifying potential CHD7 regulated candidate genes. This is of vital importance because many of the biochemical assays used to confirm genetic interactions are done on immortalized cell lines or ES cell lines. Immortalized cells and ES cells are greatly impacted by the culture conditions in which they are grown. Antibiotics and antimycotics are routinely used in cell culture with little regard to their effects on the cells themselves. Antibiotics and antimycotics have been shown to alter calcium levels, growth and apoptotic rates, and the cellular proteome (50-53).

One of the common themes that has emerged from this work is that CHD7 deficiency is associated with decreased neurogenesis. Defects in neurogenesis with CHD7 deficiency were identified in the olfactory placode (16), the developing inner ear (49), the adult olfactory epithelium, and olfactory bulb (27). Although *Chd7* is widely expressed in neurogenic regions during development and adulthood, nothing is known about the factors upstream of *Chd7* that regulate its expression. Haploinsufficiency for *CHD7* is estimated to occur in 60-80% of CHARGE patients (54-59). What accounts for the remaining 20-40% of patients accurately diagnosed with CHARGE but without a mutation in *CHD7*? The overlap in *Chd7* expression in neurogenic regions may hold the

key to discovering some of the factors involved in the regulation of *Chd7* expression. Neurogenic regions are reliant upon extrinsic and intrinsic factors within the neurogenic niche for proper neurogenesis to occur, and these have been well studied. It will be important to examine factors involved very early in regulating the neurogenic potential of the niche, and to identify factors that act similarly among neurogenic regions with *Chd7* expression. Animal models will be vital in accurately identifying factors that may regulate *Chd7* expression. It will also be important to note that some redundancy may exist between the different CHD proteins. Compensatory mechanisms for CHD7 have not yet been explored, but some of the variability in CHARGE clinical features may be due to tissue-specific compensation by additional factors such as other CHD proteins. Additionally, some CHD proteins such as CHD3 and CHD4 are binding partners (60-64), and CHD7 may bind to additional CHD proteins to regulate CHD7 function. Understanding the mechanisms underlying CHD7 regulation of neurogenesis will help identify additional factors relevant to human neurological disorders.

References

1 Gautam, S.H., Otsuguro, K.I., Ito, S., Saito, T. and Habara, Y. (2007) T-type Ca2+ channels mediate propagation of odor-induced Ca2+ transients in rat olfactory receptor neurons. *Neuroscience*, **144**, 702-713.

2 Hassenklover, T., Kurtanska, S., Bartoszek, I., Junek, S., Schild, D. and Manzini, I. (2008) Nucleotide-induced Ca2+ signaling in sustentacular supporting cells of the olfactory epithelium. *Glia*, **56**, 1614-1624.

3 Zufall, F., Leinders-Zufall, T. and Greer, C.A. (2000) Amplification of odor-induced Ca(2+) transients by store-operated Ca(2+) release and its role in olfactory signal transduction. *J Neurophysiol*, **83**, 501-512.

4 Zhang, C. (2010) Gap junctions in olfactory neurons modulate olfactory sensitivity. *BMC Neurosci*, **11**, 108.

5 Schwarting, G.A. and Henion, T.R. (2011) Regulation and function of axon guidance and adhesion molecules during olfactory map formation. *J Cell Biochem*.

6 Cho, J.H., Prince, J.E. and Cloutier, J.F. (2009) Axon guidance events in the wiring of the mammalian olfactory system. *Mol Neurobiol*, **39**, 1-9.

7 Adam, Y. and Mizrahi, A. (2010) Circuit formation and maintenance--perspectives from the mammalian olfactory bulb. *Curr Opin Neurobiol*, **20**, 134-140.

8 Bardy, C., Alonso, M., Bouthour, W. and Lledo, P.M. (2010) How, when, and where new inhibitory neurons release neurotransmitters in the adult olfactory bulb. *J Neurosci*, **30**, 17023-17034.

9 Schnetz, M.P., Bartels, C.F., Shastri, K., Balasubramanian, D., Zentner, G.E., Balaji, R., Zhang, X., Song, L., Wang, Z., Laframboise, T. *et al.* (2009) Genomic distribution of CHD7 on chromatin tracks H3K4 methylation patterns. *Genome Res*.

10 Schnetz, M.P., Handoko, L., Akhtar-Zaidi, B., Bartels, C.F., Pereira, C.F., Fisher, A.G., Adams, D.J., Flicek, P., Crawford, G.E., Laframboise, T. *et al.* (2010) CHD7 targets active gene enhancer elements to modulate ES cell-specific gene expression. *PLoS Genet*, **6**, e1001023.

11 Engelen, E., Akinci, U., Bryne, J.C., Hou, J., Gontan, C., Moen, M., Szumska, D., Kockx, C., van Ijcken, W., Dekkers, D.H. *et al.* Sox2 cooperates with Chd7 to regulate genes that are mutated in human syndromes. *Nat Genet*.

12 Pevny, L.H. and Nicolis, S.K. (2010) Sox2 roles in neural stem cells. *Int J Biochem Cell Biol*, **42**, 421-424.

13 Encinas, J.M., Michurina, T.V., Peunova, N., Park, J.H., Tordo, J., Peterson, D.A., Fishell, G., Koulakov, A. and Enikolopov, G. (2011) Division-coupled astrocytic differentiation and age-related depletion of neural stem cells in the adult hippocampus. *Cell Stem Cell*, **8**, 566-579.

14 Johansson, P.A., Cappello, S. and Gotz, M. (2010) Stem cells niches during development--lessons from the cerebral cortex. *Curr Opin Neurobiol*, **20**, 400-407.

15 Piccin, D. and Morshead, C.M. (2011) Wnt signaling regulates symmetry of division of neural stem cells in the adult brain and in response to injury. *Stem Cells*, **29**, 528-538.

16 Layman, W.S., Hurd, E.A. and Martin, D.M. (2011) Reproductive dysfunction and decreased GnRH neurogenesis in a mouse model of CHARGE syndrome. *Hum Mol Genet*.

17 Bonaguidi, M.A., Peng, C.Y., McGuire, T., Falciglia, G., Gobeske, K.T., Czeisler, C. and Kessler, J.A. (2008) Noggin expands neural stem cells in the adult hippocampus. *J Neurosci*, **28**, 9194-9204.

18 Calof, A.L., Bonnin, A., Crocker, C., Kawauchi, S., Murray, R.C., Shou, J. and Wu, H.H. (2002) Progenitor cells of the olfactory receptor neuron lineage. *Microsc Res Tech*, **58**, 176-188.

19 Cate, H.S., Sabo, J.K., Merlo, D., Kemper, D., Aumann, T.D., Robinson, J., Merson, T.D., Emery, B., Perreau, V.M. and Kilpatrick, T.J. (2010) Modulation of bone morphogenic protein signalling alters numbers of astrocytes and oligodendroglia in the subventricular zone during cuprizone-induced demyelination. *J Neurochem*.

20 Colak, D., Mori, T., Brill, M.S., Pfeifer, A., Falk, S., Deng, C., Monteiro, R., Mummery, C., Sommer, L. and Gotz, M. (2008) Adult neurogenesis requires Smad4-mediated bone morphogenic protein signaling in stem cells. *J Neurosci*, **28**, 434-446.

21 Gonzalez-Quevedo, R., Lee, Y., Poss, K.D. and Wilkinson, D.G. (2010) Neuronal regulation of the spatial patterning of neurogenesis. *Dev Cell*, **18**, 136-147.

22 Kang, K. and Song, M.R. (2010) Diverse FGF receptor signaling controls astrocyte specification and proliferation. *Biochem Biophys Res Commun*.

23 Peretto, P., Cummings, D., Modena, C., Behrens, M., Venkatraman, G., Fasolo, A. and Margolis, F.L. (2002) BMP mRNA and protein expression in the developing mouse olfactory system. *J Comp Neurol*, **451**, 267-278.

24 Shou, J., Murray, R.C., Rim, P.C. and Calof, A.L. (2000) Opposing effects of bone morphogenetic proteins on neuron production and survival in the olfactory receptor neuron lineage. *Development*, **127**, 5403-5413.

25 Shou, J., Rim, P.C. and Calof, A.L. (1999) BMPs inhibit neurogenesis by a mechanism involving degradation of a transcription factor. *Nat Neurosci*, **2**, 339-345.

26 Maier, E., von Hofsten, J., Nord, H., Fernandes, M., Paek, H., Hebert, J.M. and Gunhaga, L. (2010) Opposing Fgf and Bmp activities regulate the specification of olfactory sensory and respiratory epithelial cell fates. *Development*, **137**, 1601-1611.

27 Layman, W.S., McEwen, D.P., Beyer, L.A., Lalani, S.R., Fernbach, S.D., Oh, E., Swaroop, A., Hegg, C.C., Raphael, Y., Martens, J.R. *et al.* (2009) Defects in neural stem cell proliferation and olfaction in Chd7 deficient mice indicate a mechanism for hyposmia in human CHARGE syndrome. *Hum Mol Genet*, **18**, 1909-1923.

28 Ma, D.K., Ponnusamy, K., Song, M.R., Ming, G.L. and Song, H. (2009) Molecular genetic analysis of FGFR1 signalling reveals distinct roles of MAPK and PLCgamma1 activation for self-renewal of adult neural stem cells. *Mol Brain*, **2**, 16.

29 Wierman, M.E., Kiseljak-Vassiliades, K. and Tobet, S. (2010) Gonadotropin-releasing hormone (GnRH) neuron migration: Initiation, maintenance and cessation as critical steps to ensure normal reproductive function. *Front Neuroendocrinology*.

30 Wray, S. (2002) Development of gonadotropin-releasing hormone-1 neurons. *Front Neuroendocrinol*, **23**, 292-316.

31 Wray, S., Grant, P. and Gainer, H. (1989) Evidence that cells expressing luteinizing hormone-releasing hormone mRNA in the mouse are derived from progenitor cells in the olfactory placode. *Proc Natl Acad Sci U S A*, **86**, 8132-8136.

32 Forni, P.E., Fornaro, M., Guenette, S. and Wray, S. (2011) A role for FE65 in controlling GnRH-1 neurogenesis. *J Neurosci*, **31**, 480-491.

33 Forni, P.E., Taylor-Burds, C., Melvin, V.S., Williams, T. and Wray, S. (2011) Neural Crest and Ectodermal Cells Intermix in the Nasal Placode to Give Rise to GnRH-1 Neurons, Sensory Neurons, and Olfactory Ensheathing Cells. *J Neurosci*, **31**, 6915-6927.

34 Wray, S. (2010) From nose to brain: development of gonadotrophin-releasing hormone-1 neurones. *J Neuroendocrinol*, **22**, 743-753.

35 Camper, S., Suh, H., Raetzman, L., Douglas, K., Cushman, L., Nasonkin, I., Burrows, H., Gage, P. and Martin, D. (2002) Rossant, J. and Tam, P. (eds.), In *Mouse Development Patterning, Morphogenesis, and Organogenesis*. Academic Press, San Diego, pp. 499-518.

36 Carbajo-Perez, E. and Watanabe, Y.G. (1990) Cellular proliferation in the anterior pituitary of the rat during the postnatal period. *Cell Tissue Res*, **261**, 333-338.

37 Castinetti, F., Davis, S.W., Brue, T. and Camper, S.A. (2011) Pituitary Stem Cell Update and Potential Implications for Treating Hypopituitarism. *Endocr Rev*.

38 Fauquier, T., Rizzoti, K., Dattani, M., Lovell-Badge, R. and Robinson, I.C. (2008) SOX2-expressing progenitor cells generate all of the major cell types in the adult mouse pituitary gland. *Proc Natl Acad Sci U S A*, **105**, 2907-2912.

39 Otani, H., Otsuka, F., Takeda, M., Mukai, T., Terasaka, T., Miyoshi, T., Inagaki, K., Suzuki, J., Ogura, T., Lawson, M.A. *et al.* (2009) Regulation of GNRH production by estrogen and bone morphogenetic proteins in GT1-7 hypothalamic cells. *J Endocrinol*, **203**, 87-97.

40 Nicol, L., Faure, M.O., McNeilly, J.R., Fontaine, J., Taragnat, C. and McNeilly, A.S. (2008) Bone morphogenetic protein-4 interacts with activin and GnRH to modulate gonadotrophin secretion in LbetaT2 gonadotrophs. *J Endocrinol*, **196**, 497-507.

41 Teixeira, L., Guimiot, F., Dodé, C., Fallet-Bianco, C., Millar, R.P., Delezoide, A.L. and Hardelin, J.P. (2010) Defective migration of neuroendocrine GnRH cells in human arrhinencephalic conditions. *J Clin Invest.*, **120**, 3668-3672.

42 Imai, T., Sakano, H. and Vosshall, L.B. (2010) Topographic mapping--the olfactory system. *Cold Spring Harb Perspect Biol*, **2**, a001776.

43 Touhara, K. and Vosshall, L.B. (2009) Sensing odorants and pheromones with chemosensory receptors. *Annu Rev Physiol*, **71**, 307-332.

44 Dateki, S., Kosaka, K., Hasegawa, K., Tanaka, H., Azuma, N., Yokoya, S., Muroya, K., Adachi, M., Tajima, T., Motomura, K. *et al.* (2010) Heterozygous orthodenticle homeobox 2 mutations are associated with variable pituitary phenotype. *J Clin Endocrinol Metab*, **95**, 756-764.

45 Kelley, C.G., Lavorgna, G., Clark, M.E., Boncinelli, E. and Mellon, P.L. (2000) The Otx2 homeoprotein regulates expression from the gonadotropin-releasing hormone proximal promoter. *Mol Endocrinol*, **14**, 1246-1256.

46 Larder, R. and Mellon, P.L. (2009) Otx2 induction of the gonadotropin-releasing hormone promoter is modulated by direct interactions with Grg co-repressors. *J Biol Chem*, **284**, 16966-16978.

47 Omodei, D., Acampora, D., Mancuso, P., Prakash, N., Di Giovannantonio, L.G., Wurst, W. and Simeone, A. (2008) Anterior-posterior graded response to Otx2 controls proliferation and differentiation of dopaminergic progenitors in the ventral mesencephalon. *Development*, **135**, 3459-3470.

48 Vernay, B., Koch, M., Vaccarino, F., Briscoe, J., Simeone, A., Kageyama, R. and Ang, S.L. (2005) Otx2 regulates subtype specification and neurogenesis in the midbrain. *J Neurosci*, **25**, 4856-4867.

49 Hurd, E.A., Poucher, H.K., Cheng, K., Raphael, Y. and Martin, D.M. (2010) The ATP-dependent chromatin remodeling enzyme CHD7 regulates pro-neural gene expression and neurogenesis in the inner ear. *Development*, **137**, 3139-3150.

50 Bird, S.D., Walker, R.J. and Hubbard, M.J. (1994) Altered free calcium transients in pig kidney cells (LLC-PK1) cultured with penicillin/streptomycin. *In Vitro Cell Dev Biol Anim*, **30A**, 420-424.

51 Cohen, S., Samadikuchaksaraei, A., Polak, J.M. and Bishop, A.E. (2006) Antibiotics reduce the growth rate and differentiation of embryonic stem cell cultures. *Tissue Eng*, **12**, 2025-2030.

52 Lemeire, K., Van Merris, V. and Cortvrindt, R. (2007) The antibiotic streptomycin assessed in a battery of in vitro tests for reproductive toxicology. *Toxicol In Vitro*, **21**, 1348-1353.

53 Mathieson, W., Kirkland, S., Leonard, R. and Thomas, G.A. (2011) Antimicrobials and in vitro systems: antibiotics and antimycotics alter the proteome of MCF-7 cells in culture. *J Cell Biochem*.

54 Aramaki, M., Udaka, T., Kosaki, R., Makita, Y., Okamoto, N., Yoshihashi, H., Oki, H., Nanao, K., Moriyama, N., Oku, S. *et al.* (2006) Phenotypic spectrum of CHARGE syndrome with CHD7 mutations. *J Pediatr*, **148**, 410-414.

55 Jongmans, M.C., Admiraal, R.J., van der Donk, K.P., Vissers, L.E., Baas, A.F., Kapusta, L., van Hagen, J.M., Donnai, D., de Ravel, T.J., Veltman, J.A. *et al.* (2006)

CHARGE syndrome: the phenotypic spectrum of mutations in the CHD7 gene. *J Med Genet*, **43**, 306-314.

56 Lalani, S.R., Safiullah, A.M., Fernbach, S.D., Harutyunyan, K.G., Thaller, C., Peterson, L.E., McPherson, J.D., Gibbs, R.A., White, L.D., Hefner, M. *et al.* (2006) Spectrum of CHD7 Mutations in 110 Individuals with CHARGE Syndrome and Genotype-Phenotype Correlation. *Am J Hum Genet*, **78**, 303-314.

57 Sanlaville, D., Etchevers, H.C., Gonzales, M., Martinovic, J., Clement-Ziza, M., Delezoide, A.L., Aubry, M.C., Pelet, A., Chemouny, S., Cruaud, C. *et al.* (2006) Phenotypic spectrum of CHARGE syndrome in fetuses with CHD7 truncating mutations correlates with expression during human development. *J Med Genet*, **43**, 211-217.

58 Sanlaville, D. and Verloes, A. (2007) CHARGE syndrome: an update. *Eur J Hum Genet*, **15**, 389-399.

59 Vissers, L.E., van Ravenswaaij, C.M., Admiraal, R., Hurst, J.A., de Vries, B.B., Janssen, I.M., van der Vliet, W.A., Huys, E.H., de Jong, P.J., Hamel, B.C. *et al.* (2004) Mutations in a new member of the chromodomain gene family cause CHARGE syndrome. *Nat Genet*, **36**, 955-957.

60 Hall, J.A. and Georgel, P.T. (2007) CHD proteins: a diverse family with strong ties. *Biochem Cell Biol*, **85**, 463-476.

61 Ho, L. and Crabtree, G.R. (2010) Chromatin remodelling during development. *Nature*, **463**, 474-484.

62 Lusser, A. and Kadonaga, J.T. (2003) Chromatin remodeling by ATP-dependent molecular machines. *Bioessays*, **25**, 1192-1200.

63 Marfella, C.G. and Imbalzano, A.N. (2007) The Chd family of chromatin remodelers. *Mutat Res*, **618**, 30-40.

64 Woodage, T., Basrai, M.A., Baxevanis, A.D., Hieter, P. and Collins, F.S. (1997) Characterization of the CHD family of proteins. *Proc Natl Acad Sci U S A*, **94**, 11472-11477.